Membrane Fouling in Constant Permeate Flux Cross-Flow Microfiltration of Biological Solutions

by

Maja Stressmann

A thesis
presented to the University of Waterloo
in fulfilment of the
thesis requirement for the degree of
Doctor of Philosophy
in
Chemical Engineering

Waterloo, Ontario, Canada, 2008

I hereby declare that I am the sole author of this thesis. This is a true copy of the thesis, including any required final revisions, as accepted by my examiners.

I understand that my thesis may be made electronically available to the public.

Abstract

This thesis investigates the fouling of a microfiltration membrane by biological solutions. Membrane fouling is recognized as a major drawback for the application of microfiltration in the purification of biotechnology products. Membrane fouling was analyzed and compared for filtrations performed with a hollow fiber microfiltration module operated at constant permeate flux using bovine serum albumin (BSA) solutions or Chinese hamster ovary (CHO) cell culture broths as feed solutions.

A mechanistic model was developed to represent the fouling of a cross-flow microfiltration membrane operated at constant permeate flux. Fouling was observed as an increase in the transmembrane pressure (TMP) and assumed to occur first by pore blockage followed by cake formation over the blocked pores. The effect of the cross-flow action was described by the removal of deposits from the membrane surface thereby reducing the pore blockage and the mass of the cake. The model was fitted to the TMP profiles obtained during the filtration of BSA solutions and Chinese hamster ovary (CHO) cell culture broths with a 0.45 μm polysulfone hollow fiber membrane. According to the fitted model, pores blocked faster and more cake was formed with increasing BSA concentration. In the case of CHO cell culture broth, increasing the wall shear rate (proportional to cross-flow velocity) seemed to lead to the formation of a less pronounced cake but more pore blockage.

The cross-flow mechanistic model was applied to the microfiltration of CHO cell culture supernatants harvested at different days of the fermentation process. The filtrations were performed at two different shear rates and with two different membrane pore sizes. The cell culture supernatant caused membrane fouling observed as an increase in both the TMP and the membrane hydraulic resistance estimated from water flux measurements at the end of the filtrations. The highest TMP increase was observed for the filtrations with the smaller membrane pore size (0.2 μm) and the higher shear rate (8000 s^{-1}). The hydraulic resistance estimates of the fouled membrane also revealed a higher irreversible fouling for the smaller (0.2μm) membrane pore size while the model analysis indicates that more fouling occurred at the entrance of the membrane pores. The shear rate was found to

strongly influence the contribution of the reversible fouling to the total hydraulic resistance of the membrane. The cross-flow mechanistic model indicates a higher pore blockage for the most severe membrane fouling observed experimentally for the smaller membrane pore size and the higher shear rate. At the same time, a smaller cake deposit was predicted for the higher shear rate. The different cell culture harvest time investigated in this study did not reveal any differences in membrane fouling.

BSA solutions were used to evaluate the contribution of BSA aggregates, fresh cell culture medium and the non-ionic surfactant Pluronic F-68 to membrane fouling. A simple empirical model was developed to represent the TMP increase and to derive the initial fouling rate. The initial fouling rate, the normalized TMP and the irreversible membrane resistance at the end of the filtration were analyzed to determine the effect of BSA solution characteristics on membrane fouling. The initial fouling rate increased with increasing BSA aggregate content consistent with a two-step fouling mechanism that was proposed for membrane fouling by BSA. Increased BSA concentration and the use of fresh cell culture medium compared to potassium phosphate buffer resulted in an increase in initial fouling rate, TMP and irreversible membrane fouling. The addition of the non-ionic surfactant Pluronic-F68 to the BSA solutions decreased the long-term fouling and the irreversible fouling but did not affect the initial fouling rate.

Acknowledgements

I would like to express my sincere gratitude to my supervisor C. Moresoli for the opportunities, guidance, encouragement and financial assistance throughout the project.

I am grateful to the members of my committee, Prof. R. Ghosh from McMaster University and Profs. R. L. Legge, X. Feng and L. Meiering from the University of Waterloo for their comments on this thesis.

I am indebted to the NSERC Cellnet Research Network for funding. I wish to thank Prof. B. Marcos (University of Sherbrooke) for help with the modeling, Prof. L. Meiering for access to the DLS instrument, Dr. J. M. Scharer for providing the fresh cell culture medium, and Dr. M. Butler, Dr. M. Spearman (University of Manitoba) and Cangene Corp. (Mississauga, ON) for supplying the cell culture broths. I would also like to acknowledge Mr. D. Plaat and Mr. K. Walsh (GE Healthcare) for technical assistance with the MF system and Jan, Isabelle, Swetha, Janice and Christine for their help with experimental work.

I would like to acknowledge all former and current members of the downstairs bio-group for making the lab and office an enjoyable place to work. You were a great bunch of people. Specifically I would like to thank Joe and Dom for their valuable advice and support, Mandy for all her encouragement, Petr for interesting discussions, games and bagels, Jeremy and John for their dedication to TGIF, Kela for asking the right questions at the right time, Sarah and Marc for the great Canadian experience up north and Jason for taking me fishing so that I could catch the biggest fish.

My warmest thanks go to Jana Skorepova, for being the way she is, a true friend, great listener and dedicated runner.

I would like to thank Lori and Corey for putting up with me for yet another month, for every distraction and for every conversation which enabled me to complete this dissertation. Thanks for everything.

Last, but not least, I would like to thank my family for all their love and support.

Für meine Eltern

Contents

List of Figures

List of Tables

Nomenclature

Roman letters

$A_{blocked}$	area of membrane blocked by protein deposit (m^2)
A_c	cross sectional area of membrane fibers (m^2)
A_{open}	area of unblocked (clean) membrane (m^2)
$A_{open,o}$	initial area of unblocked (clean) membrane (m^2)
A_0	total area of the membrane (m^2)
C_b	bulk protein (organic) concentration ($g\ L^{-1}$)
F	factor for initial conditions (-)
f'	fractional amount of total protein that contributes to deposit growth (-)
i_f	initial fouling rate ($Pa\ s^{-1}$)
J	constant value of permeate flux ($m^3\ m^{-2}\ s^{-1}$)
k_p	proportionality coefficient for protein layer resistance ($m\ kg^{-1}$)
k_{pb}	cross-flow coefficient for pore blockage ($m^4\ s^{-1}\ kg^{-1}$)
k_c	cross-flow coefficient for cake formation (s^{-1})
m_p	mass of the protein deposit per unit cross-sectional area ($kg\ m^{-2}$)
n	number of fibers (-)
P	transmembrane pressure (Pa)
Q	filtrate flow rate ($m^3\ s^{-1}$)
Q_0	constant value of volumetric flow rate through membrane ($m^3\ s^{-1}$)
Q_{open}	volumetric flow rate through open pore area ($m^3\ s^{-1}$)
$Q_{blocked}$	volumetric flow rate through blocked area ($m^3\ s^{-1}$)
r	fiber radius (m)
R_f	total fouling resistance (m^{-1})
R_{irr}	hydraulic resistance of the irreversible fouling (m^{-1})
R_m	hydraulic resistance of the clean membrane (m^{-1})
R_p	resistance of the protein deposit (m^{-1})
R_{p0}	resistance of the initial protein aggregate deposit (m^{-1})

R_{rev}	hydraulic resistance of the reversible fouling (m^{-1})
R_t	total hydraulic resistance (m^{-1})
R’	specific protein layer resistance (m kg^{-1})
t	filtration time (s)
TMP	transmembrane pressure (Pa)
U	cross-flow velocity (m s^{-1})
V	cumulative filtrate volume (L)

Greek letters

α	pore blockage parameter (m^2 kg^{-1})
ε	membrane porosity (-)
μ	permeate viscosity (Pa s)

1

Introduction

Microfiltration (MF) is a key technology in the downstream processing of biopharmaceuticals in the biotechnology industry. It is used in the initial cell culture harvest step to remove the cells and cell debris from the product stream [1]. MF has been used to harvest and/or separate bacteria, yeast, fungi, and mammalian cells which produce biopharmaceuticals such as therapeutic proteins and antibiotics [2-4]. Mammalian cell systems are most suitable to produce protein pharmaceuticals that require post-translational modifications such as glycosylation and proper folding to be functional [5]. One example is the production of recombinant human tissue-plasminogen activator (t-PA) by Chinese hamster ovary (CHO) cells [5]. T-PA derived from CHO cells became commercially available after it was approved for human therapy by the FDA in 1987 [6]. CHO cells are well characterized and capable of growing in large-scale suspensions and secreting the therapeutic protein into their growth medium [6;7].

Growth media for mammalian cells are highly developed and often optimized for the specific cell line. Basic media components include carbohydrates, amino acids, salts and vitamins [6]. To enhance cell growth, serum derived from animals can be added to the media [8]. However, serum is chemically undefined, varies from batch to batch and can contaminate the cell culture with viruses or prions. Alternatively, defined and serum-free media have been developed that contain hormones and growth factors to enhance the growth of the specific cell line [6].

In MF, the separation of the cells and cell debris from the culture broth is predominantly based on the retention of particles larger than the membrane pores (e.g. CHO cells) and the passage of smaller species (e.g. proteins) through the membrane. One recognized drawback in the operation of MF systems is membrane fouling. Membrane fouling can reduce filtration efficiency and the recovery of the target protein product if its passage through the membrane is impeded. Mechanisms and factors relevant to MF membrane fouling are complex and the focus of ongoing studies. Both filtration conditions and feed composition have an impact on the MF performance and the membrane fouling in particular [9]. The feed composition is affected by the cell line and the medium used, as well as the culture conditions and the use of culture stabilizing additives. The schematic in Fig. 1.1 gives an overview of the filtration process and some of the factors affecting the process.

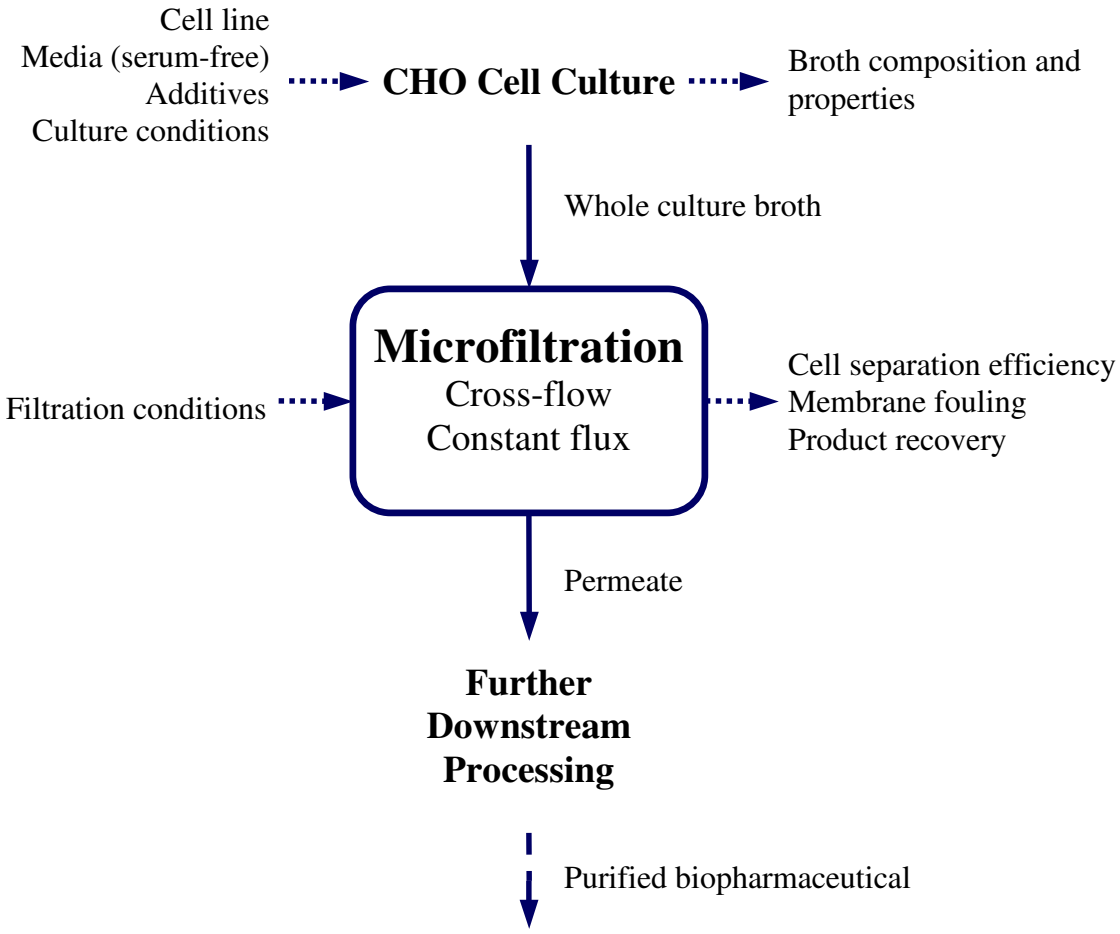

Fig. 1.1: Overview of downstream processing with microfiltration for therapeutic protein recovery from CHO cells.

Alternative technologies to MF include centrifugation and expanded bed adsorption. The advantages of MF over other techniques include mild process conditions to avoid cell rupture and protein denaturation, efficient and absolute removal of large particles, sterile operation, and the ease of scale-up to industrial scale [5;10-12]. Lower costs of MF compared to continuous disc centrifugation have also been reported [13]. Some of the disadvantages of MF are (i) the loss of the target protein due to interaction with the membrane [9], (ii) shear forces associated with the pumping of the feed solution which could lead to cell damage and subsequent contamination of the target protein with cellular proteins [14] and (iii) the sensitivity of protein transmission to culture broth properties which means that changes in the fermentation process could change the filtration

performance [15]. The major disadvantage of MF is associated with membrane fouling, which reduces filtration efficiency and possibly recovery of the protein product.

1.1 Research motivation

Processes for the production of new and existing therapeutic proteins continue to be developed and cell lines, media compositions and culture conditions are being optimized for therapeutic protein production. Changes in the production process can also affect the properties of the broth to be filtered which in turn can affect the filtration process. It is therefore important to use a filtration system and analytical models that allow for comparison of the efficiency of the filtration of different feed streams (culture broths). Filtration efficiency is greatly affected by membrane fouling and insight into fouling mechanisms and feed components causing membrane fouling are key to the improvement of the filtration process. This thesis investigates membrane fouling during the filtration of biological solutions through hollow fiber MF membranes as an initial step for mammalian cell harvest and therapeutic protein recovery.

1.2 Objectives

The objective of this thesis was to study the membrane fouling of a MF system at various filtration conditions for different feed solutions. The specific objectives were:

1. To develop a mechanistic fouling model that described the fouling by biological solutions in a hollow fiber microfiltration membrane operated in cross-flow at constant permeate flux.

2. To study the effect of shear rate, membrane pore size, presence of cells in the culture broth and time of cell culture harvest on the membrane fouling using the developed mechanistic model.

3. To assess reversible and irreversible fouling of the membrane for a variety of feeds including cell culture broth, cell culture supernatant and solutions containing model proteins.

4. To develop an empirical model that could easily describe experimental TMP profiles and that allows for derivation and calculation of the initial fouling rate.

5. To determine the effect of feed composition on membrane fouling using a model protein, where the feed composition could be altered with respect to protein concentration, solution composition and the presence of a non-ionic surfactant.

1.3 Structure of the thesis

Background information on cross-flow microfiltration, mammalian cell harvest, membrane fouling as well as filtration and solution conditions affecting the membrane fouling is provided in Chapter 2. Chapter 3 introduces a new fouling model developed for constant permeate flux cross-flow MF of biological solutions. Both the fouling by the model protein bovine serum albumin (BSA) and the fouling by CHO cell culture broth and CHO cell culture supernatant were analyzed. Chapter 4 considers the combined effect of membrane pore size and cross-flow velocity on the membrane fouling of CHO cell culture supernatant making use of the developed fouling model. The fouling of the filtration membrane by the model protein BSA is further examined in Chapter 5. An empirical model that is useful in evaluating the initial fouling rate is introduced. The effect of protein concentration, solution composition and a media additive, the non-ionic surfactant Pluronic F-68, on the initial fouling rate, overall fouling, and severity of irreversible fouling is studied. Chapter 6 highlights important conclusions from the work accomplished in this thesis and suggestions for future work are made.

Chapters 3, 4 and 5 are arranged in publication format, each with its individual abstract, introduction, materials and methods, results and discussion as well as conclusion.

2

Background

2.1 Cross-flow microfiltration

2.1.1 General concepts

Membrane filtration refers to the separation of components from a feed stream by means of a membrane where the separation is primarily a result of size differences. The liquid stream passing through the membrane, the permeate, is free of feed components larger than the membrane pores whereas the liquid stream leaving the membrane module unfiltered, the retentate, will have a higher concentration of retained particles. In cross-flow filtration (CFF), also known as tangential flow filtration (TFF), the feed flows tangentially to the membrane surface thereby sweeping away some of the deposited material and reducing the accumulation of feed components at the membrane surface. The increase in permeate flow resistance associated with the build-up of deposits is significantly reduced compared to dead-end filtration where the feed flows perpendicular to the membrane. A schematic for cross-flow filtration is shown in Fig. 2.1.

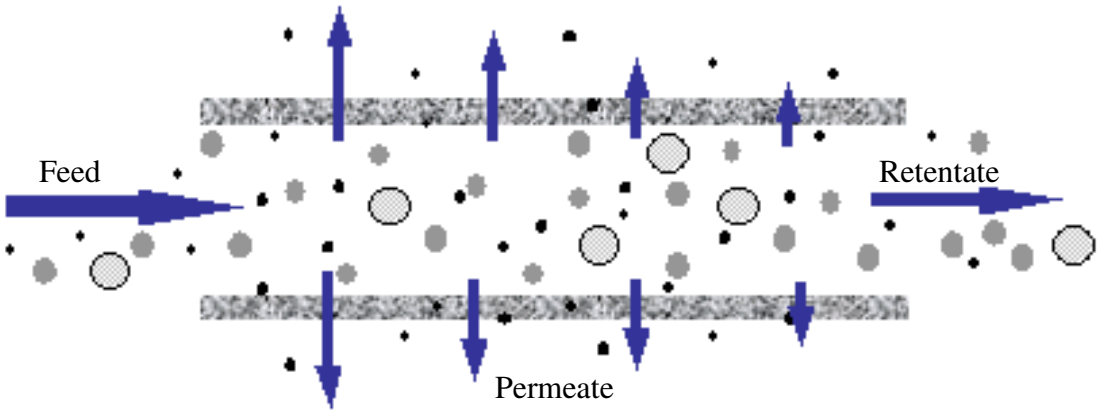

Fig. 2.1: Schematic of cross-flow filtration

The driving force in membrane filtration is the transmembrane pressure (TMP) which describes the pressure drop across the membrane and is calculated as the pressure difference between the upstream and the downstream side (permeate pressure, P_p) of the membrane (Eq. (2.1)). The upstream side pressure is taken as the average pressure between the feed pressure (P_f) and the retentate pressure (P_r) at the inlet and outlet of the membrane, respectively.

$$TMP = \Delta P = \frac{P_f + P_r}{2} - P_p \tag{2.1}$$

The velocity in the flow channel or the lumen of the membrane fiber, the cross-flow velocity U, is directly proportional to the volumetric flow rate Q,

$$U = \frac{Q}{A_c}, \tag{2.2}$$

where A_c is the cross-sectional area of the fibers. The rate at which permeate flows through the membrane is the permeate flux (J_p) or just flux (J) and often given in units of L m^{-2} h^{-1} or Lmh. It is measured as the permeate flow rate Q_p per membrane area A:

$$J = \frac{Q_p}{A}. \tag{2.3}$$

Darcy's Law (Eq. (2.4)) describes the permeate flux as a function of TMP, permeate viscosity μ_p and total resistance (R_t) to permeate flow [4].

$$J = \frac{TMP}{\mu_p (R_t)} \tag{2.4}$$

The total resistance R_t can be decomposed into intrinsic membrane resistance R_m and resistance of a fouling layer R_f:

$$R_t = R_m + R_f \tag{2.5}$$

Fouling is generally referred to as the interaction of feed components with the membrane resulting in changes of membrane characteristics. Membrane fouling is discussed in more detail in section 2.2.

2.1.2 Membrane system

Hollow fiber membrane modules were initially designed for desalination purposes but later adapted for use in ultra- and microfiltration [4]. It is common to use multiple modules in parallel to achieve high membrane surface area suitable for production scale [1]. The

feed enters the lumen of the individual fibers and a portion is passing through the pores as permeate. The inner diameter of fibers is usually between 0.2 and 1.8 mm [1].

The flow regime in a fiber is of interest because of the sensitivity of some feed components to shear forces. The Reynolds Number (Re) in a fiber can be calculated using the following equation [16]:

$$\mathrm{Re} = \frac{2\rho U r}{\mu} = \frac{2\rho Q}{\mu n \pi r}, \qquad (2.6)$$

where ρ is the fluid density, U is the cross-flow velocity, r the fiber radius and μ the solution viscosity [4]. Values typically used in this PhD thesis are $\rho = 10^3$ kg m^{-3}, U = 1 m s^{-1}, r = 5 x 10^{-4} m, μ = 9 x 10^{-4} Pa s and n = 13 which gives a Reynolds number of ~ 1100. The flow in a fiber is considered laminar for Reynolds numbers below 2000 [17].

Alternative module configurations include tubular devices, flat plate and spiral wound. The hollow fiber module configuration offers the highest packing density (membrane area per space) and the energy costs associated with the pumping are low [4].

2.1.3 Operation mode

Crossflow filtration can be operated at constant TMP or constant permeate flux. The TMP can be kept constant by adjusting a valve on the retentate line or pressurizing the feed tank. The permeate flux will change with filtration time according to the fouling behaviour of the feed solution (Fig. 2.2 A). High initial permeate flux followed by a rapid flux decrease is characteristic for constant TMP operations when membrane fouling occurs. The high initial permeate flux causes rapid particle deposition which results in a fast build-up of a boundary layer at the membrane surface with increased flow resistance. Operation at a TMP that results in fluxes much lower than this high initial flux observed for constant TMP can avoid the fast particle deposition. A careful selection of TMP is also of importance in respect to the compressibility of a potential fouling layer. If the fouling layer is compressible, increased TMP causes a more densely packed layer. As a consequence, the permeate flux will diminish with increased TMP [12;18].

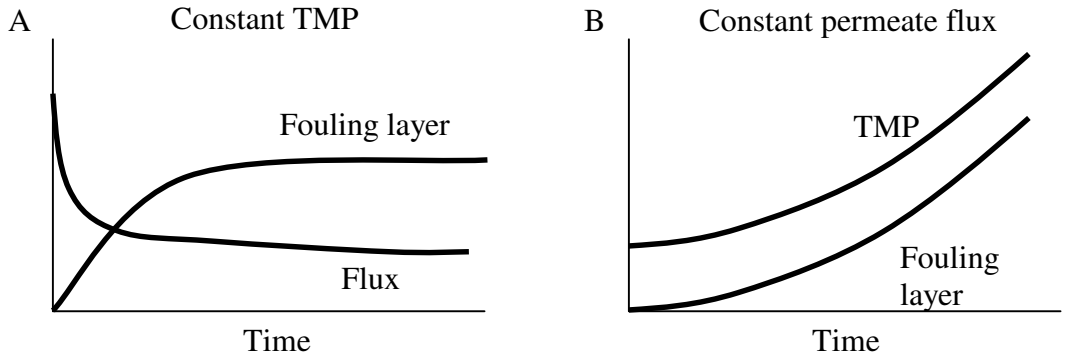

Fig. 2.2: Typical permeate flux and TMP profiles and membrane fouling layer in cross-flow filtration: (A) constant TMP and (B) constant permeate flux.

The permeate flux can be kept constant either by constantly adjusting the TMP or by making use of a permeate pump that withdraws the permeate at a constant rate. According to Eqs. (2.4) and (2.5), the TMP is a function of the resistance of a fouling layer (R_f) when the flux is kept constant. If a fouling layer forms and the hydraulic resistance increases, the TMP will increase with filtration time. The extent of the TMP increase is a function of the filtration conditions such as the permeate flux [19;20] and the feed properties [14]. A schematic TMP profile is shown in Fig. 2.2 B. Similar to choosing the TMP for operations at constant TMP, the selection of the constant permeate flux has to be made carefully. Berthold and Kempken [19] compared filtrations of hybridoma cell suspensions at different constant permeate flux. The filtration operated at the higher permeate flux showed a rapid and sharp drop of permeate pressure (and therefore TMP increase) while the permeate pressure and the TMP were constant during the filtration at the lower permeate flux. This will be discussed in more detail in the next section.

The filtration performance can be greatly influenced by the mode of operation. Harscoat et al. [21] reported that switching from constant TMP mode to constant permeate flux mode reduced the fouling considerably during the filtration of extracellular polymeric substances (EPS) with a 0.5 µm tubular ceramic membrane. The reversible fouling layer resistance was found to be 42.7 x 10^{11} m^{-1} compared to the 65.8 x 10^{11} m^{-1} resistance obtained for constant TMP operation. Both filtration operation modes showed similar irreversible fouling (9.3 and 8.2 x 10^{11}, respectively). The average flux for constant

permeate flux operations can be higher than for constant pressure operations, especially for prolonged filtration times [12].

2.1.4 Permeate flux

A critical flux has been defined as the permeate flux below which fouling is significantly reduced or even eliminated [22]. The existence of a critical flux was supported directly by a lack of particle deposition at the membrane surface when the filtration was performed below this critical flux and increasing particle deposition when the filtration was performed above this critical flux [23;24]. The observation of near constant and increasing TMP with time at a flux below and above, respectively, the critical flux was further evidence for a critical flux [24].

Using latex particle suspensions with different particle sizes, Kwon et al. [24] observed an average TMP that was very similar to the TMP obtained with filtration of clean water and remained constant over the time tested. Upon permeate flux increase, the TMP started to increase with time and was significantly different from the TMP obtained with clean water. For a given permeate flux, the particle deposition rate increased with decreasing particle size. For a given particle size, the deposition rate increased with increased permeate flux. Whether or not particles deposit depends on the force balance between transport to the membrane surface (permeate flow) and back-transport mechanisms. Back-transport mechanisms will be discussed section 2.1.6.

2.1.5 Cross-flow velocity and shear rate

As mentioned in section 2.1.1, cross-flow of the feed solution will reduce the accumulation of retained feed components at the membrane surface. Theoretically, higher cross-flow velocity (CFV) means lower particle deposition [25]. However, CFV can be restricted by the sensitivity of the feed components to the shear caused by the feed flow. The wall shear rate, γ_w, at the membrane surface is directly proportional to the CFV and calculated for hollow fiber membranes according to Eq. (2.7),

$$\gamma_w = \frac{4Q}{n\pi r^3}, \tag{2.7}$$

where Q represents the feed flow rate ($m^3\ s^{-1}$), n is the number of hollow fibers, and r (m) is the radius of the individual fiber. The effect of shear rate on the cell viability was studied for murine myeloma, human hybridoma, murine hybridoma and insect cells [14]. Cell cultures were circulated through selected filter modules at increasing flow rates and cell viability was measured before and after 20 circulation passes. Shear rates below 3000 s^{-1} had no apparent effect on the various cell lines. Shear rates above this value resulted in considerable cell damage. It is important to avoid cell damage, otherwise cell content will leak into the cell culture broth. Cell leakage can contaminate the protein product of interest and interfere with the downstream processing [19].

The choice of CFV and shear rate is balanced by both performance and economical considerations [26]. A larger pump size and higher feed flow rates will have a higher cost but are expected to provide higher permeate fluxes for most cases.

2.1.6 Particle transport

Particle transport in cross-flow membrane filtration operation is a combination of several mechanisms [16]. The feed flows tangentially to the membrane surface, carrying particles along toward the exit of the filter module. The permeate flow will transport the particles to the membrane surface where the retained particles will form a cake layer (MF) or gel layer (UF). The rate of growth and the thickness of the particle layer will depend on the dominating transport mechanism.

The size of the particles in the feed solution is an important factor that decides which transport mechanism comes to bear and has been discussed in a review by Belfort et al. [16]. Submicron particles have high diffusion coefficients so that Brownian diffusion is the most effective transport mechanism for these particles. Brownian diffusion is independent of shear rate and decreases with increasing particle size.

Proportional to shear rate and particle size is the shear-induced hydrodynamic diffusion mechanism. Particles interact and collide, causing random movement. This applies in typical cross-flow filtration with particles of about 1 micron and larger in size.

Inertial lift is yet another proposed mechanism to support back-transport of particles away from the membrane or cake layer surfaces. Particles interact with the feed stream in a nonlinear mode. The resulting lift velocity is proportional to the square of the shear rate and to the cube of the particle size.

The surface transport can drag the particles across the surface of the membrane or the fouling layer, forming a flowing layer that increases in thickness with increasing distance from the filter entrance. The cross-flow as well as the permeate flow are smallest at the filter exit. The surface transport increases linearly with increase in shear rate and particle radius.

Summarizing, the dominant transport mechanism for submicron particles and low shear rates is Brownian diffusion. Shear-induced hydrodynamic diffusion is highly relevant for micron-sized and larger particles at moderate shear rates and inertial lift for large particles and high flow rates. Belfort, Davis and Zydney [16] derived an equation that accommodates all four mechanisms to predict the long-term flux for each of the four mechanisms and provides details on the equation and assumptions.

Studies incorporating the mean size of particles forming the cake layer found a higher concentration of smaller particles in the cake compared to the concentration in the feed solution [22;27]. This was in agreement with the proposed back-transport mechanism in which particle back-transport into the flowing feed is higher for larger particles. Adapting filtration conditions in accordance with particle size could avoid cake formation or result in fouling layers with lower resistance.

2.1.7 Membrane material and pore size

A wide variety of membranes from different materials and with a range of pore sizes are available for filtrations. The choice depends on the specific feed solution to be filtered and filtration performance requirements. For example, low protein-binding membranes are desirable for the recovery of high value proteins present in low concentration since unrestricted protein transport through the membrane is absolutely necessary [28;29]. The adsorption of proteins to the membrane is more problematic with hydrophobic membranes and the use of hydrophilic membranes is recommended. The use of hydrophilic membranes

can increase the protein recovery and minimize the fouling by proteins and associated deterioration of filtration performance [25;30]. Polysulfone (PS) and polyvinylidene fluoride (PVDF) are both hydrophobic in nature but can be surface treated to increase their hydrophilicity. Ceramic and regenerated cellulose membranes are relatively hydrophilic [25]. The charge interactions between the feed components and the membrane have to be considered for surface charged membranes.

The type of membrane material will also affect the stability of the membrane. Polysulfone for example has good thermal, chemical and pH stability [31]. The reusability of membranes is determined by a consistent separation performance [25] and resistance to cleaning procedures. Frequent water flux measurements provide information on the hydraulic resistance of the membrane over time. To achieve maximum recovery of the initial water flux, cleaning procedures have to be developed with respect to the membrane stability and the specific filtration.

The pore size of a membrane principally determines which particles are retained and which can pass through the membrane. MF uses membranes with pores in the range of 0.05 to 10 µm [1]. The pore size will also affect the permeate flux or TMP during filtration, but whether increasing or decreasing the pore size affects the filtration performance positively or negatively was reported as system specific [13].

2.2 Membrane fouling

Membrane fouling is referred to as the deposition or adsorption of the particles contained in the feed stream on the membrane surface or in the membrane pores. Membrane fouling has a negative impact on filtration performance as it decreases the permeate flux or increases the TMP. It can also change the sieving characteristics of the membrane and reduce the recovery of the desired product.

2.2.1 Internal and external fouling

Different approaches can be used to describe membrane fouling. For example, depending on the location of the fouling with respect to the membrane, external and internal membrane fouling can be distinguished.

External fouling refers to particle deposition or protein adsorption to the outer surface of the membrane. If the fouling species form a deposit layer on the outer surface of the membrane, they constitute an additional resistance to the flow of the permeate through the membrane as shown in Eq. (2.5).

During internal fouling, proteins or other molecules adsorb to the pore walls. This can cause pore narrowing and pore clogging and change the effective pore size of the membrane or the pore size distribution [32;33]. If pore clogging occurs, the membrane's resistance to flow is increased in addition to changing the pore size distribution of the membrane.

2.2.2 Reversible and irreversible fouling

Another approach to describe fouling phenomena is to characterize the reversibility of fouling. Reversible fouling refers to fouling deposits that are easily removed from the membrane surface by rinsing or flushing the membrane or applying backwashing [34]. Irreversible fouling on the other hand requires cleaning under harsher conditions or with chemical agents. The attachment of the foulants to the membrane is much stronger or the fouling occurred inside the membrane structure from where the foulants are more difficult to remove. For example, fast initial fouling by pore blocking was observed during filtration of whey proteins using 0.8 µm pore size ceramic membranes [35]. The foulants could not be removed by backwashing and the authors suggested blockage of the internal membrane structure by whey protein aggregates that were small enough to enter the membrane pores.

A group of foulants that tend to foul membranes irreversibly are proteins [4;9]. Proteins can adsorb strongly to solid surfaces due to the occurrence of hydrophobic interactions, electrostatic interactions, hydrogen bonding, and van der Waals interactions [4].

2.2.3 Fouling models

To describe membrane fouling in terms of permeate flux decline or TMP increase, mechanistic fouling models have been developed over the years. There are four classical models that were first applied to constant pressure filtration [36], but later also developed for constant permeate flux filtrations [37]. These four classical models are pore blockage, pore constriction, intermediate blockage and cake filtration. A schematic showing the four different types of fouling is presented in Fig. 2.3. Pore blockage (Fig. 2.3 A) is described as the deposition of particles at the entrance of the membrane pores, thereby completely blocking the flow through those pores. Pore blockage is also termed complete blocking. Pore constriction applies when particles enter the pores and deposit along the surface of the pores which reduces the effective diameter of the pores (Fig. 2.3 B). This process is also known as standard blocking. The assumption of particle superimposition is the basis for intermediate blockage (Fig. 2.3 C). Cake filtration basically reflects external membrane fouling, where particles deposit on the membrane surface and on top of the deposited particles (Fig. 2.3 D).

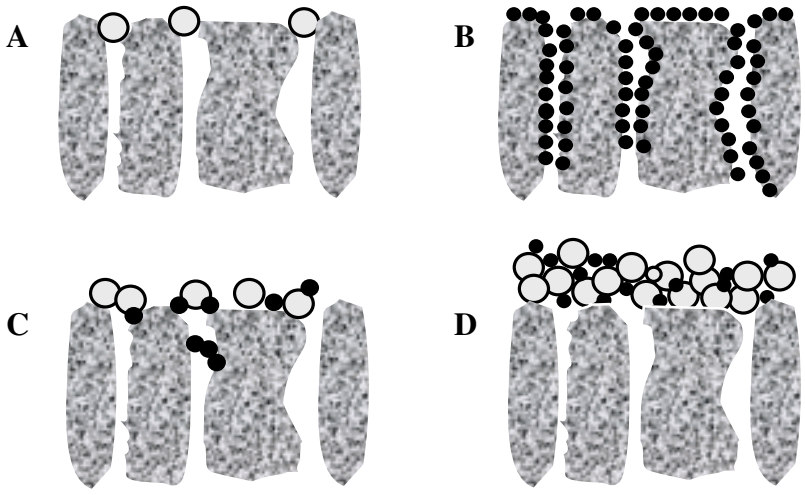

Fig. 2.3: Schematics of membrane fouling mechanisms: (A) pore blockage, (B) pore constriction, (C) intermediate blockage and (D) cake filtration.

Blocking laws for both constant pressure and constant flux are summarized in Table 2.1. Also shown are the linearized forms of the models, which are used for data analysis and the identification of fouling mechanisms [1].

Table 2.1: Governing equations for fouling models [1]

Constant pressure	Flow rate	Linearized form
Pore blockage	$\frac{Q}{Q_0} = \exp(-\beta t)$	$\ln(Q) = a\,t + b$
Intermediate blockage	$\frac{Q}{Q_0} = (1+\beta t)^{-1}$	$\frac{1}{Q} = a\,t + b$
Pore constriction	$\frac{Q}{Q_0} = (1+\beta t)^{-2}$	$\frac{t}{V} = aV + b$
Cake filtration	$\frac{Q}{Q_0} = (1+\beta t)^{-1/2}$	$\frac{t}{V} = aV + b$
Constant flux	**Pressure**	**Linearized form**
Pore blockage	$\frac{P}{P_0} = (1-\beta t)^{-1/2}$	$\frac{1}{P^2} = a - bV$
Intermediate blockage	$\frac{P}{P_0} = (1-\beta t)^{-1}$	$\frac{1}{P} = a - b\,V$
Pore constriction	$\frac{P}{P_0} = (1-\beta t)^{-2}$	$\frac{1}{P^{1/2}} = a - bV$
Cake filtration	$\frac{P}{P_0} = 1+\beta t$	$P = a + bV$

Because flux and TMP data can not always be described solely by one model, individual models were combined. Combined models were applied to filtrations that did not show consistent data fit for one individual model, but rather a shift from one fouling mechanism to another fouling mechanism [38] or a combination of two fouling mechanisms [39].

Experimental results from the filtration of the enzyme yeast alcohol dehydrogenase (YADH) through a 0.2 µm track-etched polycarbonate membrane suggested that a shift from standard blocking to cake formation occurred upon increasing the YADH concentration from 0.005 to 0.25 g L^{-1} [40]. The flux profiles matched the models for standard blocking and cake formation at low and high concentrations, respectively, and

atomic force microscopy (AFM) indicated pore narrowing at low concentrations and surface deposition at high concentrations.

Tracey and Davis [41] developed models for fouling mechanisms based on internal and external fouling. They monitored the flux decline during BSA filtration through 0.05 and 0.2 µm polycarbonate membranes. By plotting the inverse flux versus filtration time for the experimental data they obtained curves with different slopes. In accordance with the models, concave slopes pointed to internal pore blockage and convex slopes to external (surface) fouling.

2.2.4 Fouling by proteins

Despite the significant size differences between MF membrane pores and proteins, proteins are known foulants of MF membranes. The fouling is much higher than would be the case if simple monolayer adsorption occurred [40] and therefore fouling of MF membranes by proteins has become the focus of many studies. Belfort et al. [16] and Marshall et al. [9] provide extensive reviews on protein fouling.

Palecek and Zydney [42] reported on the fouling of 0.16 µm poly(ether sulfone) MF membranes in a stirred cell by a number of proteins including bovine serum albumin (BSA), immunoglobulin G (IgG), haemoglobin, ribonuclease A, and lysozyme. In each case, the permeate flux rapidly decreased by more than one order of magnitude and the quasi steady state flux after 3 h of filtration was two orders of magnitude lower compared to the initial flux in the case of ribonuclease A, IgG, and haemoglobin. The flux decline during stirred cell MF of BSA, ovalbumin, lysozyme, pepsin and β-lactoglobulin through 0.22 µm PVDF membranes was analyzed by Kelly and Zydney [43]. The authors linked the deposition of native proteins to the presence of free thiol groups in the proteins and associated thiol-disulfide interchange reactions. Fouling of MF membranes by proteins is also observed in the dairy industry during processing of whey or milk [35]. For example, ceramic membranes with a mean pore diameter around 0.8 µm were fouled by whey protein isolate solutions [35]. Due to the production process of the whey protein isolates, some of the protein was present as aggregates having an apparent size around 500 nm. The authors

suggested that aggregates blocked the membrane pores which increased the total membrane resistance.

Aggregates were suggested and identified as membrane foulants in diverse protein solutions [32;44-46]. For example, fouling was considerably reduced by removing aggregates from the feed solution by prefiltration using a smaller pore size membrane [44] or arranging membranes in series [46]. Aggregation is described as the assembly of proteins in non-native, partially unfolded configuration that is often irreversible. The mechanisms by which proteins aggregate depend on the protein itself and are affected by protein concentration and other solution conditions [47]. However, at least two steps are thought to occur. The initial step involves changes to the conformation of the native protein including partial unfolding [48]. This is followed by nucleation and the arrangement of protein molecules into growing aggregates. Solution conditions affecting the stability of the native protein include solution pH, type and concentration of electrolytes and temperature. Membrane fouling studies should therefore consider the effect of solution conditions.

Extensive studies on the fouling mechanism for proteins and protein aggregates were performed for the model protein BSA, which is discussed in more detail in section 2.2.6.

2.2.5 Effect of protein solution characteristics

2.2.5.1 Solution pH and ionic strength

Both solution pH and ionic strength influence the properties of proteins and other feed components and consequently their filtration.

The net charge of proteins is zero at their isoelectric point (IEP), which means electrostatic interactions between proteins are at their lowest and hydrophobic interactions play an increased role. Hydrophobic interactions can lead to protein aggregation and subsequently to increased protein-membrane interaction and membrane fouling [32]. In addition, proteins are most compact at their IEP and when forming a fouling layer, can pack more closely together due to the reduced electrostatic repulsion [9;49]. Both effects, compact form and packing density, lead to a denser fouling layer with increased hydraulic resistance. At a pH far from the IEP of the proteins, proteins have a high charge. This charge is negative at a pH above the IEP and positive at a pH below the IEP. For example,

the IEP of BSA is 4.7 and BSA is negatively charged at a neutral pH of 7. Palecek and Zydney [49] studied the fouling layer permeability for different proteins, including BSA, that formed on 0.16 µm PES membranes in a stirred cell system. The permeate flux of a filtration at a pH of 7.4 was higher compared to the filtration at a lower pH (closer to the IEP). This was attributed to the above mentioned difference in fouling layer deposit with higher repulsive forces leading to more permeable fouling layers.

Increasing ionic strength can have a similar effect in that it, too, decreases the electrical double layer of the proteins and their packing distance in fouling layers [13]. The combined effect of pH and ionic strength on the filtration of BSA solutions was studied by Palecek et al. [50]. The authors found that there was no difference in the permeate flux with different solution ionic strength when the filtration was operated at a pH equal to the IEP of BSA. The authors concluded that the permeability of the BSA deposit formed at the pH of zero net charge was not affected by the ionic strength of the filtered solution. Chan and Chen [32] found that the TMP increase during cross-flow filtration of BSA at pH 9 (above the IEP of BSA) was lowest in the absence of salt. Both membrane and BSA were negatively charged under these conditions and the resulting electrostatic repulsion was proposed to be the likely cause of the reduced membrane fouling observed.

2.2.5.2 Feed concentration

Membrane fouling usually increases with increased feed concentration [9;13]. However, it was also observed that different fouling mechanisms may exist at low and high feed concentrations. Kwon et al. [24] and Tarleton and Wakeman [33] suggested pore bridging in the case of high particle concentrations as the particles compete for the entrance into the pores. At low concentrations, the particles enter and plug the pores more easily, resulting in higher fouling rates compared to high particle concentrations. Bowen and Hall [40] analyzed the flux decrease during the filtration of the enzyme yeast alcohol dehydrogenase through 0.2 µm track-etched polycarbonate membranes. The authors suggested in-pore blocking at low enzyme concentration and surface deposition at high enzyme concentrations. Atomic force microscopy showed pore narrowing at low enzyme concentrations, supporting the in-pore blocking model.

2.2.6 Fouling by protein: The case of BSA

BSA is a known foulant of MF membranes and has been studied by many in respect to membrane fouling [9;16;29]. This is largely due to its availability, low costs [43] and well known characteristics [28]. Some characteristics of BSA are summarized in Table 2.2.

Table 2.2: Characteristics of bovine serum albumin (BSA)

Property		Reference
Hydrodynamic radius	8 nm (measured by DLS)	[51]
Dimensions	40 Å x 140 Å	[44]
	11.6 x 2.7 x 2.7 nm (plasma albumin)	[28]
Molecular weight	67 kDa	[28]
Isoelectric point (IEP)	4.7 - 4.9; 4.6	[28;52]
Monolayer adsorption	~ 60 Å (thickness)	[44]

The biological function of BSA is the binding and transportation of blood components. It is known to bind to fatty acids, tryptophan, bilirubin, metal ions, hormones and long chain alcohols [53].

The adsorption of BSA to membrane surfaces was studied for a variety of materials, including track-etched polycarbonate [41], cellulose [54], aluminium oxide [29], PVDF, polysulfone and nylon [55]. Information on BSA aggregation and denaturation are also available [48;56;57] and have been used to explain fouling phenomena. Solution conditions such as pH, protein concentration, salt concentration and temperature affect the conformation of the protein molecule. If a change from the native state occurs, free SH-groups and hydrophobic regions could be exposed to the outside of the protein. BSA aggregates can then form through the formation of disulfide bonds and other intermolecular interactions [48;56].

Membrane fouling by BSA has been linked to the presence of large protein aggregates [44] and the authors suggested a two-stage mechanism. At first, the large BSA aggregates deposit on the membrane surface and pore blocking occurs. Next, native BSA molecules interact with the deposits and add to the deposit. Removal of the large aggregates by prefiltration of the BSA solutions through ultrafiltration membranes reduced the fouling rate considerably and the fouling rate increased with increasing concentration of aggregates. A slower surface blocking step upon removal of BSA aggregates by

prefiltration was also observed by Jonsson et al. [10]. Chan and Chen [32] used electron microscopy to observe membrane surface changes during the cross-flow filtration of BSA solutions through 0.2 µm track-etched polycarbonate membranes at constant permeate flux. They matched those changes with changes in the TMP and found that the TMP increased once large protein aggregates started to deposit on the surface. Pore narrowing was not observed at that time and it was concluded that aggregate deposition was the initial fouling mechanism. With increasing filtration time, more aggregates deposited and in addition, pore narrowing and cake formation were visible.

Kelly and Zydney [57] could show that the interaction between native proteins and protein deposits as well as protein aggregation was linked to a free thiol group in the BSA molecule. They, too, verified the two-stage fouling mechanism by prefiltering the BSA solutions and observed reduced fouling with prefiltered BSA solutions compared to unfiltered BSA solutions. Blocking the free thiol group prevented aggregation and protein-deposit interactions such that fouling was completely eliminated for prefiltered solutions. Kelly and Zydney [43] extended this study to include other proteins with free thiol group(s). Both ovalbumin and β-lactoglobulin showed fouling characteristics very similar to BSA with increased fouling rates at the beginning of the filtration. Very similar were also the fouling characteristics for filtrations of BSA through a 0.16 µm poly(ether sulfone) membrane and a 0.2 µm polytetrafluoroethylene (PTFE) membrane [42], indicating that membrane material and pore size are not always affecting the extent and mechanism of fouling. The quasi steady-state flux after 3 h of filtration through the 0.16 µm membrane was even very similar to a 30 kDa (ultrafiltration membrane cut-off) and a 100 kDa membrane of the same material.

2.2.7 Effect of filtration conditions

2.2.7.1 Membrane pore size

All three cases, improved, unchanged and declined filtration performance were reported for increasing membrane pore size [13;58]. It seemed that not the pore size in general will determine the filtration performance, but rather the difference between pore size and particle size [33;59]. Tarleton and Wakeman [59] showed that the difference in

size between the membrane pores and the particles in the feed solution had a significant effect on the filtration performance and the predominant fouling mechanism (see section 2.2.3) during cross-flow MF of powders and yeast cells. Cake formation occurred when feed particles were larger than the membrane pores and the cake had a higher resistance to the permeate flow than the actual membrane. Particles that were in size close to or smaller than the pores entered and clogged the membrane pores. In the latter case, internal fouling occurred which was more difficult to remove than surface fouling [59]. Experiments with 0.816 µm latex particles showed that the TMP increase with filtration time at high permeate flux was significantly higher for membranes with 0.65 µm pore size than for 0.1 µm pores. This was attributed to a more efficient clogging of the larger pores [24]. Marshall et al. [60] observed very similar fouling patterns with a 0.1 µm ceramic membrane compared to a 0.05 µm membrane upon filtration of β-lactoglobulin. Because the fouling resistance of the 0.1 µm membrane increased to the same resistance level as the 0.05 µm membrane with a short delay in time, the authors suggested that the same fouling mechanism was responsible for fouling of both membranes. It was proposed that fouling occurred at the pore entrance and that the larger initial pore size of the 0.1 µm membrane lead to the delay in fouling with time.

2.2.7.2 Cross-flow velocity

High CFV not only affects filtration performance indirectly by shear damage to cells (see section 2.1.4), but directly due to particle deposition effects. Generally it is expected that higher CFV reduces membrane fouling because of increased back-transport mechanisms (inertial lift and shear-induced transport). In accordance with this theory, Todisco et al. [58] observed that increasing the CFV during MF of orange juice reduced cake formation and Choi et al. [34] reported increasing permeate fluxes in proportion to increases in CFV during MF of activated sludge. However, adverse effects were also reported. For example, the severity of fouling of a yeast cell broth increased with increasing cross-flow velocity [61]. This was due to the effect of the yeast cells. At lower CFVs, yeast cells were deposited together with other broth particulates, forming a cake of medium density. Yeast cells no longer deposited at higher CFV and the cake formed had a higher density and therefore higher flux resistance. Similarly, the size of the deposited particles in

the cake layer decreased with increasing CFV during the filtration of a quartz powder suspension [27], calcium carbonate slurries [59], yeast and latex particles [23] .

2.2.7.3 Permeate flux

The transport rate of feed components to the membrane is balanced by the permeate flux and the rate of back-transport. Operation at constant permeate flux allows for easy operation at low filtration fluxes that significantly reduce or even prevent particle deposition and/or membrane fouling. A constant TMP was maintained upon reducing the constant permeate flux by half during the MF of mouse hybridoma cell suspensions with a 0.2 µm polypropylene hollow fiber membrane [19]. Similar effects were seen for the filtration of mammalian cells using 0.65 µm PVDF flat-plate filters [14]. While the TMP increased rapidly at 100 Lmh, the TMP increase was minimal at 50 Lmh. Foley et al. [62] reported an increase in protein deposition with increasing permeate flux through 0.45 µm flat-sheet membranes.

The disadvantage of low constant permeate flux is the longer process time to filter the same volume. However, better control of filtration and the option to operate the filtration unit for longer periods of time without the need for membrane cleaning are advantageous.

2.2.8 Analysis of foulants

A number of different analytical techniques have been used in the literature to characterize membranes, fouling of membranes and particles involved in membrane fouling. Dynamic light scattering can determine the apparent size of the particles. It is important to know the size of particles in order to identify the transport mechanism affecting the deposition of particles. Another method to derive information about particle size, protein size in particular, is gel electrophoresis where particles are separated according to their mobility in polyacrylamide gels. Scanning electron microscopy is used to characterize membrane surfaces, both clean and fouled. These methods will be described in the next sections.

2.2.8.1 Dynamic light scattering

Dynamic light scattering (DLS), also known as photon correlation spectroscopy (PCS), can be used to determine the diffusion coefficient of particles in solution. Applying the Stokes-Einstein equation [63], the hydrodynamic radius of these particles can be calculated from the diffusion coefficient:

$$R_h = \frac{k\ T}{6\pi\eta D}, \tag{2.8}$$

where k is the Boltzman constant (k = 1.38 x 10^{-23} J K^{-1}), T is temperature (K), η is the solvent dynamic viscosity (Pa s) and D the diffusion coefficient (m^2 s^{-1}). The hydrodynamic radius is based on the shape of a sphere which would have the same average diffusion coefficient in solution as the particle. In the DLS analysis, a laser supplies the light source that is focussed on the liquid sample. Particles in the solution scatter the light which is measured by a detector as light scattering intensity. In some instruments, the detector is located at an angle that captures the backscatter, which reduces interferences from contaminants and multiple scattering effects. The signal from the detector is processed digitally and the light scattering intensity pattern compared at specific time intervals. Changes in the light intensity pattern are correlated to the size of the scattering particles. Smaller particles in solution move faster than larger particles and the scattering intensity pattern will change faster [64]. A correlation function is used to correlate the scatter pattern at specific time intervals to the initial scatter pattern. For a solution with small particles, the correlation coefficient will quickly decrease from 1 to almost zero. For larger particles, this decrease will be much slower. Particle size distributions are derived from the correlation function by applying algorithms [64]. Depending on the instrument and configuration, size measurements in the range of a few nanometers to several micrometers are possible. The advantages of this technique are the use of small sample volumes and liquid samples.

The larger the particle, the more light is scattered by this particle. That means even small amounts of protein aggregates can be detected in protein solutions. Several studies have used DLS to characterize BSA [32;51;52]. Ho and Zydney [51] observed two peaks in the DLS analysis of 2 g L^{-1} BSA solutions. The first peak occurred around 8 nm and the second around 360 nm, corresponding to the monomeric BSA and aggregated BSA,

respectively. DLS was also used to determine the weight fraction of the protein aggregates in the solution. Girones et al. [52] compared BSA solutions (10 g L^{-1}) at pH 4.5 and 7, the former being close to the IEP of BSA. At the IEP, larger aggregates were present and the average size of BSA was around 12 nm due to the presence of larger particles. The size of BSA at pH 7 was 9.9 nm.

2.2.8.2 SDS-PAGE and native PAGE

Sodium dodecyl sulphate (SDS)-PAGE can be used to determine the apparent size of polypeptides in solution. Solution samples are mixed with a sample buffer that contains SDS. SDS binds to the polypeptides, giving them a negative charge. The samples are loaded onto a polyacrylamide gel and an electric current is applied. The negatively charged SDS-polypeptide complexes migrate through the gel toward the anode at different speed according to the size of the complex. The migration distance at the end of the run is thus a function of their size and can be compared to standard polypeptides with known size run in the same gel. Unlike SDS-PAGE, native PAGE separates the proteins in their native state and can be used to detect protein aggregates in samples. The migration of proteins or protein aggregates through the gel is a function of their size as well as charge. The detection limit using native PAGE is relatively low and it can be difficult to observe aggregates when their fraction is small compared to the overcall protein concentration. In addition, a more open gel structure is required to allow for the migration of large aggregates into the gel. An open gel structure makes the gel less robust and more difficult to handle.

2.2.8.3 Scanning electron microscopy

A classical and well used method to characterize membrane surfaces and fouling layers is scanning electron microscopy (SEM) [4;33]. It collects data on the surface topology from secondary electron emission (the incident electrons being the primary electrons).

For example, the surface of clean membranes made from different materials were compared by SEM [51] and analyzed for porosity and pore morphology. The clean membrane surfaces were also compared to the surfaces after filtration of BSA solutions. This allowed for identification of BSA aggregates covering the pores and size estimates in comparison to the membrane pores. Similarly, SEM was used by Girones et al. [52] to

characterize microsieve membranes fouled by BSA solutions prefiltered through 5 µm membranes. The authors observed aggregates that had not been removed by the prefiltration and that partially or completely blocked pores. These aggregates were identified as the source for the membrane fouling.

Ohmori et al. [65] were able to distinguish between cake layers of bacterial cells that had formed at pH 2 and pH 5 filtrations. Using a magnification of 3000X, the cross-section of the cake layer at pH 2 showed cell aggregation and flow paths between the cell aggregates. The flow paths seemed to explain the higher permeate fluxes seen at the lower pH compared to pH 5.

2.2.9 Methods to reduce membrane fouling

If fouling occurs during a filtration process, permeate fluxes are lower and more membrane area or higher pumping cost are required to increase filtration rates. A cost effective process will therefore require strategies to reduce the extent of fouling. Approaches to reduce or prevent membrane fouling include the use of suitable filtration conditions and the reduction of particle-membrane interactions. Filtration conditions that can reduce the formation of fouling layers can involve the increased motion of the particles away from the membrane surface. This could be achieved by higher cross-flow velocity, although the positive effect is not seen in all systems (see section 2.2.7). Changes in the hydrodynamics of the flow aimed at reducing particle deposition can also be achieved with Dean vortexes, Taylor vortexes, and helical baffles [22;66]. The filtration processes can furthermore include frequent backpulsing or backflushing, where the flow of the permeate is reversed to open up the blocked pores [52;67].

Approaches to reduce particle-membrane interactions include permanent chemical modification of the membrane surface to increase the hydrophilicity of the membranes and the pre-treatment of the membrane with a surfactant. Both techniques aim at the reduction of hydrophobic interactions between the feed components and the membrane surface.

The possibility of reducing membrane fouling, caused by a model antifoam (polyoxyethylene polyoxypropylene oleyl ether), by precoating the membrane with non-ionic surfactants was investigated by Yamagiwa et al. [68]. They immersed 50 kDa

polysulfone membranes in solutions of different surfactants, rinsed the membrane and used them in ultrafiltration experiments with the model antifoam. Depending on the type of surfactant, the permeate flux during the filtration of the model antifoam through the treated membrane was increased up to three times compared to the filtration through the untreated membrane. Similar results were obtained for the filtration of different model streams including yeast extract. The flux during the filtration of yeast extract improved when the membrane was precoated with a surfactant. The improvement in permeate flux upon precoating was even better when the feed solution was a mixture of the yeast extract and the previously tested model antifoam. The benefit of precoating a membrane with surfactant prior to filtration was also shown for BSA ultrafiltration [69]. A 30 kDa polysulfone membrane was treated with a non-ionic surfactant. In comparison to the untreated membrane, higher permeate fluxes, lower protein deposition and easier membrane cleaning were observed.

2.3 Mammalian cell harvest

A number of protein pharmaceuticals are produced in mammalian cell cultures. Examples include recombinant human tissue-type plasminogen activator (tPA) [5], prothrombin [70] and monoclonal antibodies [71]. Beside the protein product and the cells, the culture broth contains for example cell debris, host cell proteins, DNA, and lipids [1]. Extensive downstream processing is required to obtain the protein product in purified form. The first step in downstream processing is the separation of the cells and cell debris from the product stream. Cells and cell debris could otherwise interfere with the subsequent downstream processing steps such as chromatography.

2.3.1 Mammalian cell cultures

Protein pharmaceuticals are preferably synthesized in mammalian cell cultures because the cells are capable of (i) proper protein folding, (ii) post-translational modifications such as glycosylation essential for the functionality of the proteins and (iii) secretion of the protein product into the suspension [6;72]. High levels of protein product concentrations

can be reached, up to several grams per litre [1;72]. Furthermore, culture techniques have been developed that allow for production on a large scale [6]. The percentage of recombinant protein pharmaceuticals produced in mammalian cells was estimated at 60 – 70 % in 2004 [72]

The mammalian cells are grown in suspensions containing nutrients and growth factors required for cell growth and protein production [6]. Growth media have been developed to optimize cell growth and recombinant protein production for specific cell lines. The media composition can be minimal or complex. Serum-free medium refers to defined medium which is usually chosen for large-scale cell cultures producing protein pharmaceuticals. Serum-containing media on the other hand are undefined. Serum is a complex mixture of plasma proteins, hormones, growth and other factors and is used as supplement in fermentation media to enhance and stabilize cell growth [6]. Serum is usually obtained from fetal or newborn bovines and varies in its exact composition [8]. The major protein component in bovine serum is bovine serum albumin (BSA). Disadvantages of using serum-containing media include batch-to-batch variation, the potential interference with the downstream purification of the target protein [6] and the risk of contamination with viruses or prions (e.g. prions causing bovine spongiform encephalitis (BSE)) [73].

Chinese hamster ovary (CHO) cells is one type of cell line widely used for recombinant protein production [6;7]. Originally derived from epithelial cells of an adult Chinese hamster in 1957, the cells have since been well characterized. The cells can be grown in suspension and the metabolism has been studied extensively. An example of large-scale production employing CHO cells is the production of tissue plasminogen activator (t-PA) originally developed by Genentech [6] and the production of monoclonal antibodies (Herceptin) for the treatment of metastatic breast cancer [74].

2.3.2 Mammalian cell harvest by microfiltration

Microfiltration is employed for mammalian cell harvest as it separates by size and the size difference between the protein product and the cells is significant. The size of mammalian cells is around 10 µm with a density close to that of aqueous suspensions [13;75]. Proteins are about 3 orders of magnitude smaller [16]. Other components that can

be found in cell culture broth include salts, carbohydrates, vitamins, hormones and peptides as these are components of cell culture media. In addition, the cell cycle produces cell debris and metabolites of different sizes, further increasing the particle size distribution of the cell culture broth [19]. Table 2.3 gives typical size characteristics of broth components for CHO cell cultures.

Table 2.3: Typical size of components found in cell culture broth

Component	Size (µm)	Reference
Chloride ion	9.9×10^{-5}	[76]
Glucose	8.6×10^{-4}	[76]
Vitamin B-12	2×10^{-3}	[77]
Bovine serum albumin	8×10^{-3}	[51]
Mammalian cell in culture	2-10	[76]
Chinese hamster ovary (CHO) cell debris	≤ 5	[70;78]
Dead CHO cell	5-8	[78]
CHO cell	10-15	[70]
CHO cell aggregate	> 15	[70]

Compared to bacterial cells, mammalian cells are more fragile and susceptible to hydrodynamic and/or interfacial stress which is even more pronounced when the cells are grown in serum-free medium [14]. Microfiltration is a suitable technique to separate cells from cell culture broth at gentle conditions that avoid cell damage and further contamination of the protein product [5;19].

2.3.3 Microfiltration membrane fouling by complex biological solutions

Fermentation or culture broths contain a wide variety of components and have a large particle size distribution. The filtration of fermentation or culture broth is challenging and can not easily be predicted from studies performed on individual components as the interaction between different components will play a significant role [25]. During the filtration of complex solutions, the fouling of one feed component could trigger the subsequent fouling by other components. A two phase TMP increase was observed during constant flux filtration of anaerobic wastewater from a bioreactor with a 0.22 µm flat sheet polyvinylidene fluoride (PVDF) membrane [79]. A slow gradual TMP increase was

followed by a phase of rapid TMP increase. The feed solution was heterogeneous and contained bacteria, colloids and dissolved macrosolutes including extracellular polymeric substances (EPS). Gradual deposition of EPS fouled the membrane slowly and the TMP increased gradually. The membrane area available for filtration (membrane capacity) decreased while local fluxes increased (constant flux operation). This caused a more rapid deposition of other feed components that accounted for the second phase of the fouling process. Similar observations of two-phase TMP increases were made by Ognier et al. [80] during the filtration of a bioreactor effluent with a 0.05 µm alumina multi-tube membrane. An interaction effect between different solution components was observed by Hughes and Field [81]. The authors compared the TMP increase during MF of unwashed yeast suspension, washed yeast suspension (EPS removed) and EPS. Using a 0.1 µm membrane, the TMP increase for the washed yeast suspension was about for times higher compared to the TMP increase seen for EPS. In the case of a 0.2 µm membrane, the TMP increase was similar for washed yeast suspension and EPS. However, for both membranes, the TMP increase for the unwashed yeast suspension was higher than the sum of the TMP increases observed for the washed yeast and EPS suspensions. The authors hypothesized that EPS was clogging the space between the yeast cells that fouled the membrane resulting in the formation of a cake with greater resistance to flow (over-clogging). Krstic et al. [2] found that the soluble components of a fungal fermentation broth after removal of the biomass caused more fouling than the biomass-containing broth. Furthermore, a higher percentage of the fouling was irreversible leading to the conclusion that more internal membrane fouling had occurred.

Fermentation conditions can also affect the downstream processing and make the filtration process even more challenging. Taddei et al. [82] reported on the MF of cider yeast broth using a 0.22 µm PVDF membrane. Permeate fluxes were lower when the fermentation was operated at higher aeration rates compared to the permeate fluxes for fermentations at low aeration. The authors suggested that a change in the composition of the yeast cell membrane had occurred due to the changes in the fermentation conditions and the availability of oxygen. These changes in the cell membrane were thought to affect the cell-membrane interactions.

When dealing with fermentation or culture broth, the effect of pH or ionic strength on filtration performance becomes more complex. Different proteins in the same broth can have opposite charges at a specific pH which can increase attraction forces between proteins as well as the hydraulic resistance of the deposit layer. The adsorption of proteins to cells and cell debris is also dependent on the solution environment and can lead to retention of the proteins along with the cells and cell debris. In a study of MF of bacterial cells [65], cell-cell interactions in the absence of proteins were found to be dependent on the pH of the solution. Decreasing the pH from 6.3 to 2 increased the permeability of the cell cake considerably. Measurements of the zeta potential and the cell hydrophobicity showed that the cells were more hydrophobic and less charged at the low pH. At the same time, scanning electron microscopy revealed cell aggregates and the presence of macropores at low pH that were absent at the higher pH. It was concluded that the higher cell-cell interaction at low pH (hydrophobic, low charge, cell aggregates) was responsible for the non-uniform cell cake with open flow paths that had a lower hydraulic resistance and therefore a higher permeate flux. The effect of cell aggregation (improved permeate flux) was thus opposite to that of protein aggregation (decreased permeate flux) discussed above.

Beside the standard medium components, fermentation additives can interfere with the downstream processing. For example, antifoams are known to foul membranes [83;84] and can affect the filtration performance more than other medium components [25]. Permeate fluxes during cross-flow filtration of *E. coli* suspensions using 0.2 µm polypropylene tubular membranes were lower when the antifoam polypropylene (PPG) was added to the fermentation medium [59]. This was observed when the cells were grown both in minimal or complex medium. A difference between the performance of minimal and complex medium was only observed in the absence of antifoam PPG, with the minimal medium having a slightly higher permeate flux.

The filtration conditions will affect individual components differently. For example, depending on the hydrodynamics of the system, individual components may or may not deposit and contribute to the formation of a fouling layer [85]. If a higher percentage of large particles deposits, it can be assumed that the fouling layer formed by the larger

particles has a higher permeability compared to a fouling layer formed by predominantly small particles.

Filtration conditions need to be adapted to the individual biological mixtures with respect to individual components. For example, in the presence of cells, conditions should be avoided that cause destruction of cells. If the cell content is leaking, contamination of the broth with nucleic acids, lipids and additional proteins can occur. These cell components can interfere with the downstream processing [5;19].

Membrane fouling by proteins, mixtures and complex solutions is highly dependent on the filtration conditions, including hydrodynamic conditions, solution properties and membrane characteristics [86], as discussed in part in section 2.2.5 and 2.2.7.

2.4 Experimental filtration conditions

Experimental conditions used in this Ph.D. thesis were selected according to conditions described in the literature for industrial scale cell harvest applications. Van Reis et al. [5] employed a hollow fiber system with 180 m^2 of membrane area to harvest CHO cells grown in serum-free cell culture media. The system was operated at a feed rate of 3.3 x 10^4 L h^{-1} which corresponded to a wall shear rate of 4000 s^{-1}. Maiorella et al. [14] recommended a shear limit of 3000 s^{-1} for mammalian cells below which cell damage due to shear is avoided. However, van Reis et al. [5] observed minimal loss in cell viability at the employed shear rate of 4000 s^{-1}. The cell harvest was operated at a constant permeate flux of 4800 L h^{-1} (27 Lmh). Under these conditions, a 15-fold concentration of cells was achieved while the TMP did not increase significantly. The product yield (in this case tissue plasminogen activator, t-PA) was above 99%. Prior to the actual industrial scale trials, a pilot scale system was used to optimize filtration performance. The scale-up to the industrial scale was relatively simple as channel length, wall shear rate, and flux were kept constant by simply adding more hollow fiber modules in parallel.

Common experimental condition chosen for this thesis were as follows unless stated otherwise.

- The permeate flux was kept constant at 30 Lmh.
- The cross-flow velocity was either 0.5 or 1 m s^{-1}, corresponding to wall shear rates of 4000 and 8000 s^{-1}, respectively. The low shear rate was chosen in consideration of some cell-containing culture broth, the high shear for cell-free systems. The flow regime at both CFVs was laminar (Re < 2000). Both constant permeate and cross-flow are applicable in industrial filtrations [87].
- The membrane pore size in most filtration experiments was 0.45 µm which will retain mammalian cells and cell debris. The achieved clarification of the broth is a requirement if subsequent downstream processing were to be performed. In some cases, a membrane with 0.2 µm pore size was used to compare filtration performance for a membrane with higher intrinsic resistance and sterilisation properties. A pore size of 0.2 µm is generally considered suitable for sterilizing liquids.
- The membrane material of the filtration cartridges was polysulfone. Polysulfone itself is hydrophobic. However the membrane was surface treated by the manufacturer to make it more hydrophilic and suitable for protein purifications.
- The optimum pH for cell cultures is usually between 6.9 and 7.4 [7] and is often maintained by bicarbonate-CO_2 buffer systems. Buffer solutions used in this thesis for BSA filtration experiments had a pH of around 7.
- BSA was chosen as a model protein because it is well characterized and fouling mechanisms described in the literature were developed specifically for BSA fouling. BSA is also a major protein component of serum, a medium additive for mammalian cell cultures [8]

3

A Model For Cross-flow Microfiltration of Biological Solutions at Constant Permeate Flux*

Membrane fouling by cell culture broth is complex with the accumulation of cells and other large particles on the membrane surface and the deposition and adsorption of small particles or macromolecules at the pore entrance or within the internal pore structure of the membrane. We have developed a new model to represent the fouling expressed as transmembrane pressure change for cross-flow microfiltration operated at constant permeate flux. Fouling is assumed to occur first by pore blockage with subsequent cake formation over the blocked areas of the membrane. The contribution of the cross-flow action is represented through the removal of aggregates from the membrane surface and the corresponding increase of open pore area and the decrease of the mass of aggregates deposit. The model fits show excellent agreement with experimental data for BSA solutions and CHO cell culture broth. The model fits indicate the formation of a more pronounced cake and a more significant decrease of open pore area for increasing BSA concentration. In the case of the CHO cell culture broth, the formation of a less pronounced cake but a more pronounced decrease of open pore area is predicted when operating at a higher shear rate.

* Adapted from Stressmann M., Marcos B., Moresoli C., submitted

3.1 Introduction

Membrane microfiltration is commonly used for the recovery of proteins from cell culture broth for which high protein transmission and short filtration times are desired. Unfortunately, membrane fouling affects the filtration performance. Fouling by cell culture broth can be caused by the accumulation of cells and other large particles on the surface of the membrane (external fouling) or the deposition and adsorption of small particles or macromolecules at the pore entrance or within the internal pore structure of the membrane (internal fouling). Higher fouling is often observed when microfiltration is operated at constant transmembrane pressure (TMP) in contrast to operation at constant permeate flux where a more uniform environment is maintained near the membrane. This reduces the high initial fouling often observed for constant TMP operation [88].

One would expect that since proteins and other small molecules are usually much smaller than the pore size of microfiltration membranes, these molecules should easily pass through the pores of the membrane. But many studies have associated proteins with significant membrane fouling. The deposition of protein aggregates on or in the membrane pores is believed to be an important factor in microfiltration fouling as described by the studies on BSA aggregates and their role in the fouling mechanisms [41;89].

The formation of a dynamic or a secondary membrane when cells are contained in a protein mixture should also be considered. Güell et al. [45] reported a flux enhancement when a small concentration of yeast cells was present or when yeast cells had formed a cake prior to the filtration of a protein mixture. It was proposed that a secondary layer had formed and would retain protein aggregates that otherwise would have fouled the primary membrane. However, higher yeast cell concentrations may lead to a reduced permeate flux when compared to the protein mixture filtered alone, likely due to cake compression. Hughes and Field [81] investigated the fouling and the role of the dynamic layer formed by yeast cells in a cone-and-plate test microfiltration cell operated at constant permeate flux. They observed a higher TMP rise for the unwashed yeast cells compared to the sum of the rates of TMP rise for the washed yeast cells and the extra polymeric substances. These

observations support the hypothesis that over-clogging of the cake was occurring, a situation where the interstices of the cake become clogged with the soluble components.

Shear conditions may also be of importance, particularly for the clarification of mammalian cells. For example, Chinese Hamster Ovary (CHO) cells are known to be susceptible to rupture when exposed to shear stress due to the lack of a rigid cell wall for protection. Typically, filtration of mixtures containing animal cells at wall shear rates as low as 3000 s^{-1} is recommended [14]. Vickroy et al. [90] assessed shear damage to CHO cells by passing suspended CHO cells through capillaries. Cell death increased with increasing shear stress as well as time of exposure.

Most membrane fouling modeling studies have concentrated on dead-end configuration and the application of the four classical fouling models describing single fouling mechanisms where the flux decline is described using one of the four mechanistic models. Briefly summarized, the fouling mechanisms are complete blocking which assumes that each particle completely plugs one pore on the membrane surface; standard blocking which assumes that small particles deposit on the walls of the pores causing a progressive restriction of the free pore; intermediate blocking which is similar to complete blocking but each particle has the ability to deposit anywhere on the membrane surface including on other deposited particles; and cake filtration where particles accumulate on the surface of the membrane in a permeable cake of increasing thickness that contributes to the resistance to the permeate flow. These models are characterized by differential equations and a limited number of global parameters estimated by the fitting of experimental filtration data. This approach may avoid the need for the characterization of the feed solution (concentration, aggregate size) but requires some initial conditions (J_0, A_0); which restricts their use to the system under investigation.

Relatively few modeling studies for constant permeate flux operation, cross-flow configuration and complex biological feeds are reported in the literature. Hlavacek and Bouchet [37] developed constant permeate flux blocking laws that were used to analyze constant permeate flux microfiltration of BSA solution for a dead-end system with 0.2 µm membranes having different porosities. Their analysis indicated that the intermediate blocking law provided the best fit for the TMP data. It was subsequently used to quantify the effect of pH and ionic strength by the estimation of the clogging coefficient,

a characteristic parameter of the feed solution. Recent work considered the complexity of biological feeds that contain cells and soluble components as for cell clarification applications. In these situations, the description of the fouling necessitates multiple mechanisms to provide an adequate representation of the filtration process. Bolton et al [39] developed new models that combine the four classical models to describe the combined effects of the individual fouling mechanisms. Analytical equations for constant pressure or constant flow operation were established and involved two fitted parameters. Validation of the model with Immunoglobulin G solution and a dead-end system showed good fits for the cake-complete and cake-intermediate models for constant permeate flux filtration.

An alternative approach presented in the literature for model development, is to divide the total permeate flux and the total membrane area into two domains, an open region and a blocked region. In this context, Ho and Zydney [91] proposed a model for constant pressure cross-flow filtration to describe the dynamics of the available number of (open) pores by assuming that the rate equation of the number of available pore is proportional to the number of available pores. Ho and Zydney represented fouling with an initial pore blockage and a subsequent cake layer growth. The model was applied to dead-end systems, initially to filtration operated at constant TMP [91] and later adapted to constant permeate flux operation [38]. The model predictions provided a very good representation of the experimental data obtained for BSA solution filtered in a dead-end microfiltration system with track-etched membranes and operated at constant permeate flux. In 2006, Duclos-Orsello et al. [92] modified the model of Ho and Zydney for constant TMP by incorporating internal fouling caused by pore blockage. The model assumes that the mechanisms are sequential where pore constriction occurs first, then internal fouling and subsequently cake formation takes place. The model predictions are in good agreement with experimental data for BSA (with and without prefiltration) and polystyrene microspheres obtained for a dead-end unstirred microfiltration system operated at constant TMP.

The objective of this study was to develop a new model to describe the cross-flow effects during constant permeate flux operation of membrane microfiltration. The model was derived from the combined pore blockage and cake filtration concepts developed by Ho and Zydney for dead-end operation [38]. Our proposed model was validated by

comparing the model fits with experimental pressure profiles for BSA feed solutions and CHO cell culture broth. The effect of shear rate and the contribution of the cells and the soluble components will also be reported.

3.2 Model development

The development of the fouling model for cross-flow operation assumes that the feed/retentate flow (cross flow) is significantly higher than the permeate flow by two orders of magnitude. Pore blocking or coverage and cake formation are considered while the polarization resistance and the adsorption resistance are assumed negligible.

Using the approach presented by Ho and Zydney [38;91], the membrane is assumed to consist of two domains, an open region and a blocked region. For instance, the total membrane area, A_0, consists of the open area, A_{open}, and the blocked area, $A_{blocked}$. The total permeate flow rate, Q_0, is constant and consists of the open permeate flow rate, Q_{open}, and the blocked permeate flow rate, Q_{block}.

$$A_0 = A_{open} + A_{blocked} \tag{3.1}$$

$$Q_0 = Q_{open} + Q_{blocked} \tag{3.2}$$

The open permeate flux and the blocked permeate flux are driven by the same trans-membrane pressure but will flow through different resistances. The open permeate flux flows through the clean membrane with resistance R_m while the blocked permeate flux flows through the cake deposit on the blocked pore and the clean membrane resistance, $Rm + R_p$:

$$\frac{Q_{open}}{A_{open}} = \frac{\Delta P}{\mu R_m}, \tag{3.3}$$

$$\frac{Q_{blocked}}{A_{blocked}} = \frac{\Delta P}{\mu(R_m + R_p)}, \tag{3.4}$$

where μ is the permeate viscosity and ΔP the transmembrane pressure. Combining equations (3.3) and (3.4), the relation between the constant permeate flux, the resistances and the transmembrane pressure has the following form:

$$\Delta P = \mu Q_0 R_m \frac{R_m + R_p}{A_0 R_m + A_{open} R_p}. \tag{3.5}$$

For initial conditions, the transmembrane pressure is given as:

$$\Delta P_0 = \mu Q_0 R_m \frac{R_m + R_{p0}}{A_0 R_m + A_{open,0} R_{p0}}. \tag{3.6}$$

The normalized TMP is obtained using equation (3.5) and (3.6):

$$\frac{\Delta P}{\Delta P_0} = \frac{R_m + R_p}{R_m + R_{p0}} \frac{A_0 R_m + A_{open,0} R_{p0}}{A_0 R_m + A_{open} R_{p0}}. \tag{3.7}$$

The fouling by a multicomponent feed, a solution that contains a wide range of proteins, is considered to begin with the formation of protein aggregates that cover rapidly the surface of the membrane. The protein aggregates block or partially block the entrance of the pores of the membrane depending on the relative size of the pores and the aggregates. The fouling continues after the initial blockage of the pore entrance where protein aggregates deposit on the blocked or partially blocked pores, leading to the formation of a protein cake.

The proposed model for the description of the blocking of the pore entrance uses the open pore area (A_{open}). As the pore is blocked by the aggregates carried to the membrane surface by the convective permeate flux, the decrease of open area is assumed to be proportional to the open convective permeate flux. At the same time, some aggregates can be removed because of the cross-flow action leading to the opening of some blocked pores and a corresponding increase of the open area. The removal of aggregates will lead to an increase of the open area which is assumed to be linearly proportional to the mass of deposited aggregates. The net rate of open area is described as:

$$\frac{dA_{open}}{dt} = -\alpha\, Q_{open} C_b + k_{pb}\, m_p\,, \tag{3.8}$$

where Q_{open} is the permeate flux passing through the open area, C_b is the bulk concentration and m_p is the mass deposit per membrane area. The parameter α is the fraction of convective permeate flux that blocks the pores; the parameter k_{pb} is the fraction of the mass deposit removed from the blocked area. Equation 8 enables the description of the characteristics associated with cross-flow operation at constant permeate flux where the transmembrane pressure reaches a quasi steady state.

The cake resistance consists of the different layers of particles forming the cake. The blocked resistance has an initial value $R_{p,0}$ corresponding to the first layer of particles which deposits instantly. During the filtration, the cake resistance R_p increases with the increase of the mass deposit and the corresponding specific resistance R' such that:

$$R_p = R'\, m_p + R_{p0}\,. \tag{3.9}$$

For a compressible cake, the specific resistance is linked to the transmembrane pressure by the classical relation:

$$R' = k_p\,(\Delta P)^S\,. \tag{3.10}$$

For a cross-flow configuration, there will be limited cake formation. Furthermore, an incompressible cake is assumed since the feed that permeates is very small and with S = 0 Eq. (3.10) is simplified to:

$$R' = k_p \quad . \tag{3.11}$$

Finally, the description of the increase of the aggregate deposit on the membrane surface is assumed to be proportional to the convective permeate flux of the blocked area but is also affected by the cross-flow action that reduces the mass of protein deposit due to shear-induced removal; the decrease is assumed to be linearly proportional to the mass of protein deposit (m_p). The net rate of change of the mass of protein deposit is given as:

$$\frac{d(m_p)}{dt} = \frac{f' Q_{blocked} C_b}{A_{blocked}} - k_c m_p . \tag{3.12}$$

The parameter *f'* is the fraction of aggregates carried by the convective permeate flux that contribute to the fouling by depositing on the cake; the parameter k_c is the fraction of the mass deposit removed from the cake. Equation (3.12) assumes no spatial variation of the cake deposit along the membrane surface.

A similar approach to account for the effect of cross-flow was presented by Foley et al. [62]. Supernatant of active dry yeast solutions was subjected to cross-flow microfiltration through 0.22 µm and 0.45 µm PVDF membranes. The fouling, observed as TMP increase, was assumed to be the net result of deposition and removal of foulant, where foulant removal was the product of a factor and the fouling layer thickness at a given time.

Solving the differential equations (3.8) and (3.12) requires initial conditions for the open area and the mass deposit. The initial open area ($A_{open,o}$) may be set as A_o (clean membrane) or when the solution is circulated prior to the filtration as:

$$A_{open,0} = F\, A_0 , \tag{3.13}$$

with *F* representing the ratio of the available open pore area compared to the initial open pore area and $A_0 = \varepsilon (A)$, with ε the membrane porosity and *A* the total membrane surface area.

The initial mass deposit is set to zero because it is assumed that no cake deposit is present at the beginning of the filtration. The differential equations were numerically integrated by a Runge-Kutta method implemented on excel datasheet.

3.3 Materials and methods

3.3.1 Microfiltration system

A schematic of the experimental setup is shown in Figure 3.1. The QuixStand benchtop system (GE Healthcare) consisting of feed reservoir, peristaltic pump and hollow fiber membrane cartridge was modified to operate at a constant permeate flux and to monitor and record system pressure during the experiments.

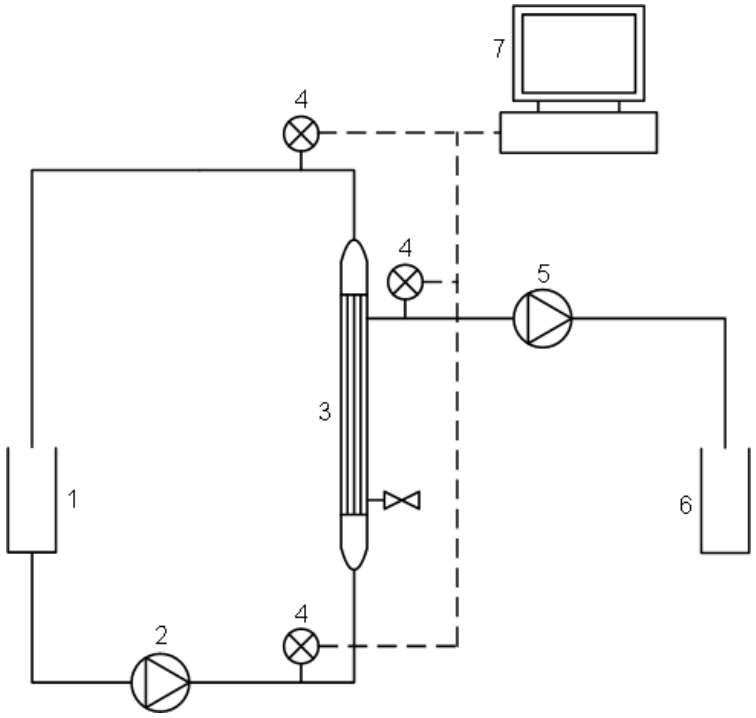

Fig. 3.1: Schematic diagram of the cross-flow hollow fiber microfiltration unit: 1 feed/retentate vessel, 2 peristaltic feed pump, 3 hollow fiber cartridge, 4 pressure transducer, 5 peristaltic permeate pump, 6 permeate vessel, 7 data acquisition system.

A peristaltic pump (Masterflex 7523-30) maintained the permeate flux at constant 30 liter/m^2/hour (Lmh). Two pressure transducers (PX303-100 G5V, Omega) were installed on the feed (P_F) and retentate line (P_R) and one pressure transducer (68075-44, Cole Parmer) on the permeate line (P_P) . All pressure transducers were connected to a data acquisition system consisting of a data acquisition hardware (PMD-1208LS, Measurement Computing) and a software (Labview 6.1 National Instruments). Pressure signals were

collected every second and averaged over 1 minute intervals and subjected to a final filtering step. Transmembrane pressure (TMP) was estimated from the pressure data according to equation (3.14):

$$TMP = \frac{P_F + P_R}{2} - P_P . \tag{3.14}$$

A 0.45 µm pore size hollow fiber microfiltration cartridge (CFP-4-E-3MA, GE Healthcare) with 30 cm fiber length, 13 fibers and 1 mm inner fiber diameter was used.

The feed was circulated continuously through the fiber lumen by a peristaltic feed pump (323E, Watson Marlow). The system was operated at two different inlet liquid shear rates, 4000 and 8000 s^{-1}, by adjusting the feed flow rate according to equation (3.15):

$$\gamma = \frac{4\,Q}{\pi\, r^3}, \tag{3.15}$$

where Q is the feed flow rate ($m^3\ s^{-1}$) and r is the fiber inner radius (m).

Membrane cleaning was performed after each filtration to recover the initial membrane resistance. The cleaning procedure included (1) rinsing with water; (2) circulation of 1 L of an Terg-A-Zyme solution (10 g L^{-1}) for 1 hour; and (3) circulation of a 100 ppm NaOCl solution for one hour; all solutions at 50°C. After cool down, the membrane was rinsed with water and stored in 30% ethanol if not used within 1 week. Success of the cleaning procedure was assessed by comparison of the water flux before filtration and after cleaning. A minimum 95% water flux recovery was reached for all experiments.

3.3.2 Feed solutions

A 2 and 4 g L^{-1} bovine serum albumin (BSA) solution was prepared by dissolving BSA (Sigma, Catalog Number A6793) in 50 mM potassium phosphate buffer pH 7.0. The solutions were prepared fresh for each experiment and used within 2 hours of preparation. Chinese Hamster Ovary (CHO) cell culture broth was provided by Cangene Corp. (Mississauga, Ontario). The cell line used was SGP45-21-3 expressing a soluble glycoprotein. Fermentation of CHO cells was performed in a 2 L fermenter with HyQ-SFX-CHO (HyClone, Logan, UT) serum free media. Half of the culture broth volume

was not centrifuged while the remaining half was centrifuged at 1000 rpm (Beckman Avanti J30-I, JA-10 rotor) for 10 min to remove the CHO cells. The supernatant was recovered and further divided in half with one half used directly for microfiltration (CFf4) and the other half frozen to –18°C (CFfr4). When used for microfiltration, CFfr4 was thawed and warmed to room temperature prior to microfiltration. Both CFfr4 and CFf4 were filtered at the low shear rate (4000 s^{-1}). The cell-containing broth was also divided in half. One half was filtered at the low shear rate, 4000 s^{-1} (CCf4), the other half at the high shear rate, 8000 s^{-1}(CCf8). An overview of the feed properties and filtration conditions is given in Table 1. The total protein content in fresh culture broth was 0.05 g L^{-1} as measured by the Bradford protein assay (standard procedure for microtiter plates, Bio-Rad Laboratories, Mississauga, ON, Canada) using BSA as standard.

Table 3.1: Experimental conditions and CHO cell culture broth properties

		Broth			
Parameter		**CCf4**	**CCf8**	**CFf4**	**CFfr4**
Treatment		fresh	fresh	fresh	frozen
Cell concentration (cells mL^{-1})	Feed	$9.8*10^5$	$1.1*10^6$	-	-
	Retentate	$4.9*10^6$	$5.0*10^6$	-	-
	Permeate	0	0	-	-
Shear rate (s^{-1})		4000	8000	4000	4000
Cell membrane integrity (%)	Feed	76.2	82.7	-	-
	Retentate	75.1	49.8	-	-
	Permeate	-	-	-	-
Solid content (g L^{-1})	Feed	18.1	17.7	17.3	17.3
Ash content (g L^{-1})	Feed	8.4	8.0	7.2	7.2
Organic content (g L^{-1})	Feed	9.8	9.8	10.1	10.1
pH	Feed	6.8	6.7	6.9	6.9

3.3.3 Total solid and ash analysis

The total solid content of the cell culture samples was determined by gravimetric analysis i.e. drying a defined volume of sample at 100^{o}C for 24 hours. After drying, each sample was burned in a furnace at 500^{o}C for at least 8 hours. The difference in weight between the dried sample (total solid) and the burned sample was defined as the organic content of the sample.

3.3.4 Cell concentration and cellular membrane integrity

Cells were counted directly under the microscope using a Petroff-Hausser chamber and trypan blue stain. Both dead cells and ruptured cells were included in the cell count. The relative number of cells with intact cellular membranes was referred to as cell membrane integrity (%).

3.4 Results and discussion

The validation of the cross-flow filtration model was achieved using a single protein solution (bovine serum albumin, (BSA)) and a multi-component solution (Chinese hamster ovary (CHO) cell culture broth with and without cells). Under the chosen conditions, fouling was present as seen by the two phase TMP increase in the pressure profile of BSA (Fig. 3.2) and cell culture broth (Fig. 3.3) filtration. TMP data were normalized by the initial TMP for the individual filtration experiments. The initial TMP was between 0.31 and 0.36 kPa for filtrations at low shear rate (4000 s^{-1}) and around 0.45 kPa for filtrations at high shear rate (8000 s^{-1}).

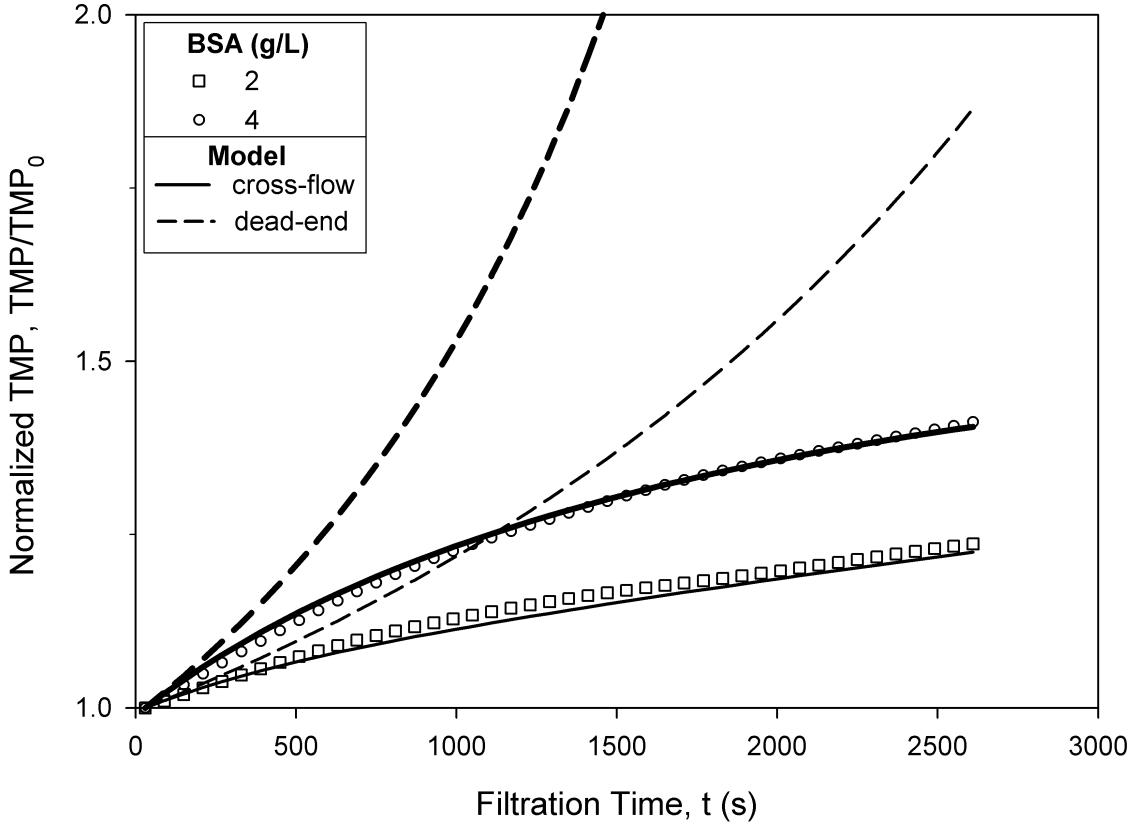

Fig. 3.2: Normalized TMP profiles for BSA solutions through 0.45 μm microfiltration membranes in a hollow fiber system for constant flux operation. Solid curves are model fits according to the best fit parameters for the cross-flow model (Table 3.2). Dashed curves are model simulations according to a dead-end model (k_{pb} = 0, Eq. (3.8) and k_c= 0, Eq. (3.12)) with BSA concentrations of 2 (– –) and 4 (**-- --**) g L^{-1}. Permeate flux is 30 L m^{-2} h^{-1} and shear rate is 8000 s^{-1}.

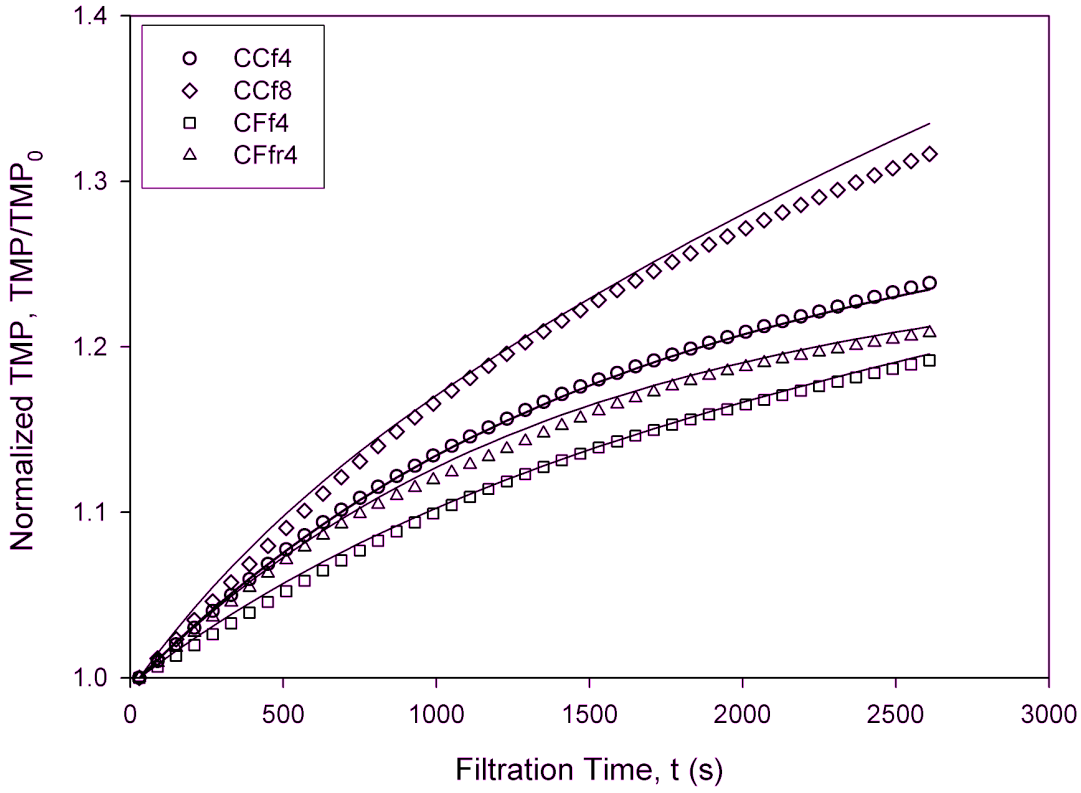

Fig. 3.3: Normalized TMP profiles for CHO cell culture broth solutions through 0.45 µm microfiltration membranes in a hollow fiber system for constant flux operation. Solid curves are model fits according to the best fit parameters for cross-flow model listed in Table 3.2. Permeate flux is 30 L m^{-2} h^{-1}. CHO cell culture broth properties listed in Table 3.1.

Input parameters required to model the TMP profile for the 0.45 µm pores polysulfone membranes, included the membrane surface area (A) of 0.011 cm^2, the membrane resistance (R_m) measured experimentally to be 3 x 10^{10} m^{-1}, the permeate viscosity taken to be that of water at 25 °C (8.9 x 10^{-4} Pa s) and the surface porosity (ε), 0.12, obtained from published estimates [93]. The resistance of the initial protein aggregate that deposits on the membrane (R_{p0}) was also obtained from published work, 4 x 10^{11} [38] and assumed to be similar for all filtrations investigated in this study. The fractional amount of protein present as aggregates was set to 0.0003 as determined by Ho and Zydney [51] using dynamic light scattering. It was assumed that all aggregates contribute to fouling and, therefore, the fractional amount of proteins present as aggregates and contributing to fouling, *f'*, was set

to 0.0003. The protein layer resistance constant R', was set to $2.0x10^{15}$ which agrees with data previously reported by Chudacek and Fane [94]. The bulk concentration (C_b) is characteristic of the feed solution to be filtered. For the BSA solutions, C_b was the actual protein concentration while the organic content was used as C_b for the CHO cell culture broth.

The initial open area factor (F), representing the effect of the initial layer due to the feed recirculation, was obtained for the corresponding filtration solution.

3.4.1 Microfiltration of bovine serum albumin

The microfiltration of BSA solutions at two different concentrations and 8000 s^{-1} shear rate was selected to validate the proposed model. BSA represents a protein extensively studied for the fouling of microfiltration membranes.

A single set of parameters (α, k_c, and k_{pb}) that provided the best fit for all the experimental TMP data of the two BSA filtrations was determined by minimizing the sum of squared residuals (SSR). The residual was equal to the difference between a data point and the model fit. Initial estimates for the three parameters were obtained by trial and error. Since k_c reflects the crossflow effect on cake formation, it was set to be equal for both BSA solutions. The TMP model fits, based on the best fit parameters listed in Table 3.2 and presented in Figure 3.2 (solid curves) are in very good agreement with the experimental TMP profiles for the entire duration of the filtration.

Table 3.2: Input parameters and fitted parameters for the cross-flow model

Parameter		**BSA 2 g L^{-1}**	**BSA 4 g L^{-1}**	**CCf4**	**CCf8**	**CFf4**	**CFfr4**
Input							
Protein conc. (g L^{-1})	C_b	2	4				
Organic content (g L^{-1})	C_b			9.8	9.8	10.1	10.1
Factor for initial conditions	F	0.485	0.485	0.56	0.37	0.56	0.52
Fitted							
Pore blockage parameter (m^2 kg^{-1})	α	0.78	0.78	0.18	0.18	0.13	0.16
Crossflow coefficient for cake (s^{-1})	k_c	0.0025	0.0025	0.0012	0.0023	0.0012	0.0012
Crossflow coefficient for pore blockage (x 10^{-3} m^4 s^{-1} kg^{-1})	k_{pb}	37.6	37.6	6.1	6.1	4.1	5.3

A comparison between model fits with and without the cross-flow effect was obtained by calculating the fits for a dead-end situation by setting $k_{pb} = 0$ (Eq. (3.8)) and $k_c = 0$ (Eq. (3.12)). The model fits assuming a dead-end situation for both BSA solutions (dashed curves, Figure 3.2) indicate significant differences between the fitted and the experimental normalized TMP profiles. The fitted normalized TMP profiles obtained for the dead-end model increase exponentially with time as reported in the literature for experimental dead-end systems [38]. While the fitted normalized TMP for the dead-end model is quite similar to the experimental normalized TMP at the beginning of the filtration, the fitted normalized TMP increases drastically with filtration time whereas the experimental normalized TMP for the cross-flow operation remains relatively constant. The significant differences of the fitted normalized TMP profiles that are obtained when assuming a dead-end configuration in comparison to the cross-flow flow configuration demonstrate the usefulness of the proposed model and the importance of considering the cross-flow flow effects.

The estimated model parameters can be used to obtain information about the characteristics of the fouling occurring during the microfiltration of the BSA solutions. The estimated pore blockage parameter (α), 0.78, is two times larger than reported by Ho and Zydney for the microfiltration of BSA solutions with 0.2 μm track etched membranes. The higher pore blockage parameter estimated for BSA in the current study may reflect the significant differences in the membrane structure of the polysulfone membranes that have an interconnected pore structure [95] in contrast to the straight through pores of the track-etched membranes used by Ho and Zydney [38]. Also, the larger membrane pore size may lead to a larger fraction of total pore area to be blocked by BSA aggregates when using 0.45 μm membranes compared to 0.2 μm membranes.

The feed with the higher BSA concentration, 4 g L^{-1}, also had the highest predicted cake formed and the more pronounced predicted decline of the open pore area during the filtration (Fig. 3.4A and Fig. 3.5A).

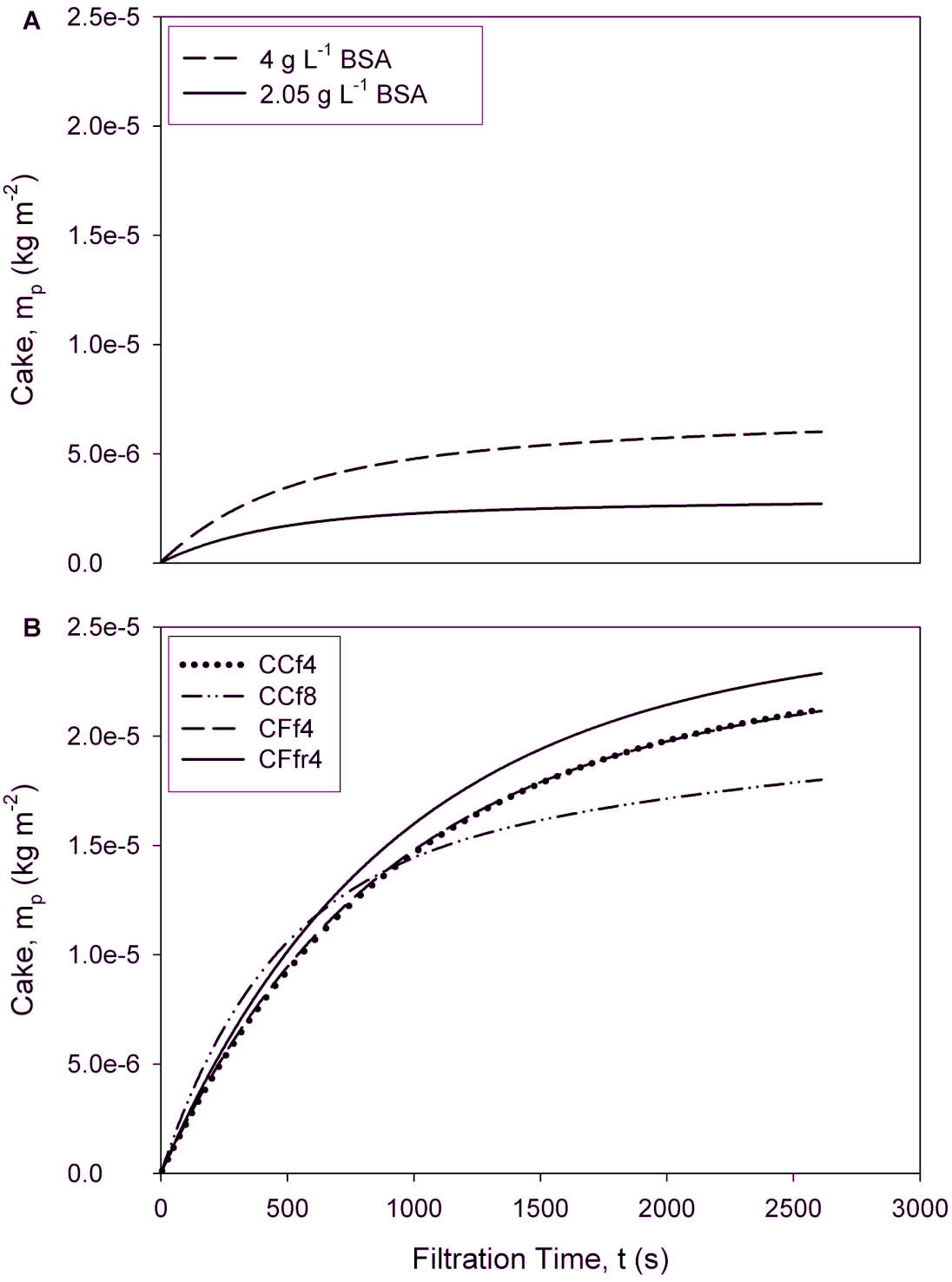

Fig. 3.4: Cake growth during microfiltration of BSA (A) and CHO cell culture broth (B) with 0.45 µm membranes at constant permeate flux of 30 L m^{-2} h^{-1}.

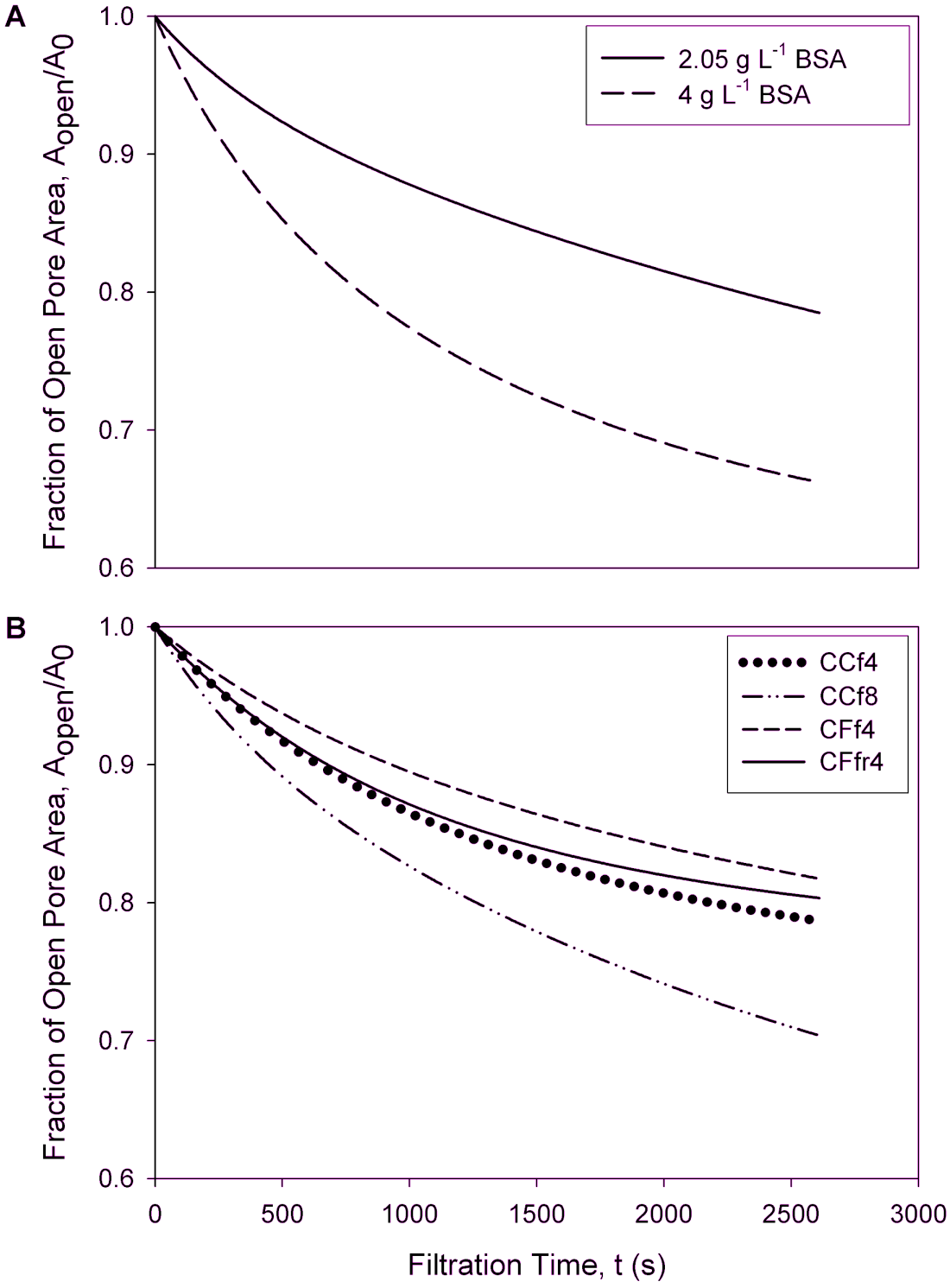

Fig. 3.5: Change in fraction of open pore area with filtration of BSA solutions (A) and CHO cell culture broths (B) with 0.45 µm membranes at constant permeate flux of 30 L m^{-2} h^{-1}.

3.4.2 Microfiltration of CHO cell culture

The fouling behaviour deduced from the normalized TMP profile for different CHO cell culture broth composition, with and without cells, fresh and frozen, low and high shear rates is illustrated in Fig. 3.3. A comparison of the filtrations at the lower shear rate (4000 s^{-1}) indicates that the cell-containing broth (CCf4) has a higher normalized TMP increase compared to the cell-free broth (CFf4) suggesting that the cells contribute to the fouling and that over-clogging of the cake was occurring as observed by Hughes and Field for yeast suspensions [81]. The cell-free broth frozen and thawed before filtration (CFfr4) had an initial normalized TMP increase similar to that of the cell-containing broth (CCf4). But the freezing and the thawing of the cell free broth induced a higher normalized TMP increase at longer filtration times. The highest normalized TMP increase was observed when using the high shear rate (8000 s^{-1} compared to 4000 s^{-1}) and the cell containing broth (CCf8). The increased fouling observed at the higher shear rate is surprising as less fouling would be expected when using a higher cross-flow. For the microfiltration of cell-containing broth, the susceptibility of the cells to shear may become important. Mammalian cells are susceptible to shear force and can rupture when exposed to high shear [14]. Mammalian cells grown in serum-free or low-protein containing media, as it was the case of the CHO cell culture used in this study, were found to be more susceptible to shear stress compared to cells grown in serum-containing media [14]. The effect of shear rate on the cells was estimated from the cell membrane integrity analysis using trypan blue exclusion technique. The cell membrane integrity remained constant at 75% during the filtration at the lower shear rate of 4000 s^{-1}, but decreased to 50% at the high shear rate (8000 s^{-1}), suggesting cell damage due to shear (Fig. 3.6).

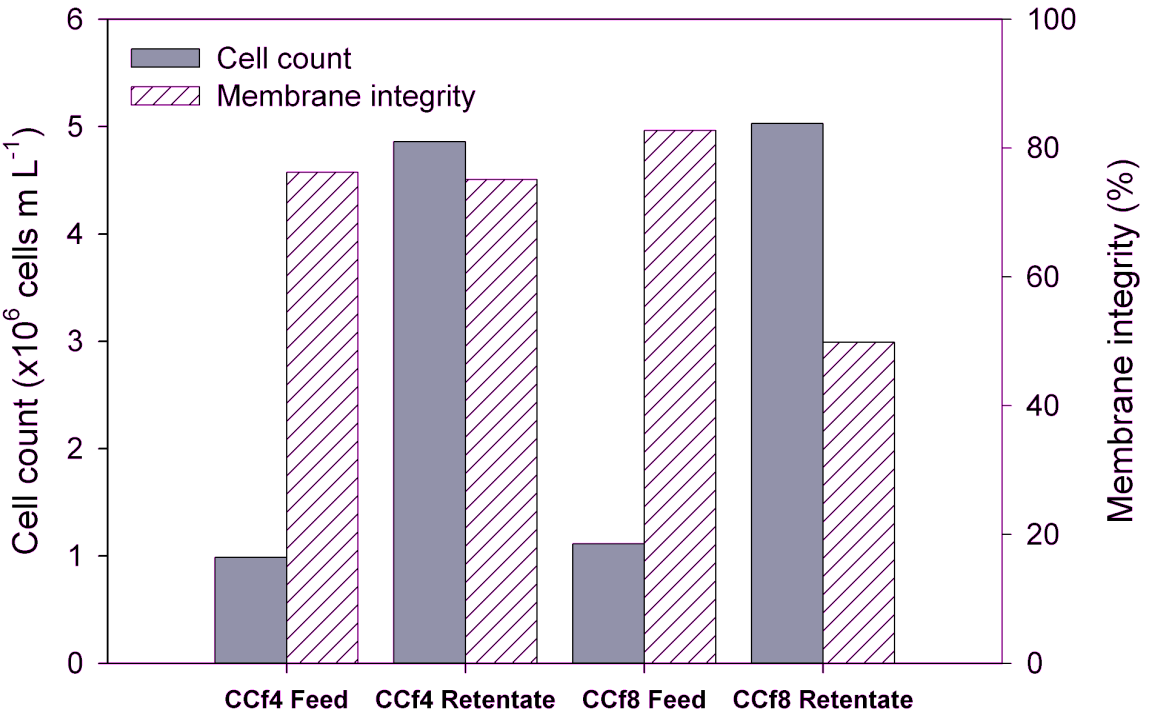

Fig. 3.6: Cell count and cell membrane integrity before (feed) and after (retentate) microfiltration of CHO cell-containing broth with 0.45 µm membranes at constant permeate flux of 30 L m^{-2} h^{-1} at low shear rate (CCf4) or high shear rate (CCf8).

A side effect of cell damage is the release of intracellular species into the feed/retentate stream that can contribute to membrane fouling [90]. According to the fitted model, it is the reduction in the fraction of open pores that causes higher fouling during the filtration of CCf8 (Fig. 3.5 B). This could be caused by the released intracellular species. The cake growth on the other hand is lower during high shear compared to low shear filtration (Fig. 3.4 B). This is in accordance with theory that higher shear can reduce the cake formation.

Model fits of the normalized TMP profile were obtained for the filtration of the four culture broths (Table 3.1). Input parameters included the fractional amount of protein present as aggregates and contributing to fouling, *f*', obtained from published data for BSA solutions, 0.0003 [51]. The bulk concentration, C_b, was estimated from the organic content of the broth obtained from the total solids and the ash content of the broth since CHO cell

culture broths contain a wide range of proteins and other unknown components that contribute to fouling.

A single set of parameters (α, k_c and k_{pb}) that provided the best fit for all the experimental TMP data of the four filtrations was determined by minimizing the sum of squared residuals (SSR). The residual was equal to the difference between a data point and the model prediction. Since k_c reflects the cross-flow effect, k_c was set equal to the k_c obtained for BSA filtrations at identical conditions (shear rate of 8000 s^{-1}) and set equal for cell culture broth filtered under the same shear conditions of 4000 s^{-1}. The value of k_c was roughly doubled for the filtration at high shear rate when compared to the low shear rate filtration. The TMP model fits, based on the best fit parameters listed in Table 3.2 and presented in Figure 3.3 (solid curves) are in good agreement with the experimental TMP profiles for the entire duration of the filtration.

The estimated parameters can provide information about the characteristics of the fouling occurring during the microfiltration of CHO cell culture broth solutions. The estimated pore blockage parameter (α), remains relatively constant, 0.13-0.18, and was four times smaller than the estimate for the BSA solutions. The lower pore blockage parameter for the CHO cell culture broth may reflect the lower propensity of the feed to block the membrane pores compared to the BSA solutions. The bulk concentration C_b deduced from the organic content of the samples was much higher than the bulk concentration of the BSA solutions and the lower value for α incorporates the diversity of species present in the cell culture broth, not all of which contribute to fouling to the same degree.

The cross-flow effect is given by the parameters k_c and k_{pb}. The estimated cross-flow coefficient for cake formation (k_c) was sensitive to the shear rate and was twice as high at high shear rate when compared to the lower shear rate. This suggests that shear induced diffusion is a possible back transport mechanism where a linear relationship with the shear rate is observed [16]. The estimated cross-flow coefficient for pore blockage (k_{pb}) was independent of shear rate when cells were present (CCf4 and CCf8) A higher k_{pb} was estimated when cells were present (CCf4 and CCf8) compared to cell free broth (CFf4 and CFfr4) which translated into a more pronounced decline of open pore area predicted for the cell containing broth (Figure 3.5 B). The proposed model that combines initial pore blockage with subsequent cake formation over the blocked area fits the

normalized TMP profile observed experimentally for cross-flow microfiltration operated at constant permeate flux of a single protein solution and a complex feed.

3.5 Conclusions

The model developed in this study combines pore blockage with subsequent cake formation and accounts for the cross-flow effect through an increase of the open pore area and a decrease of the deposition of foulant on the membrane surface. This model requires a total of 8 input parameters (four characteristics of the membrane system and four characteristics of the feed solution) and generates three parameters that provide information about the fouling behaviour of the solution. The model fits of the normalized TMP profile were validated with two very different types of biological feeds, single protein solutions (BSA) and multi-component solutions (CHO cell culture broths). A very good fit between the fitted model and the experimental data was obtained. Fouling parameters were estimated and included the pore blockage parameter (α), the cross-flow coefficient for pore blockage (k_{pb}) and the cross-flow coefficient for cake (k_c) that differed according to the feed characteristics and the shear rate.

4

Effect of Pore Size, Shear Rate and Culture Age during the Constant Permeate Flux Microfiltration of CHO Cell Culture Supernatant*

The effect of the shear rate, the membrane pore size, and the age of the culture at the time of harvest during the microfiltration of CHO cell culture supernatants operated at constant permeate flux in a hollow fiber system was analyzed using a combined pore blockage and cake formation model and hydraulic membrane resistances. Filtration of the CHO cell culture supernatant caused an initial increase of the transmembrane pressure (TMP) followed by a slower TMP increase. Filtration operation at the lower membrane pore size (0.20 μm) and the higher shear rate (8000 s^{-1}) resulted in the highest increase in TMP. Predicted pore blockage and cake formation were affected by the filtration conditions. The predicted reduction in open pore area could explain the observed TMP profiles. Treatment of the fouled membrane with water revealed the presence of larger reversible fouling at high shear rates and increased irreversible fouling with smaller membrane pore size.

* Adapted from Stressmann M., Moresoli C., submitted

4.1 Introduction

Mammalian cells such as Chinese Hamster Ovary (CHO) cells constitute a common system for the production of therapeutic glycosylated proteins [96;97]. The ability of CHO cells to excrete proteins simplifies the recovery and purification of the therapeutic protein. Membrane systems have long been used in the field of biotechnology for bioseparations [1]. Microfiltration systems in particular are used as initial step to remove cells and cell debris from feed streams containing the target product. The feasibility to use cross-flow filtration for the treatment of microorganism containing fluid streams was examined more closely in the early 1970s where the fouling of membranes was acknowledged as a major drawback in the utilization of membrane filtration in bioseparations [86]. Membrane fouling includes fouling caused by the cells and fouling caused by the soluble components.

Research on the fouling caused by the cells included the study of factors affecting the adhesion of microbial cells to surfaces [30] and the fermentation and harvest conditions [21;98]. The age of the culture and the culture conditions can affect membrane fouling by cells if cell surface properties are altered [30]. For example, the effect of culture age was studied with respect to the cell attachment ability [99] where a marine pseudomonad culture in the log-phase attached faster and in greater numbers to polystyrene surfaces than a culture in the stationary phase or death-phase. Differences in the secretion of polymers associated with adhesion were given as one possible explanation. Taddei et al. [82] observed higher fluxes for microfiltration of yeast containing cider broth with increasing content of nonviable cells and when aeration was decreased during the fermentation. The increased fluxes were attributed to altered attachment abilities of the yeast cells such as a change in yeast membrane composition that could have occurred when aeration was present.

Research on the fouling by soluble components is complicated by the heterogeneity and the polydispersity of the foulants that makes it more difficult to examine fouling mechanisms. Most studies have therefore focused on representative foulants such as proteins and their aggregates, as well as polysaccharides, both as model solutions with individual foulants and mixtures thereof [45;100;101]. The polydisperse feeds investigated have focused mostly on *E. coli* cells and yeast cells [22;45;81]. In the context of *E. coli* cells, the focus of the microfiltration is unique because the product is intracellular and a cell lysate constitutes the feed of the downstream operation. Kroner et al. [86] compared the cross-flow filtration of a *E. coli* fermentation broth with that of the washed and resuspended cells using 0.3 µm polypropylene hollow fiber membranes. The average flux for the washed and resuspended cells was about 50 L m^{-2} h^{-1} (Lmh), compared to about 28 Lmh for the *E. coli* fermentation broth. The lower average flux was attributed to additional feed components in the broth such as proteins, polysaccharides and lipids, that would have been removed during the washing steps.

In addition to feed components, the filtration operating conditions, including operating mode, membrane pore size and cross-flow velocity, generally have a significant effect on the membrane filtration performance [9;13]. In some cases, the adverse effects of membrane fouling could be reduced by operation at constant permeate flux in contrast to operation at constant transmembrane pressure (TMP). This approach avoids the operation at very high permeate flux and the associated rapid fouling that may occur at the beginning of a constant pressure filtration operation. The benefits of constant permeate flux operation have been discussed by Defrance and Jaffrin [88] for membrane bioreactors used in wastewater treatment. The average flux for constant flux operations is often higher than for constant pressure operations, especially for prolonged filtration times [12]. During constant permeate flux operation, the degree of TMP increase provides an indication of fouling. Berthold and Kempken [19] compared filtrations of hybridoma cell suspension at different constant permeate flux. A rapid and sharp drop of permeate pressure (and therefore TMP increase) was observed at the higher permeate flux while a constant permeate pressure and TMP was observed for the filtration operated at the lower permeate flux.

The effect of the membrane pore size on the fouling during the microfiltration of exopolysaccharide (EPS) solutions revealed an increased fouling with increased membrane

pore size while the fouling remained constant during the filtration of washed and unwashed yeast suspensions when using 0.1 and 0.2 micron pore size with a novel cone-and-plate microfiltration system operated at constant permeate flux [81].

The role of the cross-flow velocity during the microfiltration of the fungal fermentation broth of *Polyporus squamosus* revealed a transition from a predominantly surface fouling to a situation with mainly internal fouling when the crossflow velocity was increased for 0.2 micron aluminium oxide membranes [2]. In the context of a membrane bioreactor, both the soluble and colloidal compounds of an activated sludge were responsible for the observed fouling [20]. Futhermore, the rate at which fouling of the membrane occurred during constant permeate flux filtration was highly correlated to the set permeate flux and to the crossflow velocity. The lower the permeate flux and the higher the cross-flow velocity the lower the rate of membrane fouling rate. As crossflow velocity directly affects the wall shear rate in the system, the selection of the cross-flow velocity is an important consideration for filtration of many mammalian cells, including murine hybridoma cells, that are shear sensitive. In this context, a critical wall shear rate was defined that corresponds to limited shear damage [14]. An inlet shear rate of 4000 s^{-1} was used for the harvest of mammalian cells during the production of recombinant tissue plasminogen activator leading to the development of a successful industrial scale cross-flow microfiltration system operated at constant permeate flux [5].

The large pore size of microfiltration membranes, ranging from 0.05 to 10 µm, is expected to retain microorganisms and to allow the unhindered permeation of proteins through the membrane. However, proteins are well-known microfiltration membrane foulants, as they have a propensity to interact with the membrane surface. Adsorption to and deposition on the internal or external membrane surface can result in pore restriction, pore blockage and/or cake formation. For example, an unexpected high retention of the enzyme formate dehydrogenase with a 76 kDa molecular weight was observed during the filtration of disrupted yeast cells with hollow fiber polycarbonate membrane having a >2000 kDa cut-off [86]. The retention was unexpected since the molecular weight of formate dehydrogenase is considerably smaller than the membrane molecular weight cut-off. The authors suggested that a denser sub-layer of suspension particles was responsible

for the high retention of the enzyme. Protein aggregates specifically tend to deposit on the membrane surface [51;102] and contribute to membrane fouling.

The modeling of fouling is a powerful tool for both the understanding of the parameters responsible for fouling and the identification of the conditions where fouling will be minimized. One can use simple models to describe membrane fouling based on the four different single fouling mechanisms: standard blocking (pore constriction), complete blocking (pore blockage), intermediate blocking, and cake formation that were initially developed for dead-end systems [16]. Alternatively, various combinations of the single fouling models can be used. For example, we have recently developed a model for cross-flow microfiltration operated at constant permeate flux [103] derived from the combined pore blockage and cake filtration concepts developed by Ho and Zydney [38]. The transmembrane pressure is a function of the open pore area A_0 and the resistance of a protein deposit R_p, Eq. (4.1):

$$\Delta P = \mu Q_0 R_m \frac{R_m + R_p}{A_0 R_m + A_{open} R_p}, \tag{4.1}$$

where ΔP is TMP, μ is the solution viscosity, Q_0 is the constant flow through the membranes, R_m is the clean membrane resistance and A_0 the total area of the membrane. The change of open pore area with time is defined in Eq. (4.2):

$$\frac{dA_{open}}{dt} = -\alpha\, Q_{open} C_b + k_{pb}\, m_p, \tag{4.2}$$

where α is the pore blockage parameter, Q_{open} is the flow through the open pores, C_b is the bulk protein (organic) concentration, k_{pb} a crossflow parameter for pore blockage and m_p the mass of the protein deposit per unit area.

The change in protein deposit, Eq. (4.3), is a function of the fractional amount of total protein that contributes to fouling f', the liquid flow through the blocked membrane pores $Q_{blocked}$, C_b, the area of blocked pores $A_{blocked}$, the cross-flow coefficient for cake formation k_c and the mass of already deposited material:

$$\frac{d(m_p)}{dt} = \frac{f' Q_{blocked} C_b}{A_{blocked}} - k_c m_p . \tag{4.3}$$

Another common method to describe membrane fouling is based on the analysis of the hydraulic resistances [34;104]. The resistance of the membrane itself to the permeate flow is referred to as the intrinsic membrane resistance, R_m. In addition, adsorption and fouling layers present a resistance to flow [34]. Adsorption resistance is thought of as a resistance of a monolayer of fouling material adsorbed to the membrane surface. The resistance of the fouling layer is comprised of cake, pore blockage, and pore constriction. In this approach, the types of fouling can be distinguished according to the fouling severity. Reversible fouling can be easily removed by flushing or rinsing with water or buffer [34] while irreversible fouling removal requires the use of chemicals. In this study, the hydraulic resistances to permeate flow will be differentiated into the clean membrane resistance, R_m, and the total fouling resistance, R_f. The total fouling resistance will be further decomposed into reversible fouling resistance, R_{rev}, and irreversible fouling resistance, R_{irr}. It is distinguished by flushing the membrane after the end of the filtration experiment with water at the same operating conditions as the filtration experiment.

The objective of this study was to investigate the membrane fouling occurring during cross-flow microfiltration operation at constant permeate flux of CHO cell culture broth supernatants. The analysis is based on our recently developed model that combines pore blockage and cake filtration mechanisms and the analysis of the hydraulic resistances. The effects of the cross-flow velocity, the membrane pore size and the broth harvest time are reported.

4.2 Materials and methods

4.2.1 Microfiltration system

Figure 4.1 shows the schematic of the microfiltration system. A more detailed description can be found elsewhere [103]. Two different pore size polysulfone membranes were used in the experiments, 0.2 µm (CFP-2-E-3MA, GE Healthcare) and 0.45 µm (CFP-4-E-3MA, GE Healthcare), both having a total of 13 fibers, an inner fiber diameter of 1 mm and a total membrane area of 110 cm^2. For each filtration, 380 mL of sample were added to the feed tank. The feed solution was circulated through the lumen of the membrane fibers and returned to the feed tank for five minutes prior to opening the permeate port and starting the permeate pump to allow for system equilibrium. Filtrations were operated at constant permeate flux of 30 L min^{-1} h^{-1} (Lmh) controlled by a permeate pump. The feed flow was controlled by a peristaltic pump and either set to yield a wall shear rate of 4000 s^{-1} or 8000 s^{-1}. The permeate was collected and samples of feed, retentate and permeate were analyzed for total solid content, organic content, protein content, and viscosity.

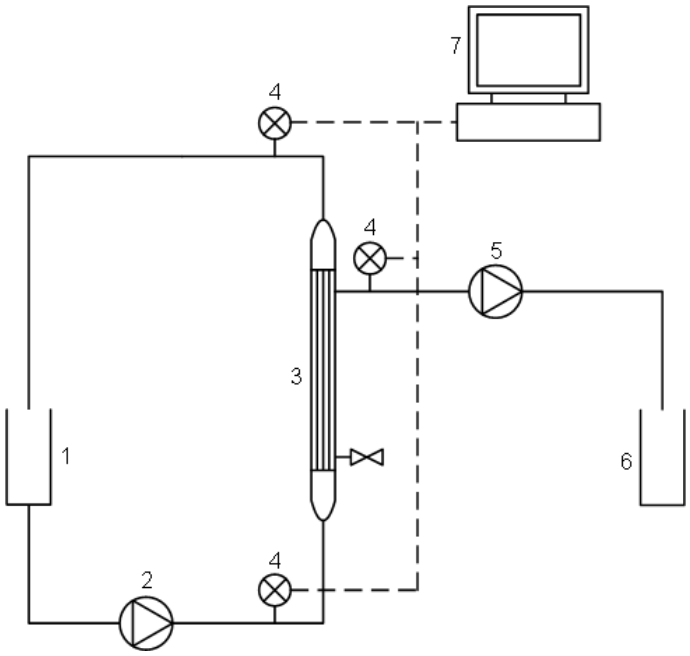

Fig. 4.1: Schematic diagram of the cross-flow hollow fiber microfiltration unit: 1 feed/retentate vessel, 2 peristaltic feed pump, 3 hollow fiber cartridge, 4 pressure transducer, 5 peristaltic permeate pump, 6 permeate vessel, 7 data acquisition system.

4.2.2 Hydraulic resistance

The clean membrane resistance, R_m, was measured using nanopure water as feed solution. The permeate was withdrawn at constant 30 Lmh and pressure in the feed, retentate, and permeate line recorded to allow for calculation of the TMP. At the end of the filtration, the membrane was flushed with 1000 mL of nanopure water at the same crossflow velocity (CFV) as during the filtration experiment. The water flux was then measured again to calculate the resistance of the irreversible fouling layer, R_{irr}. The reversible fouling resistance, R_{rev}, was calculated from the difference between the total hydraulic resistance at the end of filtration, and after the membrane flushing.

4.2.3 Cell culture supernatant

The CHO cell culture supernatant supplied by the Department of Microbiology, University of Manitoba, was frozen immediately after the cell removal by centrifugation (Sorvall RC-5, GS-3 rotor, 7000 rpm). Suspension cell cultures were performed in a 2 L perfusion bioreactor. The cells producing beta-interferon (b-IFN) were grown in serum-free media, CHO-SFM (Biogro Technology Inc., Winnipeg, Canada), to which 0.1% Pluronic F-68 was added. Cell culture broth was harvested at different times during culture and combined to obtain sufficient feed for filtration purposes. Details of the feed solution properties can be found in Table 4.1.

Table 4.1: Properties of CHO cell culture supernatant

Broth	**A**	**B**	**C**	**D**
Day of harvest	8 and 10	11 and 12	13 and 14	15 and 16
Cell concentration on day of harvest (x 10^{-6} cells m L^{-1})	2.7 and 2.9	2.4 and 2.9	3.1 and 3.2	3.6 and 3.7
Total solids (g L^{-1})	15.3 (0.86)	16.2 (0.46)	16.5 (0.38)	15.9 (0.19)
Organic content (g L^{-1})	7.3 (0.67)	7.9 (0.18)	8.1 (0.71)	8.4 (0.36)
Protein (g L^{-1})	0.083 (0.0022)	0.078 (0.0011)	0.079 (0.0053)	0.078 (0.0043)

Numbers in brackets represent standard deviation.

4.2.4 Protein analysis

Total protein content was estimated according to the Bradford method adapted for microplates by Biorad, using bovine serum albumin as standard and measuring absorbance at 590 nm.

4.2.5 Total solids and organic content

Defined volumes of feed, retentate and permeate samples of the individual filtrations were dried at 100°C and the dry weight derived. The same samples were then further dried at 500°C to determine the ash content of the sample. The difference between dry weight and ash weight was termed organic content.

4.2.6 Viscosity

The kinematic viscosity of the feed, the retentate and the permeate samples were measured using a Cannon-Fenske Routine Viscometer (Fisher, USA) of size 50. Using the density derived from the weight of 1 ml of sample, the dynamic viscosity was determined.

4.3 Results and discussion

The TMP profiles for the microfiltration of CHO cell culture supernatant at different conditions of harvest time, shear rate and membrane pore size are shown in Figures 4.2 and 4.3.

Fitted data obtained using the previously developed model (Eqs. (4.1), (4.2) and (4.3)) and the input parameters listed in Table 4.2 (taken from BSA experiments, see Chapter 3), provided a good fit for all the experimental filtration data.

Table 4.2: Input parameters for the pore-blockage cake filtration model

Parameter		**Pore size** (μm)	**Shear rate** (s^{-1})	**Broth** A	B	C	D
Organic content (g L-1)	C_b			15.3	16.2	16.5	15.9
Factor for initial conditions	F	0.20	4000	0.68	0.75	0.7	0.75
			8000	0.42	0.49	0.48	0.51
		0.45	4000	0.71	0.74	0.71	0.73
			8000	0.49	0.47	0.53	0.50
Cross-flow parameter for cake (s^{-1})	k_c	0.20	4000	0.0006 (A-D)			
			8000	0.0012 (A-D)			
		0.45	4000	0.0006 (A-D)			
			8000	0.0012 (A-D)			
Membrane resistance (m^{-1})	R_m	0.20		5.1×10^{-10}			
		0.45		3.2×10^{-10}			
Resistance of initial protein deposit (m^{-1})	R_{p0}			4×10^{11}			
Permeate viscosity (Pa s)	μ			0.00089			
Fractional amount of protein contributing to fouling	*f*’			0.0003			

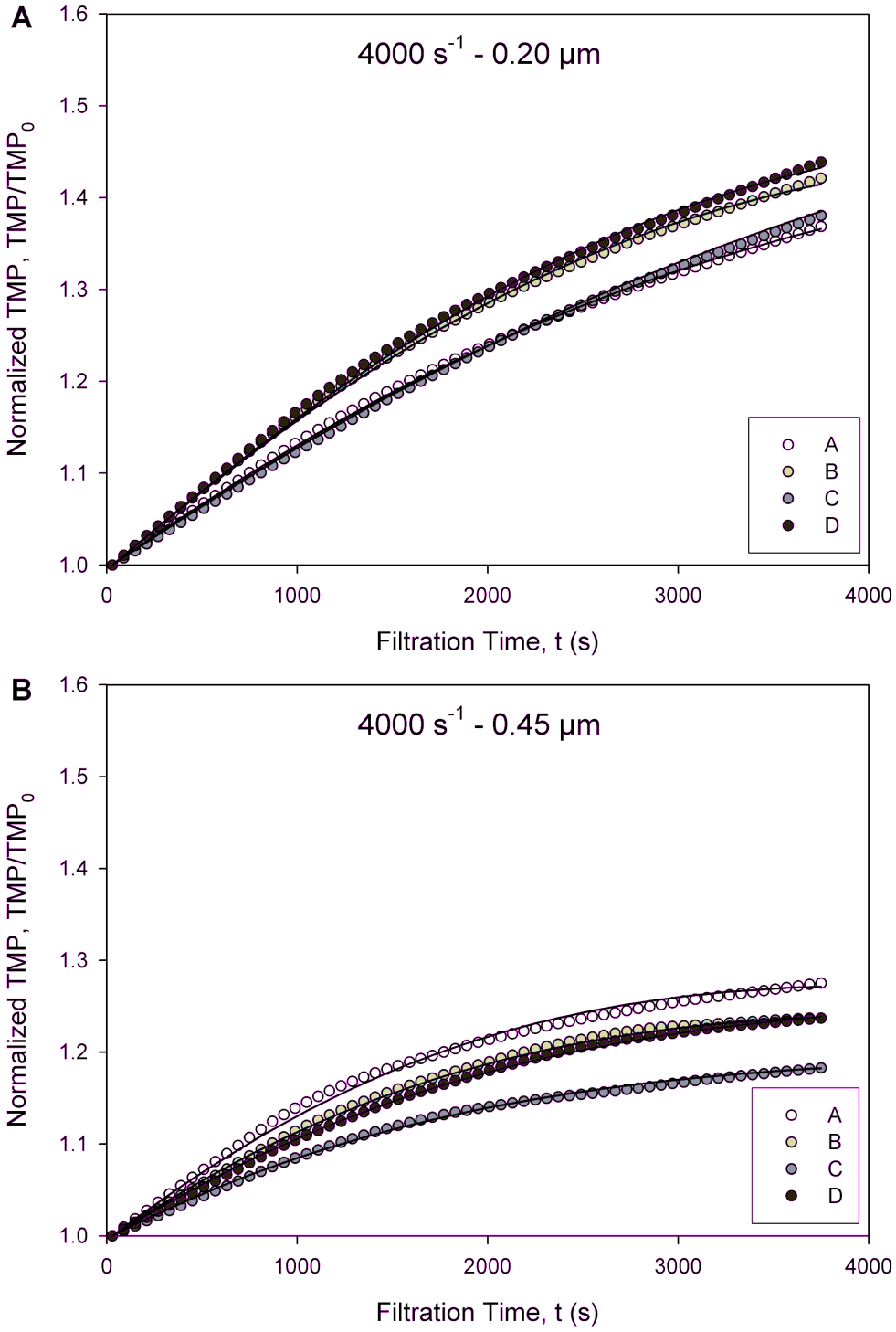

Fig. 4.2: Normalized TMP profiles for CHO cell culture supernatants at the low shear rate (4000 s^{-1}) with 0.2 µm (A) and 0.45 µm (B) microfiltration membranes in a hollow fiber system for constant flux operation. Solid curves are the model fit according to the best fit parameters listed in Table 4.2. Permeate flux is 30 Lmh. CHO cell culture broth A-D properties are listed in Table 4.1.

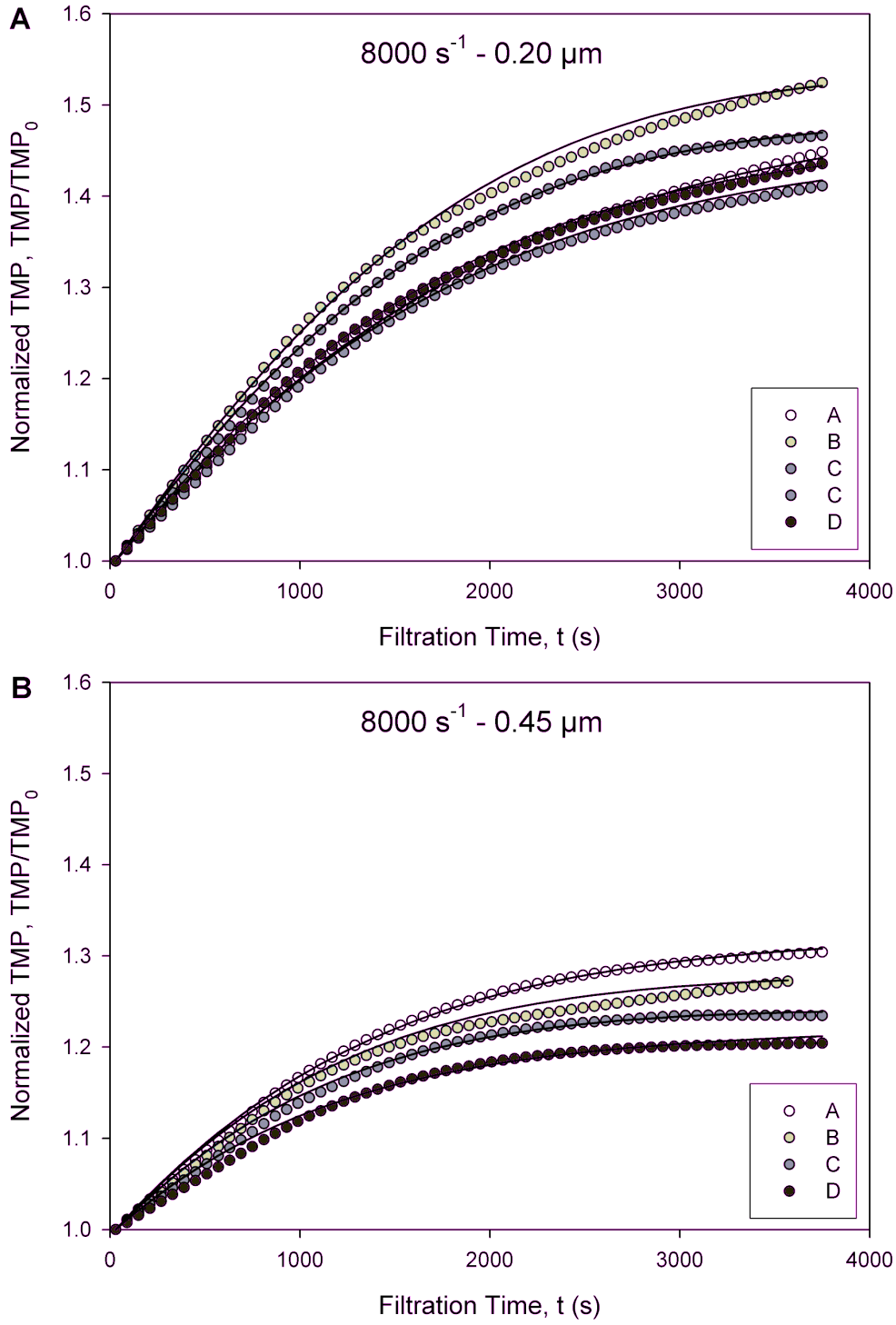

Fig. 4.3: Normalized TMP profiles for CHO cell culture supernatants at the high shear rate (8000 s^{-1}) with 0.2 µm (A) and 0.45 µm (B) microfiltration membranes in a hollow fiber system for constant flux operation. Solid curves are the model fit according to the best fit parameters listed in Table 4.2. Permeate flux is 30 Lmh. CHO cell culture broth A-D properties are listed in Table 4.1.

The highest TMP increase was observed for the lower membrane pore size (0.20 µm). A higher TMP increase was observed at the higher shear rate (8000 s^{-1}) than at the lower shear rate (4000 s^{-1}). This difference was more pronounced for the smaller membrane pore size and is reflected by the fitted values for alpha, the pore blockage parameter, and $k_{pb,}$ the cross-flow parameter for pore blockage (Table 4.3).

Table 4.3: Fitted parameters (average for broth A to D) for the pore blockage and cake formation crossflow model.

Membrane pore size (µm)	**Shear rate (s^{-1})**	**pore blockage parameter α (m^2 kg^{-1})**	**Cross-flow parameter k_{pb} (x 10^{-3} m^4 s^{-1} $kg^{-}1$)**
0.20	4000	0.38 (0.0509	7.1 (1.56)
	8000	0.49 (0.057)	11.2 (2.14)
0.45	4000	0.20 (0.043)	4.8 (1.02)
	8000	0.24 (0.033)	7.0 (0.83)

Numbers in brackets represent standard deviation.

The time at which the broth was harvested had a negligible effect on the filtration performance for the cell harvest time frame studied (8 days). Broth A (day 8-10) to D (day 15-16) could be grouped together according to the filtration conditions and no consistent trend among A, B, C, and D was identifiable.

The higher TMP increase observed at the high shear rate was surprising as high shear conditions are generally considered to be beneficial in reducing the membrane fouling. However, Devereux and Hoare [105] gave examples where increased cross-flow did not provide the expected improvement. A break-up of precipitate aggregates and a shift from external to internal fouling, respectively, were proposed as possible explanations. If particles break up into smaller particles they could enter the pores more easily and deposit within the pores, resulting in more severe fouling at high shear. A change in the fouling mechanism could have occurred for the filtrations of the CHO cell fermentation broth upon increase of the shear rate from 4000 to 8000 s^{-1}. Alternatively, Taddei et al. [82] suggested that the material already deposited might be less susceptible to the shear force provided by the higher shear.

Using the model that considers pore blockage and cake formation as fouling mechanisms, the open membrane pore area and the cake formation were predicted as illustrated in Fig. 4.4 and Fig. 4.5.

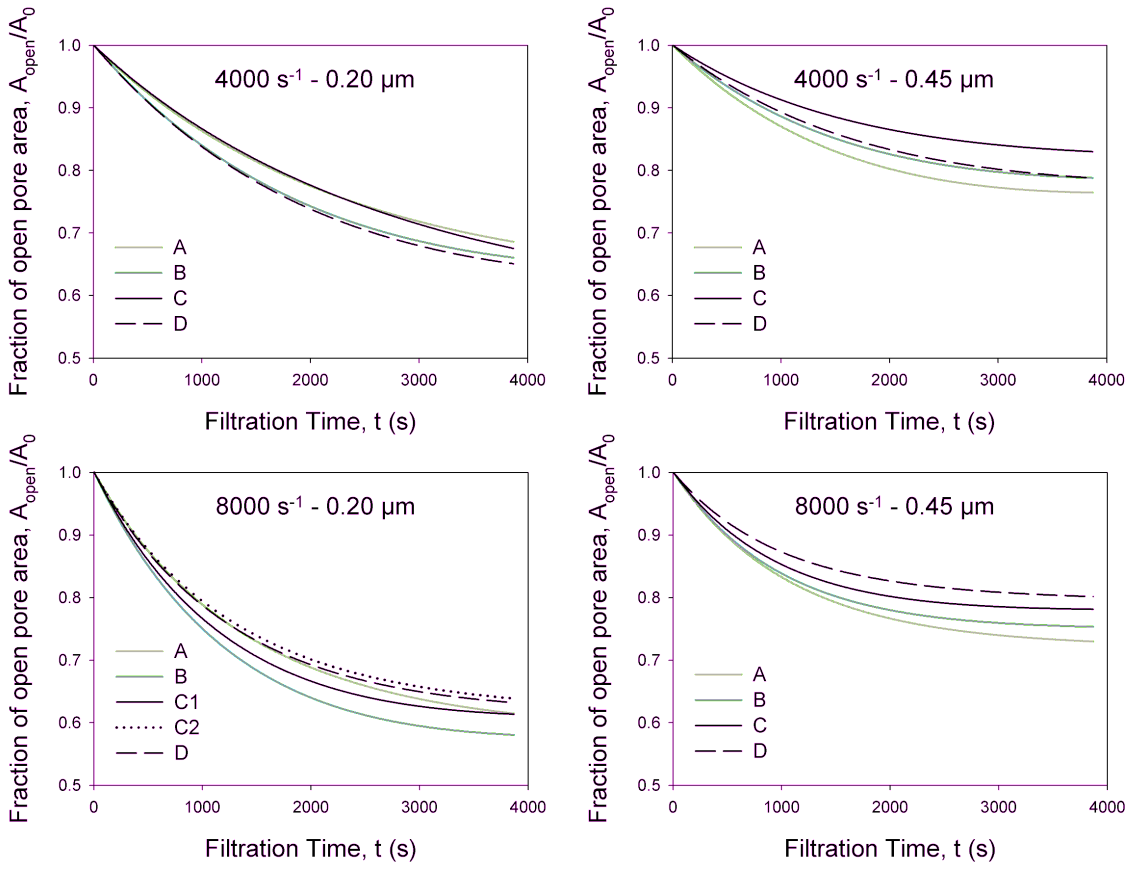

Fig. 4.4: Reduction in open pore area according to the model fit for low (4000 s^{-1}) and high (8000 s^{-1}) shear conditions, and small (0.20 µm) and large (0.45 µm) membrane pore size. Permeate flux was constant at 30 Lmh.

The most significant decrease in membrane open pore area is predicted for the smaller membrane pore size and at the high shear conditions while the lowest decrease is predicted for the larger membrane pore size and at the low shear conditions. The effect of the membrane pore size could be explained by a higher tendency of feed components to block the smaller pores or block them more severely. The effect of the shear rate is less important compared to the effect of the membrane pore size.

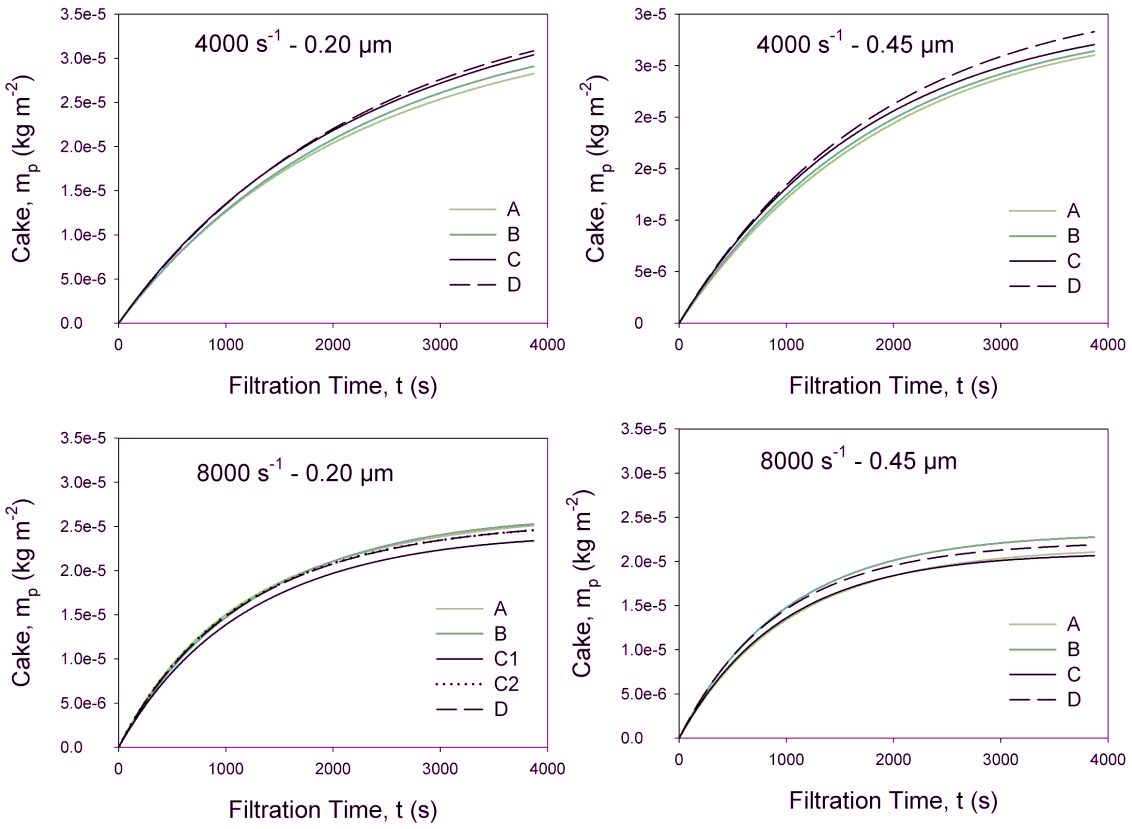

Fig. 4.5: Increase in deposited cake according to the model fit for low (4000 s^{-1}) and high (8000 s^{-1}) shear conditions, and small (0.20 µm) and large (0.45 µm) membrane pore size. Permeate flux was constant at 30 Lmh.

The predicted cake growth as a function of filtration time shown in Fig. 4.5 indicates a lower cake formation for the high shear conditions which is consistent with theory. The higher the shear force, the more material will be removed from the membrane surface. The predicted cake formation is somewhat more important with the smaller membrane pore size at both shear rates. It can be seen that the shear rate affects the cake growth, whereas the membrane pore size affects the pore blockage. Experimental conditions can affect concurrent fouling mechanisms differently [9], changing which fouling mechanism is predominant. In this study, pore blockage seems to have the most pronounced effect on TMP increase. The higher TMP increase at the higher shear rate and with the smaller membrane pore size is consistent with the highest reduction of open pore area at those same filtration conditions. Despite a prediction of smaller cakes at higher shear rates, the observed TMP increase was higher at the higher shear rate.

Hydraulic resistances, intrinsic membrane resistance (R_m), total fouling resistance (R_f), reversible fouling resistance (R_{rev}) and irreversible fouling resistance (R_{irr}) calculated from the water flux measurements before filtration and after rinsing the membranes after each experiment are shown in Fig. 4.6.

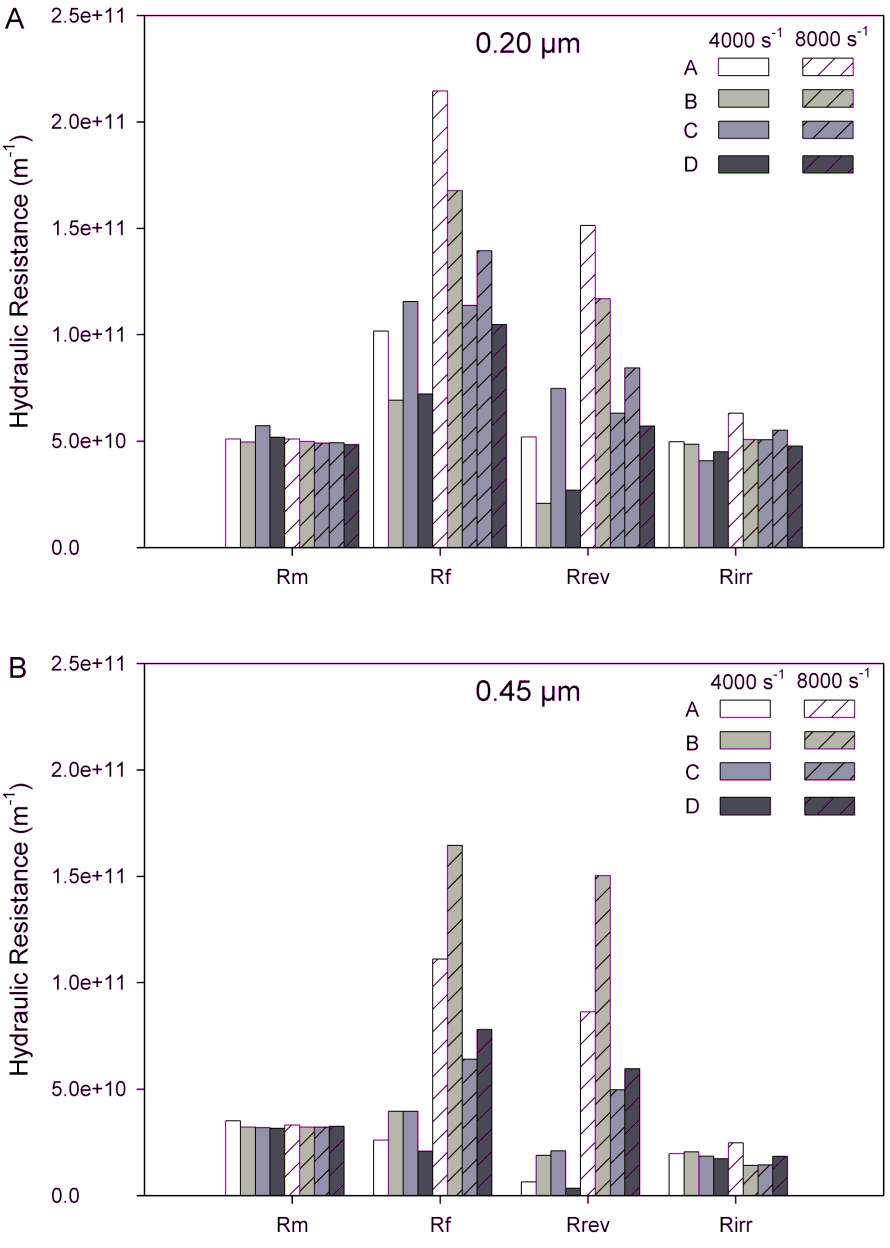

Fig. 4.6: Hydraulic resistance for 0.2 µm (A) and 0.45 µm (B) microfiltration membranes in a hollow fiber system for constant flux operation at low (4000 s^{-1}) and high (8000 s^{-1}) shear conditions.

The resistance of the clean membrane was consistent throughout the set of experiments for both membranes confirming the efficiency of the cleaning protocol with about 3.2 x 10^{10} m^{-1} for the 0.45 µm membrane pore size and 5.1 x 10^{10} m^{-1} for the 0.20 µm membrane pore size. The total fouling resistances calculated from the TMP and the permeate flux at the end of each filtration showed a higher R_f for the higher shear rate conditions that could result from the inherent higher pressure in the system when operating at the higher shear rate conditions. For both the low and high shear rates, the total fouling resistance was higher when the smaller membrane pore size was used. For the lower shear rate, the average R_f estimate for all broths (A to D) was 8.9 x 10^{10} m^{-1} when using the 0.20µm membrane, about three times higher compared to 3.1 x 10^{10} m^{-1} for the 0.45 µm membrane pore size. At the high shear conditions, a 50% increase of the average R_f estimate was observed, 1 x 10^{11} m^{-1} for the 0.45 µm membrane compared to 1.5 x 10^{11} m^{-1} for the 0.20 µm membrane. Thus, the impact of membrane pore size on the overall fouling is more significant at the lower shear rate. In contrast, the irreversible fouling was affected only by the membrane pore size. The irreversible fouling was doubled for the 0.20 µm membrane when compared to the 0.45 µm membrane. Such a difference would support a predominant pore blockage fouling mechanism where the shear rate has a negligible impact on the irreversible fouling. The membrane pore size was the major factor governing the irreversible fouling. The reversible fouling however was strongly influenced by the shear rate where the reversible fouling was significantly higher at the high shear conditions for both membrane pore sizes investigated. The contribution of the reversible fouling to the total fouling, presented in Table 4.4, indicates a higher proportion of reversible fouling when filtrations were operated at the high shear conditions. About 80% of the fouling observed for the filtrations at the high shear conditions with the larger membrane pore size was reversible i.e. easily removed by water rinsing. This is generally considered desirable as it is easier to remove. In contrast, only about 36% of the fouling observed at the low shear conditions and with the larger pore size was reversible. Despite such differences, the irreversible fouling i.e. remaining after flushing the membrane with water was similar for both shear conditions investigated for the same membrane pore size.

Table 4.4: Contribution of the reversible fouling at different filtration conditions.

Membrane pore size (µm)	Shear rate (s^{-1})	Reversible fouling (% of total fouling R_f)
0.2	4000	45.8 ± 15.3
	8000	62.2 ± 7.6
0.45	4000	35.5 ± 17.7
	8000	80.7 ± 7.1

Choi et al. [34] observed the opposite effect when filtering activated sludge through 0.3 µm PVDF flat sheet membranes. Flushing the membrane after filtration at high cross-flow velocity did not remove a significant portion of the fouling whereas membranes fouled at the lower cross-flow velocity were partially cleaned by flushing. The range of cross-flow velocity tested, 0.1 to 4.5 m s^{-1}, was significantly wider than the ones investigated in the current study (0.5 to 1.0 m s^{-1}).

Viscosity changes during the filtration could contribute to TMP changes (Eq. (4.1)). A previous study identified an increase in bulk concentration and the associated viscosity increase as one of the causes of permeate flux decrease during microfiltration of a bacterial fermentation broth [3]. To test the possibility of a viscosity effect on the filtration of the CHO cell culture supernatant, the viscosity of feed, retentate and permeate solutions was measured. However, no change in viscosity was observed. Permeate samples were not significantly different from the feed solutions or from water. Therefore, the viscosity of water was used for modeling purposes and an increase in TMP over time due to increase in viscosity with progressing concentration was ruled out. Analysis of solid content revealed no significant change in the retentate or permeate sample compared to the feed samples, either. This could indicate that the components contributing to fouling represented only a very small portion of the solid content in the samples and their loss due to interaction with the membrane was not detectable.

4.4 Conclusions

The influence of cross-flow velocity, membrane pore size, and culture broth harvest time on TMP increase and membrane fouling during microfiltration of CHO cell culture supernatants was studied. The TMP increase was more severe at the smaller membrane pore size and the higher shear rate, but was not affected by the day of culture harvest. According to the combined pore blockage and cake formation model previously introduced (Chapter 3), a larger decrease in the open pore area can explain the more severe membrane fouling observed with the smaller membrane pore size and the higher shear rate. The predicted cake growth indicated a dependence on shear rate, with a smaller cake deposits at the higher shear rate. At the same time, the total fouling resistance calculated from the membrane hydraulic resistances, was affected in a similar way by the membrane pore size and the shear rate. The membrane pore size affected the irreversible fouling, consistent with the model analysis that more fouling occurs at the entrance of the membrane pores. Shear rate however strongly influenced the contribution of reversible fouling to the total fouling. .

5

Pluronic F-68 Reduces Membrane Fouling during Cross-flow Microfiltration of Bovine Serum Albumin*

Cross-flow microfiltration experiments at constant permeate flux were performed with bovine serum albumin solutions. A simple empirical model was introduced to model the normalized TMP increase with time and to calculate the initial fouling rate i_f. The initial fouling rate increased with increased aggregate content, consistent with a two-step mechanism that was proposed for BSA fouling. Furthermore, the initial fouling rate was correlated to the irreversible fouling measured at the end of filtrations. The initial fouling rate, the normalized TMP at the end of the filtration and the irreversible fouling increased with increasing BSA concentrations from 0.1 g L^{-1} to 4 g L^{-1} and when the base solution potassium phosphate buffer was changed to fresh cell culture medium. The presence of the non-ionic surfactant Pluronic F-68 in the feed decreased the long-term fouling and the irreversible fouling, but did not decrease the initial fouling rates.

* Adapted from Stressmann M., Moresoli C., submitted

5.1 Introduction

Microfiltration is a key technology in the downstream processing of pharmaceutical products from cell cultures, in particular in the initial steps of cell harvest and the removal of the cells and cell debris from the product stream [1]. One recognized drawback in the operation of microfiltration systems is membrane fouling, mostly associated with proteins. It not only affects the filtration performance negatively by reducing the process throughput and increasing the costs associated with the membrane cleaning, but it also reduces the recovery of the target protein if its passage through the membrane is impeded. In order to understand the complex mechanisms and factors relevant to microfiltration fouling, several studies focussed on the membrane fouling by individual protein species under defined conditions. One protein often chosen for this purpose is bovine serum albumin (BSA). It is a known foulant of microfiltration membranes despite the significant size difference between the membrane pores (0.05 – 10 μm) and the BSA molecule (~8 nm) [9;16;51]. The more serious fouling susceptibility of BSA was found to be its partial denaturation products [106] or aggregates [44]. Kelly et al [44] proposed a two-step fouling mechanism to explain the flux decline seen with microfiltration of BSA. The first step consists of the deposition of aggregated BSA molecules on the membrane surface. The second step concerns the deposition of bulk BSA on the initial BSA deposits. The factors influencing protein denaturation that would initiate membrane fouling according to the two-step mechanism proposed by Kelly et al. [44] are the operating conditions such as the cross-flow velocity and temperature [106]. Alternatively, protein aggregates can also be present in commercial BSA products [44]. An example of a BSA product that contains aggregates is the heat-shock precipitated commercial BSA. Ho and Zydney [51] used dynamic light scattering (DLS) to determine the presence and size of BSA monomers and aggregates responsible for fouling of microfiltration membranes.

The study of simplified model feed solutions can shed light on more complex feed solutions such as fermentation broth. The critical factors that impact the filtration performance can be identified, and more importantly, used to suggest how these factors can be manipulated to improve the filtration performance. It is important to know if and how

individual feed components affect the filtration performance as a change in media composition during the upstream process can significantly affect downstream processing operations such as membrane filtration [11].

Pluronic F-68 (PF68) is commonly added at concentrations of 0.01% - 0.1% to mammalian cell cultures to protect cells from damage due to shear and bubble sparging [107]. PF68 is a poly(ethylene oxide)$_m$-poly(propylene oxide)$_n$-poly(ethylene oxide)$_m$ (PEO_m-PPO_n-PEO_m) triblock copolymer and on average m is 30 and n is 80 [108]. The molecular weight is about 8400. As a non-ionic surfactant, PF68 is foam stabilizing, reduces cell-bubble attachment and can reduce the susceptibility of mammalian cells to shear forces in bioreactors [109]. Pluronic copolymers have also been studied as a means to pretreat surfaces to reduce adsorption of macromolecules. The hydrophobic portion (PPO) can attach noncovantly to the hydrophobic surface thereby making it more hydrophilic due to the hydrophilic PEO groups facing the surrounding solution [110]. Recently, a variety of Pluronic polymers were blended with polyethersulfone to produce membranes that displayed improved fouling resistance [111]. Although Pluronic is known to reduce protein adsorption by either coating or permanent surface modification, the direct addition of Pluronic to protein solutions has not been studied to our knowledge.

In this study, the fouling behaviour of BSA, a representative protein foulant, in potassium phosphate buffer and fresh mammalian cell culture medium was examined in the presence or absence of PF68 during constant permeate flux microfiltration. The mammalian cell culture medium selected, RPMI 1640, contains a variety of inorganic salts, amino acids and vitamins as well as glucose and other ingredients. RPMI 1640 is less complex than a true animal cell culture media, but contains the essential components that are found in typical commercial mammalian culture media. An empirical model was introduced to obtain data on the initial rate of fouling. The membrane fouling was studied for a variety of feed conditions and related to the content of BSA aggregates and the estimated initial rates of fouling. The abundance of BSA aggregates was analyzed using dynamic light scattering technique and the magnitude of the irreversible membrane fouling was determined by waterflux measurements before and after each filtration experiment. The initial rate of fouling, the overall fouling and the aggregate content were examined in the context of the two step fouling mechanism proposed by Kelly et al (1993).

5.2 Materials and methods

5.2.1 BSA solutions

Experiments were performed using BSA (fraction V heat shock precipitated BSA, catalogue number A6793, Sigma, St.Louis, MO) as model protein. The protein powder was dissolved either in potassium phosphate buffer solution (0.05 M, pH 7) or fresh cell culture medium RPMI 1640 (Gibco Invitrogen, Grand Island, NY) (pH 7.5), subsequently referred to as PPB and CCM, respectively. Where indicated, Pluronic F-68 (Sigma, St. Louis, MO) was added to the solution and dissolved by stirring. The protein solutions were stirred for approximately 30 min and used in the filtration experiments within 2 h of preparation. For permeate filtration (PermFilt) experiments, the permeate of an initial filtration was stored overnight at 4^{o}C and warmed to room temperature before use.

5.2.2 Filtration experiments

Filtration experiments were performed using the QuixStand benchtop system (GE Healthcare, USA). A schematic of the experimental setup is shown in Fig. 5.1. A peristaltic pump (Masterflex 7523-30, Cole Parmer, Vernon Hills, IL) was added to the system to operate the filtration at constant permeate flux. Pressure transducers (PX303-100 G5V, Omega, Stamford, CT and 68075-44, Cole Parmer, Vernon Hills, IL) installed on the feed, retentate and permeate line measured the pressure in the system throughout the filtrations.

The transmembrane pressure (TMP) was calculated from the time averaged pressure data according to:

$$TMP = \frac{P_f + P_r}{2} - P_p, \tag{5.1}$$

where P_f is the feed pressure, P_r is the retentate pressure and P_p is the permeate pressure.

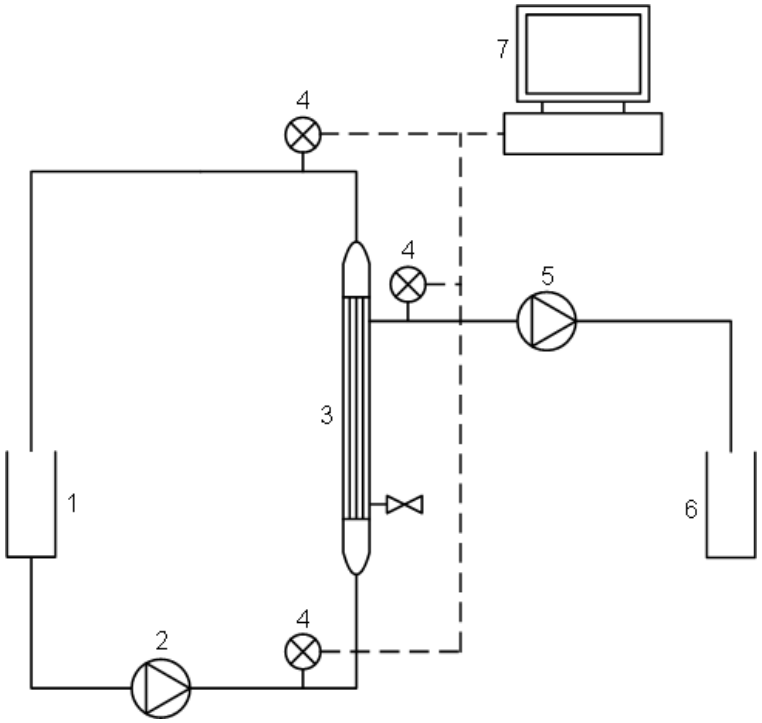

Fig. 5.1: Schematic of the cross-flow hollow fiber microfiltration unit: 1 feed/retentate vessel, 2 peristaltic feed pump, 3 hollow fiber cartridge, 4 pressure transducer, 5 peristaltic permeate pump, 6 permeate vessel, 7 data acquisition system

The hollow fiber cartridge used in the experiments (CFP-4-E-3MA, GE Healthcare) contained 13 polysulfone fibers of 30 cm length with inner diameter of 1 mm and a pore size of 0.45 µm according to the manufacturer. The cross-flow velocity was either 1 m s^{-1} or 0.5 m s^{-1} which corresponds in this system to wall shear rates of about 8000 s^{-1} and 4000 s^{-1}, respectively. Waterflux measurements were conducted before each filtration experiment at the same cross-flow velocity as the subsequent experiment. Before the start of the filtration, the feed solution was circulated through the membrane fiber lumen (permeate port closed off) for 5 min to allow for equilibrium of the system. At the end of this start-up procedure, the permeate port was opened, the permeate pump started and TMP data were collected. All experiments were conducted at room temperature (24 ± 2°C). After each filtration experiment, the membrane was flushed with 1 L of nanopure water (Milli-Q system) followed by the measurement of the waterflux. From the difference in hydraulic membrane resistance before the filtration and after membrane flushing, the irreversible fouling resistance (R_{irr}) was determined. A membrane cleaning procedure involving

consecutive circulation of Tergazyme detergent, nanopure water, and NaOCl solution at 50°C through the membrane restored the membrane resistance after each cleaning cycle to approximately the initial clean membrane resistance (max 5% higher).

5.2.3 Data analysis

As the measured TMP obtained from the pressure transducer signals constituted an impressive number of data points with some pressure fluctuations due to the use of a peristaltic pump, a methodology was developed where the pressure transducer signals were averaged over 1 min intervals and fitted to an empirical mathematical equation that could describe the TMP pattern of a rapid TMP increase followed by a slower TMP increase (Eq. (5.2)):

$$TMP = \frac{a\,t}{b+t} + c\,. \tag{5.2}$$

The parameters a and b were estimated using the solver function of Excel while c was set equal to the initial TMP (TMP_0) and t was the filtration time in seconds. A very good representation of the pressure transducer signals was obtained using Eq. (1) by capturing the non-linearity of the TMP change with time. A typical profile of the fit of the normalized TMP is shown in Fig. 5.2.

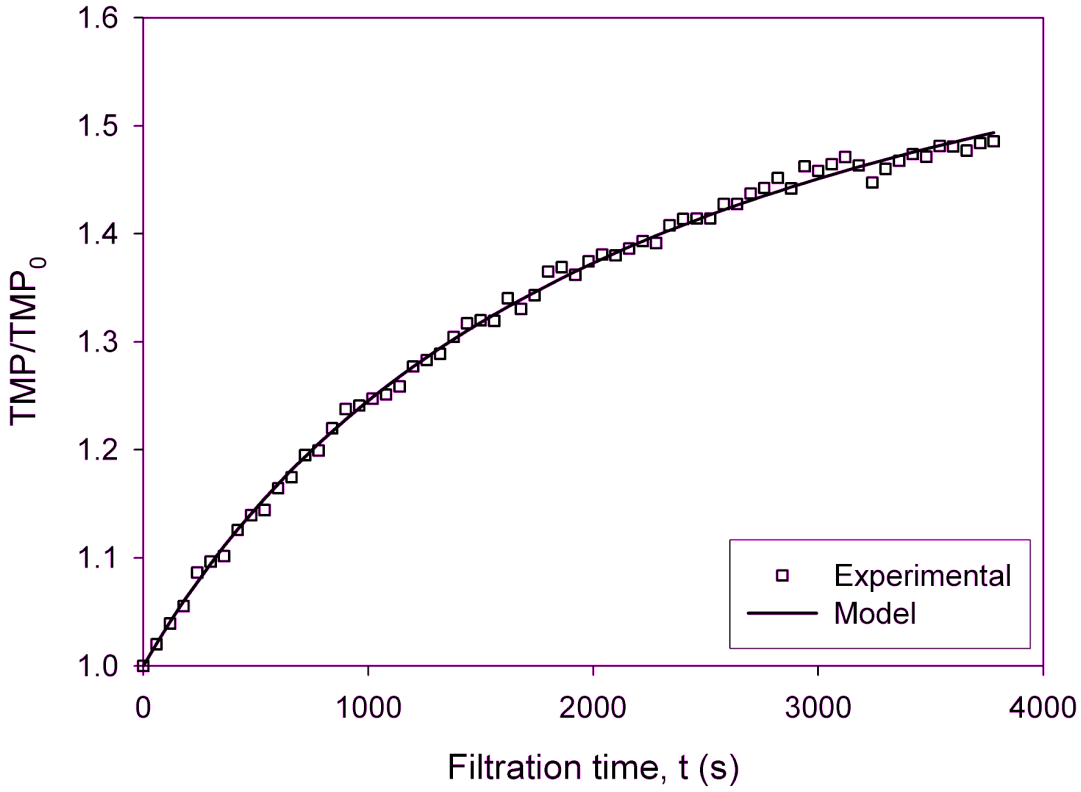

Fig. 5.2: Normalized TMP during the filtration of a BSA solution with a 0.45 µm polysulfone hollow fiber membrane at cross-flow velocity of 1 m s^{-1} (8000 s^{-1}). Squares represent actual data and the solid curve represents the fit of the empirical model .

Further analysis of the TMP change with time was obtained by taking the derivative with time of Eq. (5.2) and estimating at time = 0 as given by Eq. (5.3):

$$\left[\frac{d}{dt}(TMP)_{t=0}\right] = \frac{a}{b} = i_f , \tag{5.3}$$

where i_f was termed initial fouling rate (Pa s^{-1}).

5.2.4 Dynamic light scattering

Feed, retentate and permeate samples were directly analyzed for particle size distribution using a Zetasizer Nano ZS (Malvern Instruments, Worcestershire, UK) with backscatter detection at 173°. Measurements were performed the same day as the filtrations. Particle size distributions are displayed as intensity distribution function. For the purpose of this study, it was sufficient to qualitatively assess the level of aggregates in individual solutions and number distributions were not analyzed. However, since large particles, in this case aggregates, scatter more light than small particles [112], one has to keep in mind that the amount of aggregates in the samples was actually very small, with this small amount causing a relatively high scattering intensity.

5.3 Results

5.3.1 Effect of feed composition on membrane fouling

The normalized TMP increase was used to evaluate the fouling as the filtration proceeded for constant flux operation. The effect of PF68 for three BSA concentrations, 0.1, 2 and 4 g L^{-1}, in potassium phosphate buffer (PPB) feed was investigated (Fig. 5.3).

When no PF68 was present, the estimated initial rate of fouling for the 4 g L^{-1} BSA in PPB solution was twice the initial rate estimated for the 2 g L^{-1} BSA in PPB solution and eight times the initial rate estimated for the 0.1 g L^{-1} BSA in PPB solution (Table 5.1). Also, the highest normalized TMP increase was observed when no PF68 was present for all three BSA concentrations. The normalized TMP reached at the end of the filtration was 16% higher for the 4 g L^{-1} BSA in PPB solution when compared to the 2 g L^{-1} BSA in PPB solution and the 0.1 g L^{-1} BSA in PPB solution was 8.6% lower when compared to the 2 g L^{-1} BSA in PPB solution.

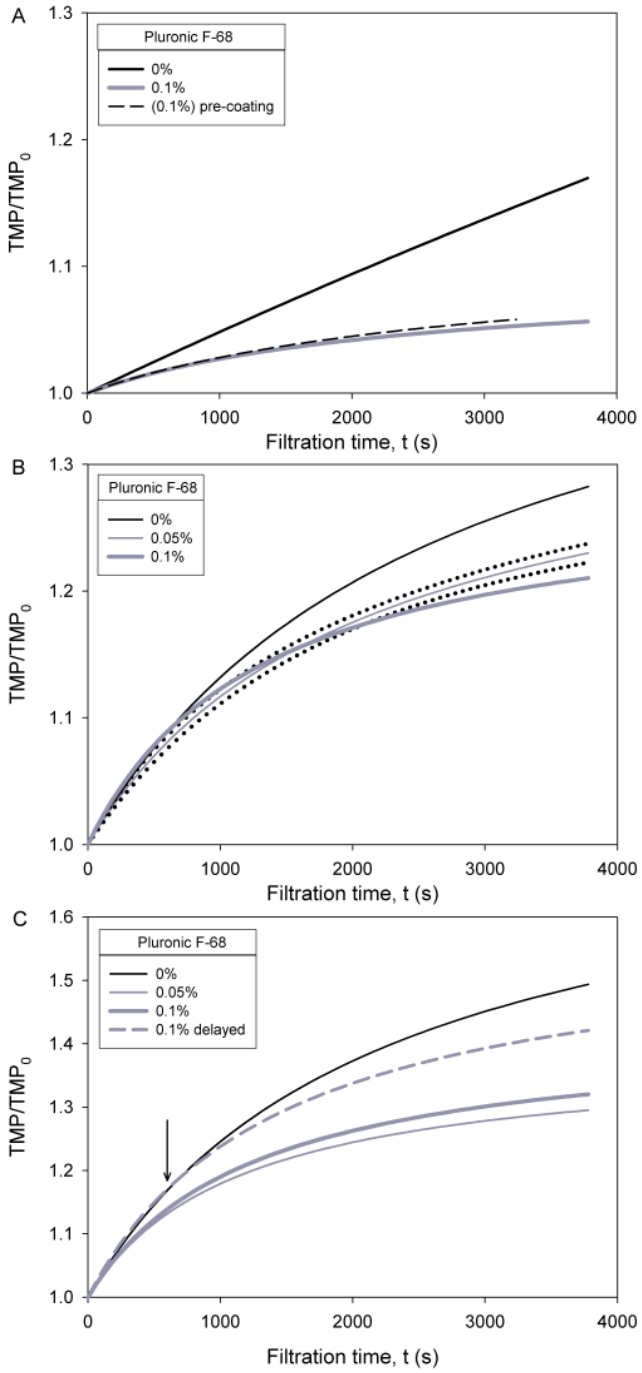

Fig. 5.3: Fitted normalized TMP profiles, Eq. (5.2) for the filtration of BSA in PPB solutions with a 0.45 µm polysulfone hollow fiber membrane at 8000 s^{-1}. (A) 0.1 g L^{-1}, (B) 2 g L^{-1}, (C) 4 g L^{-1} BSA. Pluronic F-68 was added to the BSA solution before the start of the filtration at a concentration of 0.05% or 0.1%, circulated through the membrane lumen before the filtration ((0.1%) pre-coating, details in text), or added to the feed tank 600 s after the start of the filtration (0.1% delayed) as indicated by the arrow.

Table 5.1: Initial fouling rates (i_f), normalized TMP increase at the end of the filtration (TMP/TMP_0 end) and irreversible fouling resistance (R_{irr}) for various feed conditions.

BSA ($g\ L^{-1}$)	Feed	PF68 (%)	comment	i_f ($Pa\ s^{-1}$)	TMP/TMP_0 (end)	R_{irr} ($x\ 10^{10}\ m^{-1}$)
0.1	PPB	0		0.16	1.17	0.29
0.1	PPB	0.1		0.12	1.06	0.42
0.1	PPB	(0.1)	pre-coating	0.12	1.06	0.23
2	PPB	0		0.65	1.28	1.16
2	PPB	0.05		0.66 ± 0.08[a]	1.23 ± 0.01[a]	0.79 ± 0.04[a]
2	PPB	0.1		0.78	1.21	0.83
4	PPB	0		1.28	1.49	2.28
4	PPB	0.05		1.23	1.30	1.10
4	PPB	0.1		1.22	1.32	1.02
4	PPB	0.1	delayed addition	1.45	1.42	1.39
2	CCM	0		1.32	1.37	1.51
2	CCM	0.1		1.72	1.27	1.17
2	CCM	0.1	delayed addition	1.43	1.30	0.97
1.6[b]	CCM	0	PermFilt	0.62	1.35	0.83
1.7[b]	CCM	0.1	PermFilt	0.18	1.03	0
2.0[b]	CCM	0 + 0.1	PermFilt (+ PF68)	0.05	1.03	0
4.0[b]	PPB	0.1	PermFilt	0.00	1.00	0
2	CCM	0	heat-treatment	1.95	1.39	2.39

[a]Average ± standard deviation, n = 4
[b]BSA concentration measured using the Bio-Rad Protein Assay (based on the method of Bradford)

The addition of PF68 for a given BSA concentration in PPB did not affect the initial normalized TMP profile but reduced the normalized TMP increase at longer filtration times. The filtration with 0.05% PF68 added to 2 $g\ L^{-1}$ BSA in PPB solution was repeated four times and exhibited similar fouling behaviour. The addition of 0.1% PF68 was effective in reducing the normalized TMP increase at longer filtration times, 64% for the 0.1 $g\ L^{-1}$ BSA concentration, 25% for the 2 $g\ L^{-1}$ BSA and 35% for the 4 $g\ L^{-1}$ BSA concentration. The addition of 0.05% PF68 was not significantly different from the 0.1% PF68.

The role of PF68 on membrane fouling by BSA was further investigated by pre-coating of the hollow fiber membrane with PF68. For this purpose, a 0.1% PF68 in PPB solution was circulated through the hollow fiber membrane with the permeate line closed for 10 min and subsequently drained. A 0.1 $g\ L^{-1}$ BSA in PPB solution was then filtered

according to the standard procedure. As can be seen in Fig. 5.3 A, the reduction of the membrane fouling was similar to the addition of PF68 to the 0.1 g L^{-1} BSA solution. The role of PF68 on the membrane fouling by BSA was further investigated by conducting a filtration with 4 g L^{-1} BSA in PPB alone initially with the subsequent addition at 600 s (arrow Fig. 5.3 C) of a small volume of PF68 in PPB solution to the feed tank that would bring the concentration of PF68 to 0.1%. The addition of PF68 at 600 s reduced the normalized TMP increase (20% reduction at the end of filtration) when compared to the experiment with no PF68 present during the filtration. These observations suggest that PF68 is effective in reducing further membrane fouling even after the membrane has already been fouled by BSA. The filtration of a 0.1% PF68 in PPB solution with no BSA present (not shown), showed that the TMP remained constant, indicating that PF68 did not cause membrane fouling.

The use of cell culture media (CCM) instead of PPB as base for a 2 g L^{-1} BSA solution caused generally more membrane fouling as shown by the higher estimated initial rate of fouling and the higher normalized TMP reached at the end of the filtration (Table 1). The addition of 0.1% PF68 to a 2 g L^{-1} BSA in CCM solution reduced the normalized TMP increase (Fig. 5.4).

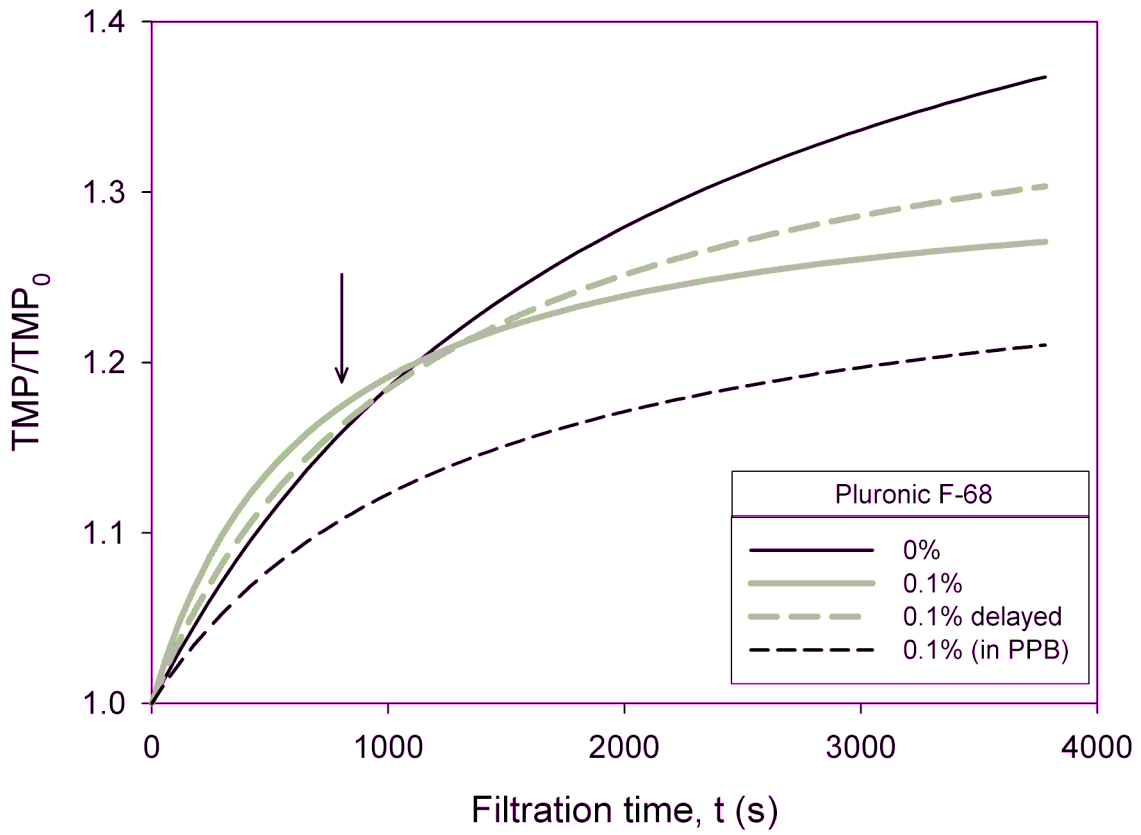

Fig. 5.4: Fitted normalized TMP profile, Eq. (5.2), for the filtration of 2 g L^{-1} BSA in fresh cell culture medium (CCM) with a 0.45 µm polysulfone hollow fiber membrane at 8000 s^{-1}. Pluronic F-68 was added at a concentration of 0.1% before the filtration or 600 s after the begin of the filtration (0.1% delayed) as indicated by the arrow. For comparison, the TMP profile of a 2 g L^{-1} BSA and 0.1% PF68 in phosphate buffer solution (0.1% (in PPB)) is shown.

At the end of the filtration, the normalized TMP was reduced by 27%, a comparable reduction as seen with PPB solutions. However, the estimated initial rate of fouling increased by 30% in the presence of PF68, suggesting interaction with CCM components that are not present in the PPB solution. The delayed addition of PF68 affected the behaviour of the normalized TMP upon the addition of PF68 (arrow in Fig. 4). Despite the slightly higher initial increase in TMP, the overall fouling at the end of the filtration with delayed PF68 addition was lower when compared to the PF68-free 2 g L^{-1} BSA in CCM solution, with a 19% reduction of the normalized TMP increase at the end of the filtration.

To test whether the fouling components present in the feed had been removed during the filtration, the permeate collected during the filtration was used as feed solution in a subsequent filtration (PermFilt) operated under the same experimental conditions as the initial filtration (Fig. 5.5).

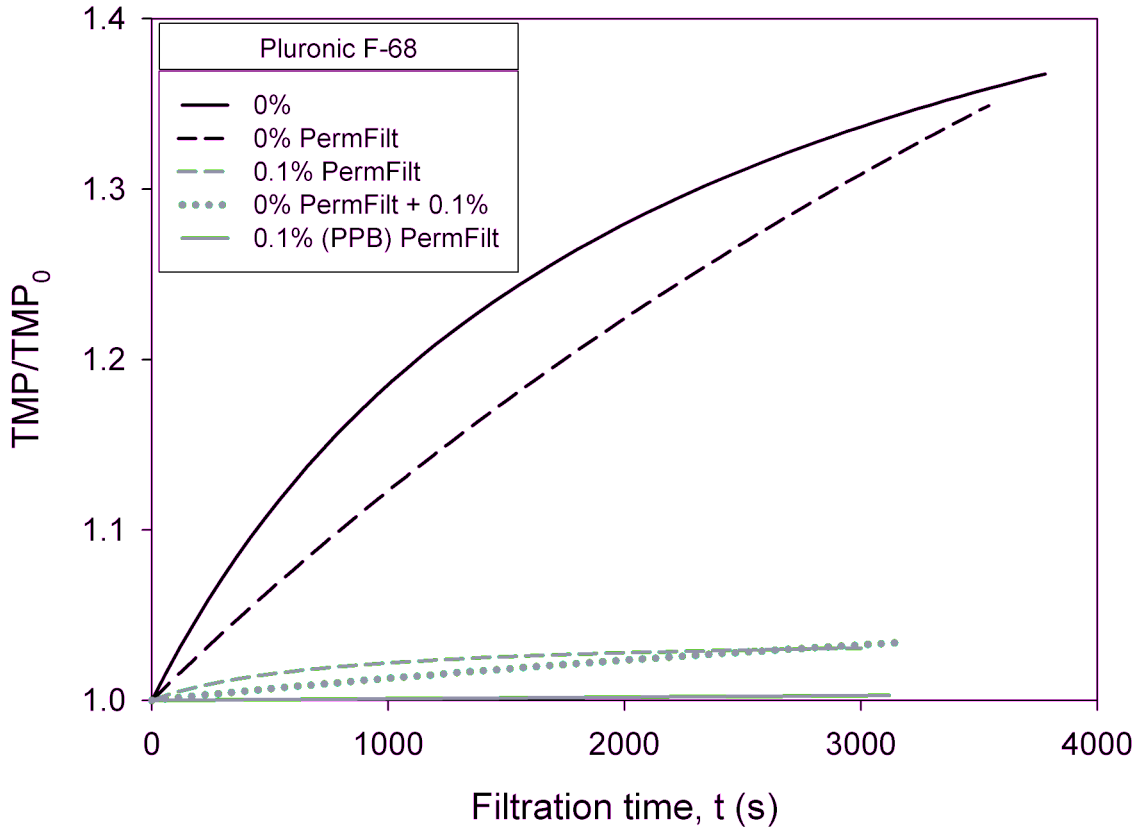

Fig. 5.5: Fitted normalized TMP profiles, Eq. (5.2) for the filtration and permeate filtration (PermFilt) of 2 g L^{-1} BSA in cell culture medium (CCM) with a 0.45 µm polysulfone hollow fiber membrane at 8000 s^{-1}. Pluronic F-68 was either not present (0%), added to the initial filtration (0.1%) or added just before the permeate filtration of an initially Pluronic F-68-free solution (+ 0.1%). Additionally, the profile of a permeate filtratioin of a 4 gL^{-1} BSA in phosphate buffer (PPB) solution is shown.

The filtration of the permeate collected during a 2 g L^{-1} BSA in CCM filtration displayed fouling but a different behaviour was observed, with an initial rapid linear increase followed by a slower linear increase. At the end of the permeate filtration, the TMP increase was similar to the TMP increase for the initial filtration (1.37 and 1.35 respectively, Table 5.1). The permeate filtration of a feed solution containing 0.1% PF68 and 2 g L^{-1} (0.1% PermFilt) was associated with a much lower normalized TMP increase

during the first half of the permeate filtration and the increase of the normalized TMP at the end of the filtration was negligible (1.03, Table 5.1). A similar observation was obtained for the filtration of a permeate collected during the filtration of a 2 g L^{-1} BSA solution without PF68 where 0.1% PF68 was added just prior the filtration of the permeate (0% + 0.1% PermFilt). As for the filtration of the permeate for a 2 g L^{-1} BSA PF68-free solution (0% PermFilt), the normalized TMP increased linearly, but the increase was also negligible (1.03, Table 5.1). Membrane fouling was not observed for the permeate filtration of a 4 g L^{-1} BSA in PPB solution containing 0.1% PF68, the normalized TMP remained almost constant throughout the filtration experiment (Fig. 5.5). The filtrations of pure PPB solution and CCM did not reveal any detectable fouling, indicating that no unspecific fouling occurred (data not shown) confirming that the observed fouling during permeate filtration of BSA in CCM solution can be attributed to the presence of BSA and its interaction with the CCM components. The estimated initial rates of fouling during the permeate filtration were reduced significantly when compared to the initial filtrations (Table 5.1), about half for the PF68-free solution and even more significantly for the PF68-containing solutions.

5.3.2 Aggregate characteristics

According to the two-step mechanism for MF fouling by BSA [44], the deposition of the protein aggregates plays a major role in the initial fouling of the membrane and is a precondition for long-term fouling. The feed, the retentate and the permeate of selected filtrations were analyzed for aggregate content and particle size distribution (PSD) by dynamic light scattering (DLS). An example of the particle size distribution is shown in Fig. 5.6 for a 2 g L^{-1} BSA in CCM solution. The scattering intensity plotted against the particle size reveals two distinct peaks. The first peak, around 8 nm, can be attributed to BSA monomers in the solution [51]. The second peak between 200 to 300 nm, corresponds to BSA aggregates. About 28% of the light scattering intensity was attributed to aggregates. Aggregates were present most likely because the BSA used in this study was produced by heat-shock precipitation [44].

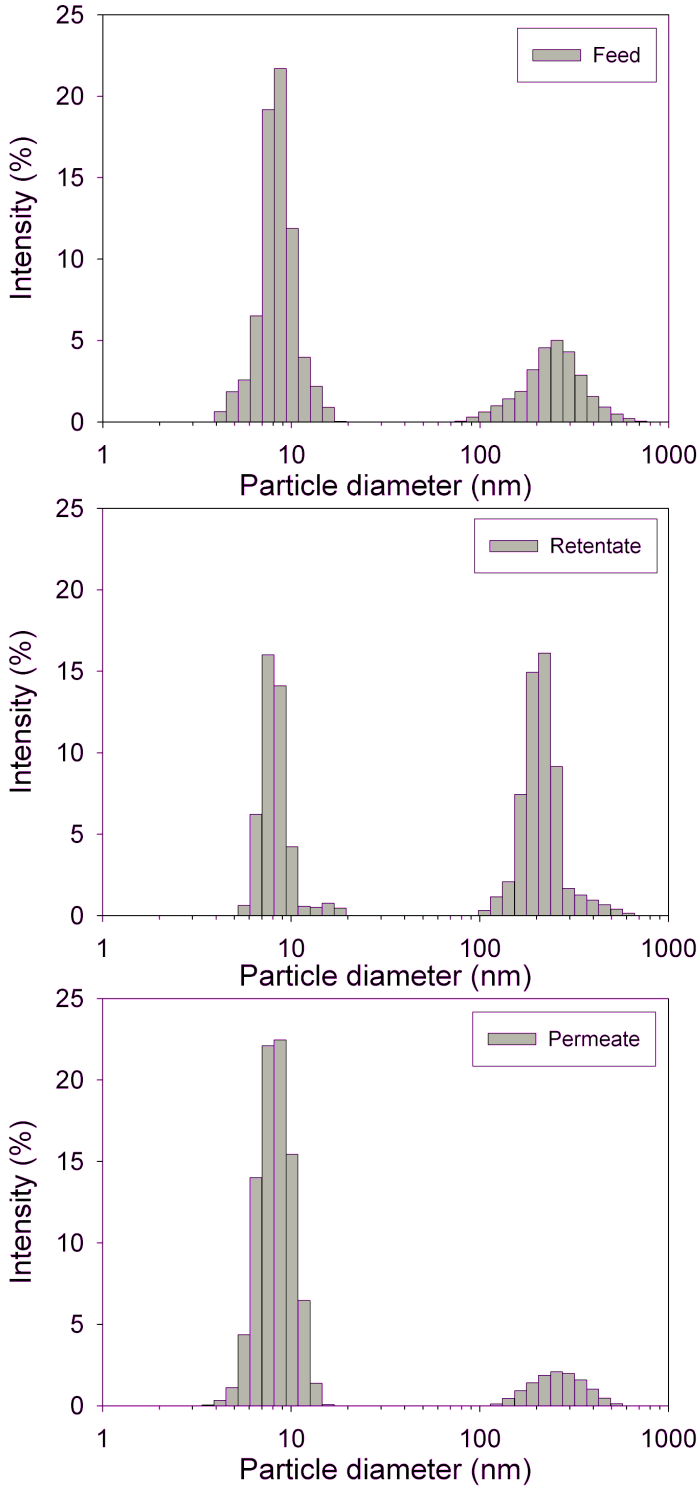

Fig. 5.6: Particle size distribution obtained by dynamic light scattering for the feed, retentate and permeate sample of a 2 g L^{-1} BSA in cell culture medium (CCM) solution filtered with a 0.45 µm polysulfone hollow fiber membrane.

The light scattering intensity of aggregates in the retentate was about 56%, likely due to a concentration effect and the retention of aggregates even though the membrane pores (450 nm on average) were larger than the aggregates (250 nm on average). Aggregates were also present in the permeate solution. This was not surprising since the aggregates were found to be slightly smaller than the membrane pores, ~250 nm compared to ~450 nm. However, the amount of aggregates in the permeate solution was significantly reduced indicating that a large portion of the aggregates was retained by the membrane or lost due to adsorption to the membrane.

The effect of PF68 on the aggregate intensities for 2 g L^{-1} BSA in CCM filtrations at 8000 s^{-1} is displayed in Fig. 5.7. Upon filtration of the permeate that was collected in the first filtration, the aggregate pattern was similar to the pattern observed during the initial filtration where the aggregate intensity increased significantly for the retentate and decreased for the permeate when no PF68 was present.

When 0.1% PF68 was added to the feed solution, the aggregate intensity in the retentate at the end of the filtration was similar to the feed, while the aggregate intensity for the permeate was much lower. The aggregate content in the permeate in the presence and absence of PF68 was similar. Upon filtration of the permeate collected for a feed solution that contained 0.1% PF68, the aggregates content of the retentate increased when compared to the feed while no aggregates were detected in the permeate solution. The addition of PF69 to the BSA solution did not affect the aggregate composition. Both BSA aggregate size and BSA aggregate intensity were similar for PF68-free and PF68-containing BSA solutions.

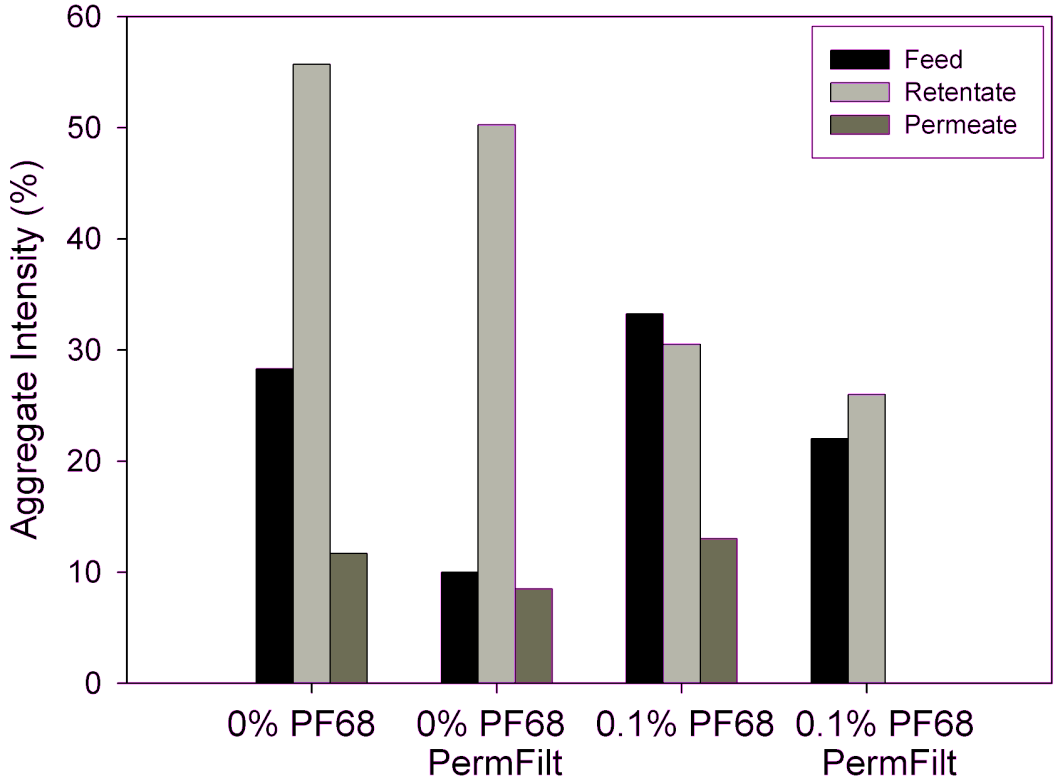

Fig. 5.7: Aggregate intensity in feed, retentate and permeate samples of filtrations of 2 g L^{-1} BSA in cell culture medium (CCM) at constant permeate flux of 30 Lmh and 8000 s^{-1} without (0%) and with (0.1%) added Pluronic F-68 and permeate filtrations thereof.

For all filtrations, a lower membrane fouling was observed during permeate filtration compared to the initial feed filtration. At the same time, aggregate levels were lower in the permeate solutions compared to the feed solutions. To test whether an increased aggregate content would result in increased membrane fouling, BSA aggregation was induced by heating a 2 g L^{-1} BSA in CCM solution to 65°C for 1h. The particle size distribution of the heat-treated sample, shown in Fig. 5.8, is quite different from the non-heat-treated BSA solution (Fig. 5.6). The aggregate intensity is much more important and accounts for about 75% of the total intensity. Besides the large aggregates, particles having a size of about 30 nm were detected in the sample (feed).

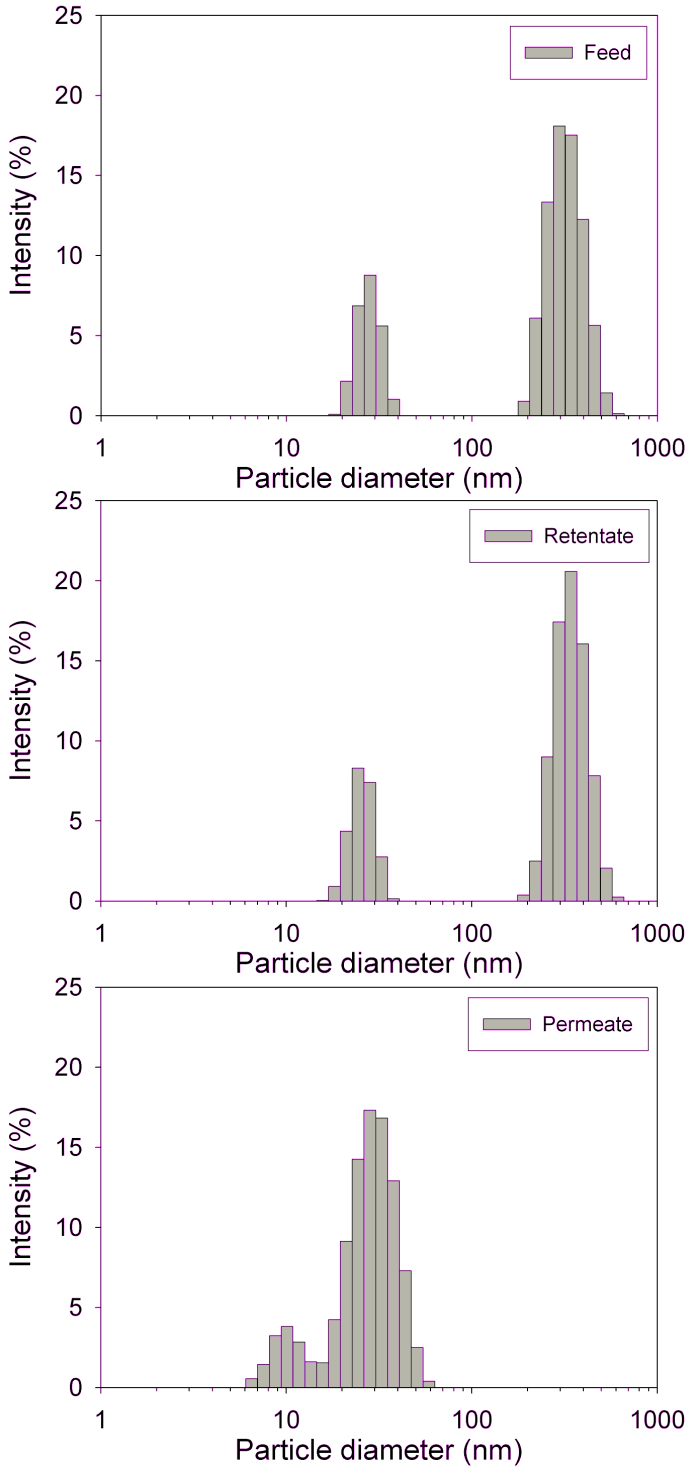

Fig. 5.8: Particle size distribution obtained by dynamic light scattering for a solution of 2 g L^{-1} BSA in cell culture medium (CCM) after heat-treatment (incubation at 65°C for 1 h) (feed) and after filtration with a 0.45 µm polysulfone hollow fiber membrane (retentate, permeate).

Heating the BSA solution and letting it cool down to room temperature prior to filtration increased the initial fouling rate significantly (Table 5.1), whereas the overall normalized TMP increase was similar to the filtration without prior heat-treatment (Fig. 5.9).

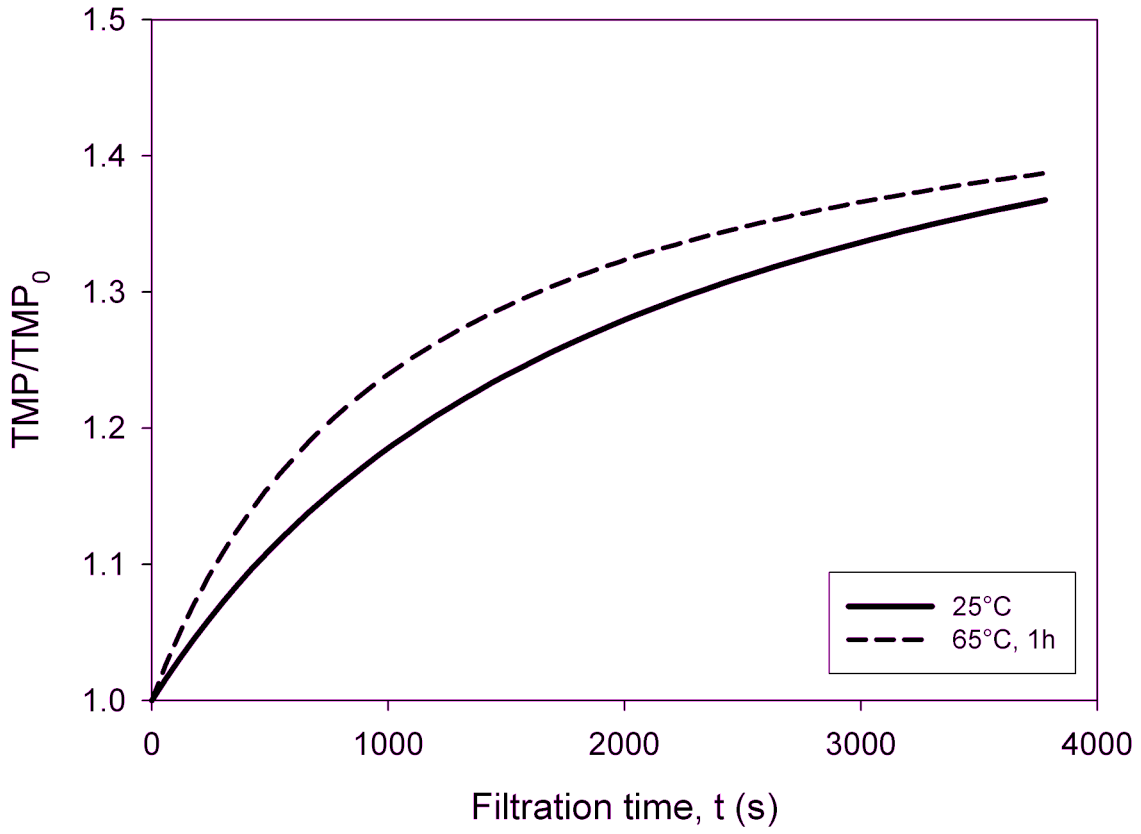

Fig. 5.9: Fitted normalized TMP profile for the filtration of 2 g L^{-1} BSA in cell culture medium (CCM) with a 0.45 µm polysulfone hollow fiber membrane at constant permeate flux. Dashed line represents filtration of feed solution after heat-pretreatment (65°C, 1 h), filtrations itself were operated at room temperature (~25°C).

The intensity distribution in the retentate of the heat-treated sample was very similar to the feed sample of this filtration (Fig. 5.8). The permeate on the other hand did not contain large aggregates and the scattering intensity of particles of size 30 nm increased to 85%. Furthermore, 14% of the intensity came from particles of about 10 nm. The small particles represent the BSA monomers which were not detected in the feed and permeate sample

most likely because of the interference from the higher amount of large particles with very high scattering intensity. After removal of the large aggregates, BSA monomers were detected again. A study on heat-induced BSA denaturation revealed the formation of irreversible small-order oligomers and aggregates [48] consistent with the aggregate profiles reported in the current study.

5.3.3 Effect of feed composition on the irreversible fouling

The water flux estimates obtained before the filtration and after flushing the membrane were used to estimate the contribution of the irreversible membrane fouling (R_{irr}) (Table 5.1). The highest irreversible fouling resistance was observed for the higher BSA concentration in the PPB solution and for the heat-treated BSA in CCM solution. The addition of PF68 clearly reduced the irreversible fouling, although no difference could be observed for the effect of PF68 for the concentration range investigated in this study for the PPB system. The irreversible fouling for the PF68 containing PPB solutions was reduced by 28% for 2 g L^{-1} BSA and by 55% for 4 g L^{-1} BSA. For CCM solution with 2 g L^{-1} BSA, the irreversible fouling was reduced by 23% with the addition of 0.1% PF68. Delayed addition of PF68 still reduced the irreversible fouling by 39% for 4 g L^{-1} BSA in PPB and by 36% for 2 g L^{-1} BSA in CCM. Surprisingly, the delayed PF68 addition for 2 g L^{-1} BSA in CCM solution resulted in a reduction of irreversible fouling (36%) beyond the reduction achieved when PF68 was present at the beginning of the filtration (23%).

The irreversible fouling of the permeate filtration when no PF68 was present for the 2 g L^{-1} BSA CCM solution was reduced by half compared to the initial filtration. The permeate filtration with PF68 containing CCM solutions (including PF68 added prior to the permeate filtration) stood out in that no irreversible fouling was detected which is consistent with the extremely low fouling deduced from the normalized TMP increase observed (Fig. 5.5).

As the high irreversible fouling conditions were associated with conditions of high initial rates of fouling for filtrations under the same conditions (PPB or CCM, absence or presence of PF68), the irreversible fouling, R_{irr}, was plotted as a function of the initial fouling rate, i_f. The plot revealed a linear relationship between the irreversible fouling

resistance and the initial fouling rate for BSA solutions in both PPB and CCM solutions (Fig. 5.10).

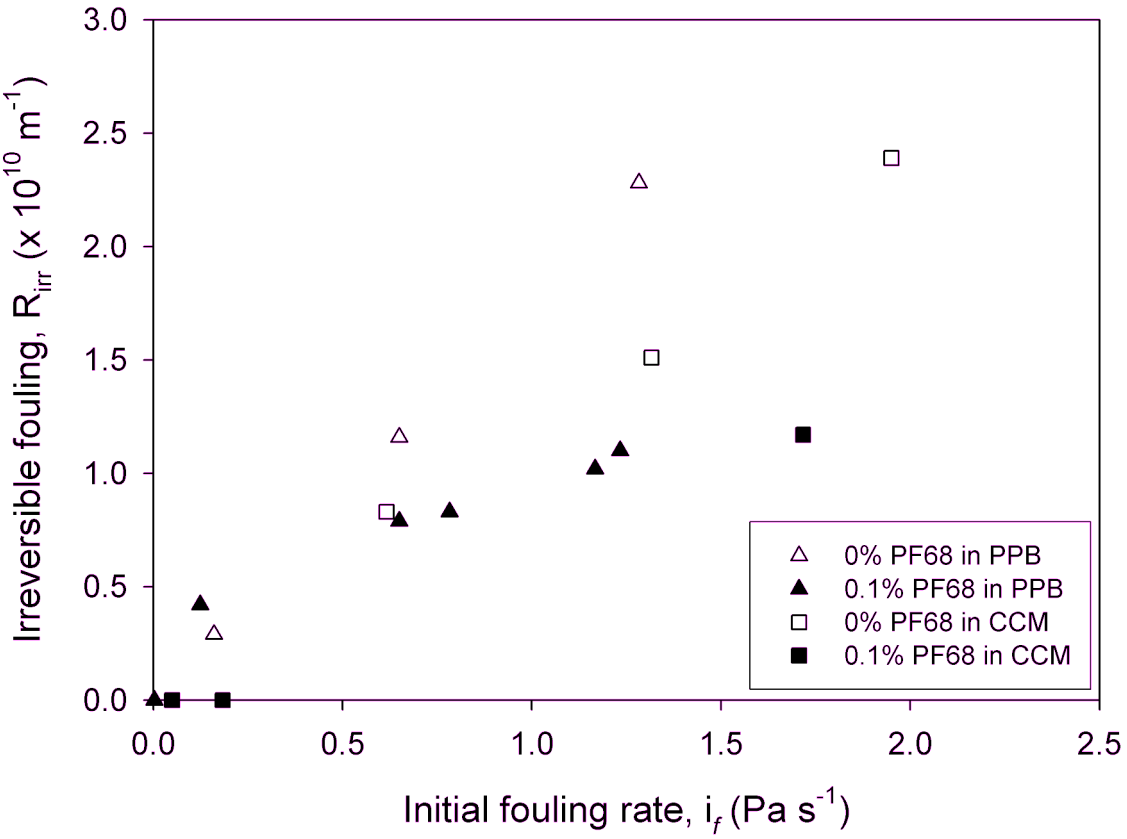

Fig. 5.10: Irreversible fouling resistance obtained for the microfiltration of BSA in phosphate buffer (PPB) (triangle) or cell culture medium (CCM) (square) solution without (open symbol) and with (closed symbol) addition of Pluronic F-68 as a function of the initial fouling rate.

The slope of the linear relationship appears to be a characteristic of the presence of PF68 and the type of solution (PPB or CCM). The linear relationship for the PF68 containing solutions falls below those without added PF68, suggesting that PF68 affected the fouling mechanism or at least the severity of the irreversible fouling.

5.4 Discussion

5.4.1 Effect of solution composition

Membrane fouling as deduced from normalized TMP profiles was observed for BSA solutions in both PPB and CCM during microfiltration using a 0.45 µm polysulfone hollow fiber membrane module operated at constant permeate flux. The estimated initial fouling rates, the normalized TMP at the end of the filtrations and the irreversible fouling all increased with increasing BSA concentration which is in agreement with previous studies [9;89]. The fouling was more pronounced for CCM when compared to PPB solutions likely because CCM contains a variety of components, such as salts, that can impact on the interactions of BSA with the membrane. The estimated initial rate of membrane fouling by BSA, deduced from a simple empirical model (Eq. (5.2)), was linked to the presence of aggregates as seen from the permeate filtration experiments for the 2 g L^{-1} BSA in CCM solutions (Fig. 5.7) and the filtration of the heat-treated 2 g L^{-1} BSA in CCM solution (Fig. 5.8). The estimated initial fouling rate was reduced by half for the permeate filtration but increased by 50% for the filtration of the solution with a more significant aggregate content. In contrast, the normalized TMP at the end of the filtration was quite similar for both systems. The differences in initial fouling rate are consistent with the two-step mechanism for BSA fouling proposed by Kelly et al. [44] where the relative amount of aggregates and monomers present in the feed solution is related to the overall membrane fouling while the initial rate of fouling is directly related to the deposition of protein aggregates [44;89]. For the low aggregate solutions obtained by collection of the permeate during initial filtration operations, the filtration through the 0.45 µm pore size membrane did not remove completely the aggregates as was shown by DLS analysis (Fig. 5.6). The presence of aggregates in the permeate explains why membrane fouling could still be seen upon subsequent filtration of the permeate. Previous studies reported fouling-free filtration or considerable reduction in the extent of fouling when protein solutions were pre-filtered. For example, the filtration of the permeate collected during the filtration of 4 g L^{-1} whey protein solution through a 0.8 µm ceramic membrane proceeded almost fouling free and DLS revealed that particles around 500 nm in size were removed during the initial filtration

[35]. Kelly and Zydney [43] used a 100,000 MWCO membrane to eliminate aggregates prior to filtration using a 0.22 μm membrane which more or less prevented membrane fouling based on minimal flux decline criteria.

A linear correlation seen between the estimated initial fouling rate and the experimentally measured irreversible fouling (Fig. 5.12) suggests that the fouling occurred early during the filtration operation and would constitute the premise for the irreversible fouling measured at the end of the filtration operation. As the irreversible fouling requires stronger interactions between foulants and the membrane and considering that the initial fouling is associated with the protein aggregates, we suggest that protein aggregates adsorbed strongly to the membrane, causing the higher irreversible fouling resistance.

5.4.2 Effect of Pluronic F-68

The filtrations of BSA solutions containing PF68 presented in Fig. 5.3 to 5.5 indicate that the addition of PF68 affects the BSA fouling characteristics. The effect is based on PF68-BSA interactions since the filtration of PF68 in PPB solutions was not different from the filtration of nanopure water. Although the initial rate of fouling for PF68-containing solutions was similar to PF68-free solutions, the long-term fouling was reduced by about 25% when PF68 was present. Pluronic copolymers are known to reduce the adsorption of proteins to hydrophobic surfaces by binding to hydrophobic surfaces via the hydrophobic PPO chains which leaves the hydrophilic PEO to act like a guard [110]. In the present study, a polysulfone microfiltration membrane was used which is considered relatively hydrophobic. However, according to the manufacturer, the surface has been treated to make it more hydrophilic though no information on surface hydrophilicity is available. Higuchi et al. [108] reported a 50% reduction in human serum albumin adsorption to polysulfone disk membranes when the membranes were coated with Pluronic F-68 prior to static adsorption experiments.

Since the effect of PF68 is directed essentially to the long-term fouling, it is possible that PF68 does not prevent aggregate deposition, but does reduce the deposition of BSA monomers that occurs once aggregate deposition has taken place. The filtration of the

permeate of previous solutions was highly interesting and revealed that the filtration of permeate or the addition of PF68 to a feed solution reduced the initial rate of fouling or the overall fouling, respectively. The filtration of permeate containing PF68 eliminated most of the membrane fouling (Fig. 5.6) suggesting that PF68 reduces protein-membrane interaction, as well as protein-protein interaction and associated aggregate formation. Pluronic is known to reduce cell damage in aerated bioreactors by reducing hydrophobic interactions between cells and bubbles [113]. A similar mechanism could prevail in the filtration experiments reported in this study whereby protein-protein interactions are reduced. If only a limited number of aggregates are present and PF68 reduces or prevents the generation of more aggregates, fouling would be minimal as observed for the 2 g L^{-1} BSA in CCM solution (Fig. 5.6). The similar fouling profile observed for the filtration of the PF68-free permeate with added PF68 and the filtration of the PF68-containing permeate indicates that the low fouling was not caused by the removal of the fouling species during the initial fouling, but rather by a direct effect of the presence of PF68 in the 2 g L^{-1} BSA in CCM solution.

The effect of sodium dodecyl sulphate (SDS), also an amphiphilic molecule like PF68, on the fouling of zirconium oxide membranes (pore size 0.1µm) by lactoferrin was investigated by Chilukuri et al. [87]. The presence of SDS from the start significantly reduced total fouling resistance which was determined from the TMP during constant permeate flux filtration. The total fouling resistance even decreased when the addition of SDS was delayed and occurred after 60 min of filtration, indicating that SDS affected the fouling that had already occurred. The preferential adsorption of SDS and the possible displacement of adsorbed protein was proposed as possible explanation for the behaviour observed. One can hypothesize that PF68 may act like SDS by preventing the formation of additional aggregates leading to reduced irreversible fouling. However, PF68 did not reverse fouling and fouling continued even in the presence of PF68 though at a lower rate for the 4 g L^{-1} BSA in PPB solution (Fig. 5.3 C) and the 2 g L^{-1} BSA in CCM solution (Fig. 5.4).

5.5 Conclusions

The effect of initial and long term fouling for BSA in PPB and CCM solutions was quantified using an empirical model that fitted the TMP profiles obtained during cross-flow microfiltration in constant permeate flux mode. The aggregate content was modulated by heat-treatment of the feed and the use of permeate from prior filtrations. The estimated initial fouling rate was related to the level of aggregate content in the feed solution and to the irreversible fouling resistance estimated experimentally at the end of the filtration of BSA in PPB and CCM solutions. The apparent increase of the estimated initial fouling rate with increase in aggregate content is in agreement with the two-step fouling mechanism for BSA proposed by Kelly et al. [44].

Increasing the BSA concentration in the feed from 0.1 to 4 g L^{-1} and replacing potassium phosphate buffer by the more complex cell culture medium, lead to increased initial fouling rates, higher normalized TMPs at the end of the filtrations and increased irreversible fouling.

The addition of Pluronic F-68 to the BSA solution did not affect the estimated initial fouling rate for the BSA in PPB solutions but increased for the 2 g L^{-1} BSA in CCM solution. Long term fouling was affected by PF68 and the normalized TMP at the end of the filtration was reduced for all protein concentrations tested and for both BSA in PPB and BSA in CCM solutions. Irreversible fouling was also reduced upon addition of PF68 to both 2 g L^{-1} BSA in PPB and CCM solutions. It appears that PF68 acts predominantly at a later stage of the fouling, possibly reducing protein-protein and/or protein-aggregate interactions. This is supported by the observation of reduced long-term fouling and irreversible fouling for delayed addition of PF68 to 2 g L^{-1} BSA in CCM and 4 g L^{-1} in PPB solutions. The structure of PF68 would allow for noncovalent binding of the hydrophobic block (PPO) to hydrophobic regions of the protein aggregates, thereby reducing hydrophobic interactions between the deposited aggregates and the bulk protein.

A correlation exists between the initial fouling rate and the irreversible fouling of BSA in PPB and CCM solutions, suggesting the formation of irreversible fouling early on during the filtration. The correlation was linear for PF68-free solutions and the slope was higher

for PPB solutions when compared to CCM solutions. The presence of PF68 in the BSA in PPB and CCM solutions reduced the slope, a lower irreversible fouling at similar estimated initial fouling rates were observed when compared to the PF68-free solutions.

While previous studies concentrated on membrane coating or other forms of membrane pre-treatment with surfactants to reduce protein adsorption, we added Pluronic F-68 directly to the solution. The positive effect of Pluronic F-68 addition is reassuring since it is quite frequently added to serum-free cell culture media. It would be important to further investigate and confirm that the positive effect of PF68 is also observed with other membrane material and proteins.

6

Conclusions

Membrane fouling was studied for a hollow fiber microfiltration (MF) system operated at constant permeate flux. The hollow fiber system represented a bench-scale system suitable to separate cells and large particles from cell culture broth as an initial step in the downstream processing of biopharmaceuticals. Feed solutions subjected to the MF included solutions of two types (beta-interferon and immunoglobulin G producing lines) of Chinese Hamster Ovary (CHO) cell culture broth (cell-containing and supernatant) and solutions of bovine serum albumin (BSA) as a representative model protein foulant.

Membrane fouling was observed for all biological solutions filtered using the hollow fiber system, though the observed fouling was low. The low fouling can be attributed to the filtration conditions chosen, with a constant permeate flux of 30 Lmh and a 0.45 µm polysulfone membrane. The membrane fouling was observed as an increase in normalized TMP with filtration time and as an increase in the hydraulic resistance assessed by measuring the water flux. The typical experimental TMP profile consisted of an initial rapid increase followed by a slower long-term increase. A relatively stable TMP was observed only for the cell culture supernatant filtered at a shear rate of 8000 s^{-1} with the 0.45 µm membrane. The TMP increase at the end of the filtration ranged from about 1.25 for the CHO cell culture supernatant, 1.28 for 2 g L^{-1} BSA in phosphate buffer and 1.37 for 2 g L^{-1} BSA in CHO cell culture medium to 1.49 for 4 g L^{-1} BSA in phosphate buffer. This showed that BSA is a strong foulant, comparable to the complex CHO cell culture broth.

A new mechanistic model applicable to cross-flow MFs operated at constant permeate flux was developed. Fouling was assumed to occur first by pore blockage with subsequent cake formation over the blocked areas of the membrane. The model accounted for cross-flow effects by a term for deposit removal and reduction in blocked area. The model fitted the TMP data of CHO cell culture broth (cell-containing and supernatant) as well as BSA solutions. The fit was good for filtrations at two different shear rates (4000 s^{-1} and 8000 s^{-1}) and 0.45 µm and 0.2 µm membrane pore sizes. The model also correctly reflected the differences in fouling rates when the BSA concentration increased from 2 g L^{-1} to 4 g L^{-1}.

The estimated model parameters included the pore blockage parameter (α) and the cross-flow parameters for cake formation (k_c) and pore blockage (k_{pb}). At a shear rate of

8000 s^{-1} and 0.45 µm pore size, the best fit value for α (m^2 kg^{-1}) was 0.78 for the BSA solutions, 0.18 for the CHO cell-containing culture broth and 0.24 for the CHO cell culture supernatant. The significantly higher α value for BSA could reflect the higher adsorption properties of BSA or the differences in the fouling species contained in the CHO cell culture broth. In fact, the total protein content of the broth was significantly lower than its organic content. For the cell culture supernatant, significant differences for the α estimates were obtained according to the pore size of the membrane. The estimated α increased from 0.2 to 0.38 at low shear rate and from 0.24 to 0.49 at high shear rate when decreasing the membrane pore size from 0.45 µm to 0.20 µm.

At a shear rate of 8000 s^{-1} and 0.45 µm pore size, the best fit value for k_c (s^{-1}) was 0.0025 for the BSA solutions, 0.0023 for the CHO cell containing broth and 0.0012 for the CHO cell culture supernatant. It is likely that a difference in the feed composition affected the effectiveness of the cross-flow in the fibers and the cake removal.

The fitted cross-flow parameter for pore blockage, k_{pb} (m^4 s^{-1} kg^{-1}), at a shear rate of 4000 s^{-1} and 0.45 µm pore size was very similar for filtrations of CHO cell culture broth (6.1×10^{-3}) and CHO cell culture supernatant (7.0×10^{-3}) but higher for BSA solutions (38×10^{-3}). As with the pore blockage parameter, differences in the fouling mechanism can be attributed to differences in the feed composition. Filtration conditions also affected the best fit for k_{pb}. For the cell culture supernatant, the estimated k_{pb} increased by a factor of ~1.5 upon decrease of the pore size from 0.45 to 0.20 µm while decreasing the shear rate from 8000 s^{-1} to 4000 s^{-1} resulted in a decrease of the k_{pb} estimate.

The membrane pore size was a significant factor for the extent of irreversible fouling during the filtration of CHO cell culture supernatant. Irreversible fouling resistance was about twice as high for the 0.2 µm membrane pore size compared to the 0.45 µm membrane pore size. In contrast, reversible fouling was affected by the cross-flow velocity where the reversible fouling increased by a factor of 2 to 3 upon doubling the cross-flow velocity.

An empirical model with two fitted parameters was introduced to describe TMP profiles and to derive and calculate the initial fouling rate (i_f) for the filtration of BSA solutions. The model reflected the typical TMP increase of higher TMP initial increase with

subsequent levelling off. An increase in the estimated initial fouling rate was observed for the filtration of BSA solutions with a higher aggregate content. This was in agreement with a proposed two-step fouling mechanism for BSA, where the fouling is initiated by the deposition of BSA aggregates followed by the deposition of BSA molecules on the initial BSA aggregate deposits.

The effect of CHO cell culture medium (CCM) was examined by comparing BSA solutions in potassium phosphate buffer (PPB) and CCM. Both the estimated initial fouling rate and the extent of irreversible fouling increased with increasing BSA concentration. A linear correlation between the estimated initial fouling rate and irreversible fouling was observed for both BSA in PPB and CCM, with a higher slope for BSA in PPB. The linear correlation suggested that the irreversible fouling was associated with the initial fouling by the BSA aggregates.

The role of the non-ionic surfactant Pluronic F-68 (PF68), an additive present in CHO cell culture media, was studied for the filtration of BSA solutions. PF68 can be added to cell cultures to protect the cells from damage due to shear. The addition of PF68 to BSA solutions reduced the overall fouling (normalized TMP at the end of the filtration), essentially by reducing the irreversible fouling. The reduction in irreversible fouling ranged from 23% for 2 g L^{-1} BSA in CCM to 55% for 4 g L^{-1} BSA in PPB. The estimated initial fouling rates were surprisingly not reduced when PF68 was present. PF68 did not seem to affect the initial protein-membrane interactions. The positive effect of PF68 on the long-term membrane fouling by BSA could be explained by a reduction of protein-protein and/or protein-aggregate interactions in the presence of PF68.

The positive effect of PF68 on the overall membrane fouling was however not observed during the filtration of the supernatant for b-IFN producing CHO cell culture containing PF68 in comparison to IgG producing CHO cell culture that did not contain PF68. One can suspect that the diverse composition of CHO cell culture broth may have interfered with the effects associated with PF68.

This study revealed different membrane fouling behaviour using solutions of the model protein BSA and CHO cell culture supernatant. Fig. 6.1 shows the irreversible fouling as well as the estimated initial fouling rates for both CHO cell supernatants and BSA solutions filtered at a shear rate of 8000 s^{-1} with a 0.45 µm pore size membrane. The irreversible fouling and estimated initial fouling rate for BSA in PPB were very similar to that of the CHO cell supernatant. The CHO cell supernatant contained PF68 (0.1% was added to the b-IFN producing CHO cell culture). In comparison to the BSA solutions containing 0.1% PF68, the irreversible fouling was slightly higher at comparable initial fouling rate estimates. This could indicate that some of the fouling species in the CHO cell broth were adsorbed more strongly to the membrane.

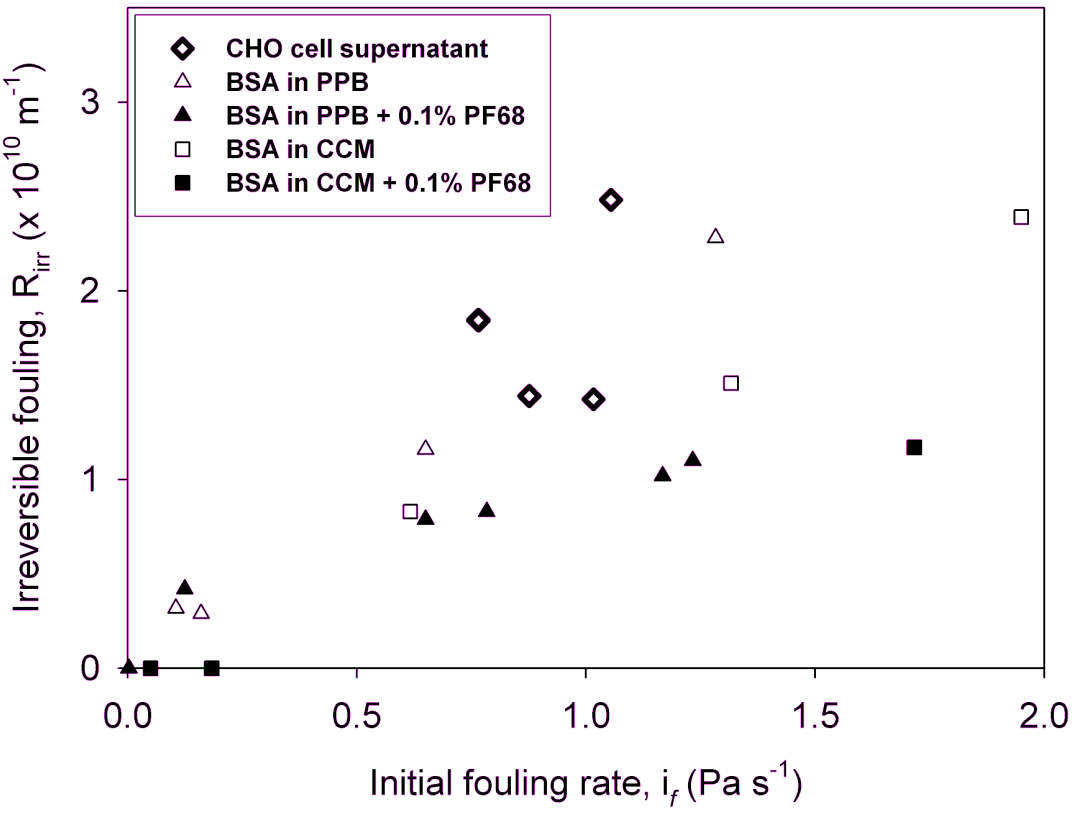

Fig. 6.1: Irreversible fouling resistance obtained for the microfiltration of CHO cell culture supernatant and BSA solutions as a function of the initial fouling rate. The filtration was operated at constant flux (30 Lmh), a shear rate of 8000 s^{-1} and with a 0.45 µm pore size hollow fiber membrane.

In summary, this thesis presents a newly developed mechanistic model and an empirical model for the description of the TMP profiles obtained during the cross-flow microfiltration of BSA solutions and CHO cell culture broths. The shear rate, membrane pore size and feed composition (e.g. presence of cells, BSA concentration, buffer solution, presence of media additive) affected the fouling mechanisms and the extent of membrane fouling. Based on the results presented in this thesis, the following future work is suggested:

1. Experimental determination of the input parameters for the mechanistic model for individual cell culture broths including the fractional amount of bulk components contributing to membrane deposit growth (*f'*), the proportionality coefficient for deposit layer resistance (k_p) and the resistance of the initial deposit (R_{p0}).

2. Microfiltration and membrane fouling analysis for other types of mammalian cell culture broths that would enable the identification of the cell culture components and culture conditions critical to the initial, overall and irreversible membrane fouling.

3. Determination of the target protein concentration and estimation of its recovery in the permeate for different filtration conditions.

4. Investigation of the effect of Pluronic F-68 on the membrane fouling caused by cell culture components.

5. Investigation of the specific effect of Pluronic F-68 on the membrane fouling caused by bovine serum albumin.

.

References

[1] van Reis, R., Zydney, A. Bioprocess membrane technology. *J. Membr. Sci.* **297** (2007) 16-50.

[2] Krstic, D. M., Markov, S. L., Tekic, M. N. Membrane fouling during cross-flow microfiltration of *Polyporus squamosus* fermentation broth. *Biochem. Eng. J.* **9** (2001) 103-109.

[3] Nagata, N., Herouvis, K. J., Dziewulski, D. M., Belfort, G. Cross-Flow membrane microfiltration of a bacterial fermentation broth. *Biotechnol. Bioeng.* **34** (1989) 447-466.

[4] Zeman, L. J., Zydney, A. L. Microfiltration and Ultrafiltration: Principles and Applications. Marcel Dekker, Inc., New York.1996

[5] van Reis, R., Leonard, L. C., Hsu, C. C., Builder, S. E. Industrial-Scale harvest of proteins from mammalian-cell culture by tangential flow filtration. *Biotechnol. Bioeng.* **38** (1991) 413-422.

[6] Butler, M. Animal cell culture and technology. IRL Press, New York.1996

[7] Butler, M. The characteristics and growth of cultured cells. In Mammalian cell biotechnology (Butler, M., ed) pp. 1-25, Oxford University Press, Oxford, 1991.

[8] Macleod, A. J. Serum and its fractionation. In Mammalian cell biotechnology (Butler, M., ed) pp. 27-37, Oxford University Press, Oxford, 1991.

[9] Marshall, A. D., Munro, P. A., Tragardh, G. The effect of protein fouling in microfiltration and ultrafiltration on permeate flux, protein retention and selectivity - A literature-review. *Desalination* **91** (1993) 65-108.

[10] Jonsson, G., Pradanos, P., Hernandez, A. Fouling phenomena in microporous membranes. Flux decline kinetics and structural modifications. *J. Membr. Sci.* **112** (1996) 171-183.

[11] Russotti, G., Göklen, K. E., Wilson, J. J. Development of a pilot-scale microfiltration harvest for the isolation of physostigmine from *Streptomyces griseofuscus* broth. *J. Chem. Tech. Biotechnol.* **63** (1995) 37-47.

[12] Frenander, U., Jonsson, A. S. Cell harvesting by cross-flow microfiltration using a shear-enhanced module. *Biotechnol. Bioeng.* **52** (1996) 397-403.

[13] Lojkine, M. H., Field, R. W., Howell, J. A. Crossflow microfiltration of cell suspensions: A review of models with emphasis on particle size effects. *Trans. Inst. Chem. Eng.* **70** (1992) 149-164.

[14] Maiorella, B., Dorin, G., Carion, A., Harano, D. Crossflow microfiltration of animal cells. *Biotechnol. Bioeng.* **37** (1991) 121-126.

[15] Glimenius, R. Microfiltration - state of the art. *Desalination* **53** (1985) 363-372.

[16] Belfort, G., Davis, R. H., Zydney, A. L. The behavior of suspensions and macromolecular solutions in crossflow microfiltration. *J. Membr. Sci.* **96** (1994) 1-58.

[17] Wilkes, J. O. Fluid Mechanics for chemical engineers. Prentice-Hall, New Jersey.1999

[18] Faibish, R. S., Elimelech, M., Cohen, Y. Effect of interparticle electrostatic double layer interactions on permeate flux decline in crossflow membrane filtration of colloidal suspensions: An experimental investigation. *J. Colloid Interface Sci.* **204** (1998) 77-86.

[19] Berthold, W., Kempken, R. Interaction of cell-culture with downstream purification - A case-study. *Cytotechnology* **15** (1994) 229-242.

[20] Tardieu, E., Grasmick, A., Geaugey, V., Manem, J. Influence of hydrodynamics on fouling velocity in a recirculated MBR for wastewater treatment. *J. Membr. Sci.* **156** (1999) 131-140.

[21] Harscoat, C., Jaffrin, M. Y., Bouzerar, R., Courtois, J. Influence of fermentation conditions and microfiltration processes on membrane fouling during recovery of glucuronane polysaccharides from fermentation broths. *Biotechnol. Bioeng.* **65** (1999) 500-511.

[22] Field, R. W., Wu, D., Howell, J. A., Gupta, B. B. Critical flux concept for microfiltration fouling. *J. Membr. Sci.* **100** (1995) 259-272.

[23] Li, H., Fane, A. G., Coster, H. G. L., Vigneswaran, S. Direct observation of particle deposition on the membrane surface during crossflow microfiltration. *J. Membr. Sci.* **149** (1998) 83-97.

[24] Kwon, D. Y., Vigneswaran, S., Fane, A. G., Ben Aim, R. Experimental determination of critical flux in cross-flow microfiltration. *Sep. Purif. Technol.* **19** (2000) 169-181.

[25] Russotti, G., Göklen, K. E. Crossflow membrane filtration of fermentation broth. In Membrane Separations in Biotechnology (Wang, W. K., ed) pp. 85-159, Marcel Dekker Inc., New York, 2001.

[26] Howell, J. A. Sub-critical flux operation of microfiltration. *J. Membr. Sci.* **107** (1995) 165-171.

[27] Klein, G. M., Meier, J., Kottke, V. Fouling in membrane apparatus: The mechanisms of particle deposition. *Food Bioprod. Process.* **77** (1999) 119-126.

[28] Bowen, W. R., Gan, Q. Properties of microfiltration membranes: flux loss during constant pressure permeation of bovine serum albumin. *Biotechnol. Bioeng.* **38** (1991) 688-696.

[29] Bowen, W. R., Hughes, D. T. Properties of microfiltration membranes. Part 2. Adsorption of bovine serum albumin at aluminium oxide membranes. *J. Membr. Sci.* **51** (1990) 189-200.

[30] Defrise, D., Gekas, V. Microfiltration membranes and the problem of microbial adhesion - A literature survey. *Process Biochem.* **23** (1988) 105-116.

[31] Yamagiwa, K., Kobayashi, H., Onodera, M., Ohkawa, A. Antifoam fouling and its reduction by surfactant precoat treatment of polysulphone ultrafilter. *Biotechnol. Tech.* **8** (1994) 267-270.

[32] Chan, R., Chen, V. The effects of electrolyte concentration and pH on protein aggregation and deposition: critical flux and constant flux membrane filtration. *J. Membr. Sci.* **185** (2001) 177-192.

[33] Tarleton, E. S., Wakeman, R. J. Understanding flux decline in cross-flow microfiltration: Part III - Effects of membrane morphology. *Chem. Eng. Res. Des.* **72** (1994) 521-529.

[34] Choi, H., Zhang, K., Dionysiou, D. D., Oerther, D. B., Sorial, G. A. Influence of cross-flow velocity on membrane performance during filtration of biological suspension. *J. Membr. Sci.* **248** (2005) 189-199.

[35] Mourouzidis-Mourouzis, S. A., Karabelas, A. J. Whey protein fouling of microfiltration ceramic membranes - Pressure effects. *J. Membr. Sci.* **282** (2006) 124-132.

[36] Hermia, J. Constant pressure blocking filtration laws - Application to power-law non-newtonian fluids. *Trans. Inst. Chem. Eng.* **60** (1982) 183-187.

[37] Hlavacek, M., Bouchet, F. Constant flow-rate blocking laws and an example of their application to dead-end microfiltration of protein solutions. *J. Membr. Sci.* **82** (1993) 285-295.

[38] Ho, C. C., Zydney, A. L. Transmembrane pressure profiles during constant flux microfiltration of bovine serum albumin. *J. Membr. Sci.* **209** (2002) 363-377.

[39] Bolton, G., LaCasse, D., Kuriyel, R. Combined models of membrane fouling: Development and application to microfiltration and ultrafiltration of biological fluids. *J. Membr. Sci.* **277** (2006) 75-84.

[40] Bowen, W. R., Hall, N. J. Properties of microfiltration membranes - mechanisms of flux loss in the recovery of an enzyme. *Biotechnol. Bioeng.* **46** (1995) 28-35.

[41] Tracey, E. M., Davis, R. H. Protein fouling of track-etched polycarbonate microfiltration membranes. *J. Colloid Interface Sci.* **167** (1994) 104-116.

[42] Palecek, S. P., Zydney, A. L. Intermolecular electrostatic interactions and their effect on flux and protein deposition during protein filtration. *Biotechnol. Prog.* **10** (1994) 207-213.

[43] Kelly, S. T., Zydney, A. L. Protein fouling during microfiltration: Comparative behavior of different model proteins. *Biotechnol. Bioeng.* **55** (1997) 91-100.

[44] Kelly, S. T., Senyo Opong, W., Zydney, A. L. The influence of protein aggregates on the fouling of microfiltration membranes during stirred cell filtration. *J. Membr. Sci.* **80** (1993) 175-187.

[45] Güell, C., Czekaj, P., Davis, R. H. Microfiltration of protein mixtures and the effects of yeast on membrane fouling. *J. Membr. Sci.* **155** (1999) 113-122.

[46] Chandavarkar, A. S. Dynamics of fouling of microporous membranes by proteins. 1990. PhD thesis. Massachusetts Institute of Technology, Cambridge, MA.

[47] Chi, E. Y., Krishnan, S., Randolph, T. W., Carpenter, J. F. Physical stability of proteins in aqueous solution: mechanism and driving forces in nonnative protein aggregation. *Pharmaceutical Research* **20** (2003) 1325-1334.

[48] Vaiana, S. M., Emanuele, A., Palma-Vittorelli, M. B., Palma, M. U. Irreverible formation of intermediate BSA oligomers requires and induces conformational changes. *Proteins: Struct. , Funct. , Bioinf.* **55** (2004) 1053-1062.

[49] Palecek, S. P., Zydney, A. L. Hydraulic permeability of protein deposits formed during microfiltration: effect of solution pH and ionic strength. *J. Membr. Sci.* **95** (1994) 71-81.

[50] Palecek, S. P., Mochizuki, A. L., Zydney, A. L. Effect of ionic environment on BSA filtration and the properties of BSA deposits. *Desalination* **90** (1993) 147-159.

[51] Ho, C. C., Zydney, A. L. Effect of membrane morphology on the initial rate of protein fouling during microfiltration. *J. Membr. Sci.* **155** (1999) 261-275.

[52] Girones, M., Lammertink, R. G. H., Wessling, M. Protein aggregate deposition and fouling reduction strategies with high-flux silicon nitride microsieves. *J. Membr. Sci.* **273** (2006) 68-76.

[53] Foster, J. F. Some aspects of the structure and conformational properties of serum albumin. In Albumin structure, function and uses (Rosenoer, V. M., Oratz, M., and Rothschild, M., eds.) pp. 53-84, Pergamon Press, Oxford, 1977.

[54] Zhang, J., Cai, Z., Cong, W., Su, Z., Ouyang, F. Mechanisms of protein fouling in microfiltration. II. adsorption and deposition of proteins on microfiltration membranes. *Sep. Sci. Technol.* **37** (2002) 3039-3051.

[55] Pitt, A. M. The non-specific protein binding of polymeric microporous membranes. *J. Parenter. Sci. Technol.* **41** (1987) 110-113.

[56] Militello, V., Casarino, C., Emanuele, A., Giostra, A., Pullara, F., Leone, M. Aggregation kinetics of bovine serum albumin studied by FTIR spectroscopy and light scattering. *Biophys. Chem.* **107** (2004) 175-187.

[57] Kelly, S. T., Zydney, A. L. Effects of intermolecular thiol-disulfide interchange reactions on BSA fouling during microfiltration. *Biotechnol. Bioeng.* **44** (1994) 972-982.

[58] Todisco, S., Peña, L., Drioli, E., Tallarico, P. Analysis of the fouling mechanism in microfiltration of orange juice. *J. Food Process. Preserv.* **20** (1996) 453-466.

[59] Tarleton, E. S., Wakeman, R. J. Understanding flux decline in cross-flow microfiltration: Part I - Effects of particle and pore-size. *Chem. Eng. Res. Des.* **71** (1993) 399-410.

[60] Marshall, A. D., Munro, P. A., Trägårdh, G. Influence of permeate flux on fouling during the microfiltration of β-lactoglobulin solutions under cross-flow conditions. *J. Membr. Sci.* **130** (1997) 23-30.

[61] Tanaka, T., Kamimura, R., Fujiwara, R., Nakanishi, K. Crossflow filtration of yeast broth cultivated in molasses. *Biotechnol. Bioeng.* **43** (1994) 1094-1101.

[62] Foley, G., Macloughlin, P. F., Malone, D. M. Membrane fouling during constant flux cross-flow microfiltration of dilute suspensions of active dry yeast. *Sep. Sci. Technol.* **30** (1995) 383-398.

[63] Li, W., Cui, S. W., Wang, Q. Solution and conformational properties of wheat β-D-glucans studied by light scattering and viscometry. *Biomacromolecules* **7** (2006) 446-452.

[64] Nguyen, L. T., Wiencek, J. M., Kirsch, L. L. Characterization methods for the physical stability of biopharmaceuticals. *PDA J Pharm. Sci. Technol.* **57** (2003) 429-445.

[65] Ohmori, K., Glatz, C. E. Effects of pH and ionic strength on microfiltration of *C. glutamicum*. *J. Membr. Sci.* **153** (1999) 23-32.

[66] Wakeman, R. J., Williams, C. J. Additional techniques to improve microfiltration. *Sep. Purif. Technol.* **26** (2002) 3-18.

[67] Parameshwaran, K., Fane, A. G., Cho, B. D., Kim, K. J. Analysis of microfiltration performance with constant flux processing of secondary effluent. *Water Res.* **35** (2001) 4349-4358.

[68] Yamagiwa, K., Kobayashi, H., Onodera, M., Ohkawa, A. Surfactant pretreatment of a polysulfone ultrafilter for reduction of antifoam fouling. *Biotechnol. Bioeng.* **43** (1994) 301-308.

[69] Fane, A. G., Fell, C. J. D., Kim, K. J. The Effect of surfactant pretreatment on the ultrafiltration of proteins. *Desalination* **53** (1985) 37-55.

[70] Iding, K., Lutkemeyer, D., Fraune, E., Gerlach, K., Lehmann, J. Influence of alterations in culture condition and changes in perfusion parameters on the retention performance of a 20 µm spinfilter during a perfusion cultivation of a recombinant CHO cell line in pilot scale. *Cytotechnology* **34** (2000) 141-150.

[71] Lutkemeyer, D., Ameskamp, N., Tebbe, H., Wittler, J., Lehmann, J. Estimation of cell damage in bench- and pilot-scale affinity expanded-bed chromatography for the purification of monoclonal antibodies. *Biotechnol. Bioeng.* **65** (1999) 114-119.

[72] Wurm, F. M. Production of recombinant protein therapeutics in cultivated mammalian cells. *Nature Biotechnology* **22** (2004) 1393-1398.

[73] van der Pol, L., Tramper, J. Shear sensitivity of animal cells from a culture-medium perspective. *Trends Biotechnol.* **16** (1998) 323-328.

[74] Chu, L., Robinson, D. K. Industrial choices for protein production by large-scale cell culture. *Curr. Opin. Biotechnol.* **12** (2001) 180-187.

[75] Lightfoot, E. N., Moscariello, J. S. Bioseparations. *Biotechnol. Bioeng.* **87** (2004) 259-273.

[76] Ghosh, R. Principles of bioseparations engineering. World Scientific Publishing Co., New Jersey.2006

[77] Cheryan, M. Ultrafiltration and microfiltration handbook. Technomic Publishing Company, Inc., Lancaster, Pennsylvania.1998

[78] Seewoster, T., Lehmann, J. Cell size distribution as a parameter for the predetermination of exponential growth during repeated batch cultivation of CHO cells. *Biotechnol. Bioeng.* **55** (1997) 793-797.

[79] Cho, B. D., Fane, A. G. Fouling transients in nominally sub-critical flux operation of a membrane bioreactor. *J. Membr. Sci.* **209** (2002) 391-403.

[80] Ognier, S., Wisniewski, C., Grasmick, A. Membrane bioreactor fouling in sub-critical filtration conditions: a local critical flux concept. *J. Membr. Sci.* **229** (2004) 171-177.

[81] Hughes, D., Field, R. W. Crossflow filtration of washed and unwashed yeast suspensions at constant shear under nominally sub-critical conditions. *J. Membr. Sci.* **280** (2006) 89-98.

[82] Taddei, C., Aimar, P., Howell, J. A., Scott, J. A. Yeast-cell harvesting from cider using microfiltration. *J. Chem. Tech. Biotechnol.* **47** (1990) 365-376.

[83] Kroner, K. H., Hummel, W., Völkel, J., Kula, M. R. Effects of antifoams on cross-flow filtration of microbial suspensions. In Membranes and membrane processes (Drioli, E. and Nakagaki, M., eds.) pp. 223-232, Plenum Press, New York, 1986.

[84] Hanisch, W. Cell harvesting. In Membrane separations in biotechnology (McGregor, W. C., ed.) pp. 61-88, Marcel Dekker, Inc., New York, 1986.

[85] Keskinler, B., Yildiz, E., Erhan, E., Dogru, M., Bayhan, Y., Akay, G. Crossflow microfiltration of low concentration-nonliving yeast suspensions. *J. Membr. Sci.* **233** (2004) 59-69.

[86] Kroner, K. H., Schutte, H., Hustedt, H., Kula, M. R. Cross-Flow filtration in the downstream processing of enzymes. *Process Biochem.* **19** (1984) 67-74.

[87] Chilukuri, V. V. S., Marshall, A. D., Munro, P. A., Singh, H. Effect of sodium dodecyl sulphate and cross-flow velocity on membrane fouling during cross-flow microfiltration of lactoferrin solutions. *Chem. Eng. Process.* **40** (2001) 321-328.

[88] Defrance, L., Jaffrin, M. Y. Comparison between filtrations at fixed transmembrane pressure and fixed permeate flux: application to a membrane bioreactor used for wastewater treatment. *J. Membr. Sci.* **152** (1999) 203-210.

[89] Kelly, S. T., Zydney, A. L. Mechanisms for BSA fouling during microfiltration. *J. Membr. Sci.* **107** (1995) 115-127.

[90] Vickroy, B., Lorenz, K., Kelly, W. Modeling shear damage to suspended CHO cells during cross-flow filtration. *Biotechnol. Prog.* **23** (2007) 194-199.

[91] Ho, C. C., Zydney, A. L. A combined pore blockage and cake filtration model for protein fouling during microfiltration. *J. Colloid Interface Sci.* **232** (2000) 389-399.

[92] Duclos-Orsello, C., Li, W., Ho, C.-C. A three mechanism model to describe fouling of microfiltration membranes. *J. Membr. Sci.* **280** (2006) 856-866.

[93] Mueller, J., Davis, R. H. Protein fouling of surface-modified polymeric microfiltration membranes. *J. Membr. Sci.* **116** (1996) 47-60.

[94] Chudacek, M. W., Fane, A. G. The dynamics of polarisation in unstirred and stirred ultrafiltration. *J. Membr. Sci.* **21** (1984) 145-160.

[95] Ritchie, S. Polymer grafted membranes. In New insights into membrane science and technology: Polymeric and biofunctional membranes (Bhattacharyya, D. and Butterfield, D., eds) pp. 299-327, Elsevier Science B.V., 2003.

[96] Sethuraman, N., Stadheim, T. A. Challenges in therapeutic glycoprotein production. *Curr. Opin. Biotechnol.* **17** (2006) 341-346.

[97] Butler, M. Optimisation of the cellular metabolism of glycosylation for recombinant proteins produced by mammalian cell system. *Cytotechnology* **50** (2006) 57-76.

[98] Meireles, M., Lavoute, E., Bacchin, P. Filtration of a bacterial fermentation broth: harvest conditions effects on cake hydraulic resistance. *Bioprocess and Biosystems Engineering* **25** (2003) 309-314.

[99] Fletcher, M. The effects of culture concentration and age, time, and temperature on bacterial attachment to polystyrene. *Can. J. Microbiol.* **23** (1977) 1-6.

[100] Güell, C., Davis, R. H. Membrane fouling during microfiltration of protein mixtures. *J. Membr. Sci.* **119** (1996) 269-284.

[101] Thomassen, J. K., Faraday, D. B. F., Underwood, B. O., Cleaver, J. A. S. The effect of varying transmembrane pressure and crossflow velocity on the microfiltration fouling of a model beer. *Sep. Purif. Technol.* **41** (2005) 91-100.

[102] Zydney, A. L., Ho, C. C. Effect of membrane morphology on system capacity during normal flow microfiltration. *Biotechnol. Bioeng.* **83** (2003) 537-543.

[103] Stressmann, M., Marcos, B., Moresoli, C. A model for cross-flow microfiltration of biological solutions at constant permeate flux. *J. Membr. Sci.* **submitted** (2007)

[104] Daufin, G., Labbé, J.-P., Quémerais, A., Michel, F. Fouling of an inorganic membrane during ultrafiltration of defatted whey protein concentrates. *Neth. Milk Dairy J.* **45** (1991) 259-272.

[105] Devereux, N., Hoare, M. Membrane Separation of Protein Precipitates - Studies with Cross Flow in Hollow Fibers. *Biotechnol. Bioeng.* **28** (1986) 422-431.

[106] Meireles, M., Aimar, P., Sanchez, V. Albumin denaturation during ultrafiltration: Effects of operating conditions and consequences on membrane fouling. *Biotechnol. Bioeng.* **38** (1991) 528-534.

[107] Kilburn, D. G. Monitoring and control of bioreactors. In Mammalian cell biotechnology (Butler, M., ed) pp. 159-186, Oxford University Press, Oxford, 1991.

[108] Higuchi, A., Sugiyama, K., Yoon, B. O., Sakurai, M., Hara, M., Sumita, M., Sugawara, S., Shirai, T. Serum protein adsorption and platelet adhesion on pluronic (TM)-adsorbed polysulfone membranes. *Biomaterials* **24** (2003) 3235-3245.

[109] Ghebeh, H., Handa-Corrigan, A., Butler, M. Development of an assay for the measurement of the surfactant pluronic F-68 in mammalian cell culture medium. *Anal. Biochem.* **262** (1998) 39-44.

[110] Govender, S., Jacobs, E. P., Bredenkamp, M. W., Swart, P. A robust approach to studying the adsorption of Pluronic F108 on nonporous membranes. *J. Colloid Interface Sci.* **282** (2005) 306-313.

[111] Wang, Y.-Q., Su, Y.-L., Ma, X.-L., Sun, Q., Jiang, Z.-Y. Pluronic polymers and polyethersulfone blend membranes with improved fouling-resistant ability and ultrafiltration performance. *J. Membr. Sci.* **283** (2006) 440-447.

[112] Yang, S.-T., Marchio, J. L., Yen, J.-W. A dynamic light scattering study of β-galactosidase: environmental effects on protein conformation and enzyme activity. *Biotechnol. Prog.* **10** (2008) 525-531.

[113] Ghebeh, H., Gillis, J., Butler, M. Measurement of hydrophobic interactions of mammalian cells grown in culture. *J. Biotechnol.* **95** (2002) 39-48.